М. ӘУЕЗОВ АТЫНДАҒЫ ОҢТҮСТІК ҚАЗАҚСТАН УНИВЕРСИТЕТІ

ПЕРНЕБАЕВ ЖАҚСЫЛЫҚ ДӘУЛЕТБАЙҰЛЫ

ҚОРҒАСЫН-МЫРЫШ ҚОЖДАРЫН ҚАЙТА ӨҢДЕУ ӨНІМДЕРІМЕН ТОПЫРАҚТЫҢ ЛАСТАНУЫН ЭКОЛОГИЯЛЫҚ БАҒАЛАУ ЖӘНЕ БОЛЖАУ

8D05210 – Экология

Философия докторы (PhD) дәрежесін алу үшін
ғылыми мақалалар сериясы түрінде ұсынылған диссертация

Ғылыми кеңесшілер:

Исаева Ақмарал Өмірбекқызы,
биология ғылымдарының докторы, профессор

Шетелдік ғылыми кеңесші:

Махмуд-ур-Рахман Ансари, PhD,
Фейсалабад мемлекеттік университеті, Пәкістан

Қазақстан Республикасы
Шымкент, 2026

sustainability

MDPI

Review

Scoping Review on Soil Contamination from Pb–Zn Slag and Environmental Assessment Methods

Zhaksylyk Pernebayev and Akbota Aitimbetova *

Department of Ecology, M. Auezov South Kazakhstan University, Shymkent 160012, Kazakhstan; zhaksylykpernebaev@gmail.com
* Correspondence: akbota.askarkyzy@auezov.edu.kz

Abstract

Pb–Zn slag and smelting activities represent a persistent global source of soil contamination, releasing toxic heavy metals—lead (Pb), zinc (Zn), cadmium (Cd), and arsenic (As)—with documented risks to ecosystems and human health. Although previous reviews have addressed heavy metal contamination near smelters and pollution indices as assessment tools, no review has specifically mapped environmental assessment methods for Pb–Zn slag-contaminated soils, and evidence from Central Asia remains absent. This scoping review, following PRISMA-ScR 2018 guidelines, maps the global evidence base on soil contamination from Pb–Zn slag and associated assessment methods. Searches across Dimensions, PubMed, and OpenAlex identified 410 records; 56 studies (2010–2025) met the inclusion criteria. Studies were concentrated in China (35.7%), Poland (8.9%), and Brazil (7.1%); no studies from Kazakhstan were identified despite major Pb–Zn smelting operations in the Shymkent region. All studies reported heavy metal concentrations exceeding regulatory thresholds, with cadmium as the primary ecological risk driver and lead posing the greatest health risk to children. Assessment methods included pollution indices (73.2%), ecological risk assessment (67.9%), GIS-based spatial analysis (57.1%), human health risk frameworks (51.8%), and source apportionment models (50.0%). Post-2018 studies increasingly applied integrated multi-method frameworks. Critical gaps include the absence of Central Asian research, limited predictive modeling, and a lack of standardized protocols. Findings provide a structured evidence map to guide environmental monitoring and remediation at slag-contaminated sites globally.

Keywords: Pb–Zn slag; PRISMA-ScR; soil contamination; Kazakhstan; heavy metals

Check for updates

Academic Editor: Guannan Liu

Received: 17 March 2026
Revised: 6 April 2026
Accepted: 9 April 2026
Published: 15 April 2026

Copyright: © 2026 by the authors. Licensee MDPI, Basel, Switzerland. This article is an open access article distributed under the terms and conditions of the Creative Commons Attribution (CC BY) license.

1. Introduction

Soil contamination by heavy metals represents a pervasive global environmental challenge, affecting agricultural productivity, ecosystem health, and human well-being [1]. Heavy metals such as lead, zinc, cadmium, and arsenic persist in soils due to their non-biodegradable nature, leading to bioaccumulation in food chains and posing risks of chronic toxicity, including neurological disorders, renal damage, and carcinogenicity [2]. According to global estimates, over 50 million hectares of agricultural land are contaminated with heavy metals [3], with Asia bearing the heaviest burden due to rapid industrialization and intensive mining [3]. In Europe and North America, legacy pollution from historical smelting operations continues to affect soils decades after facility closures [4,5]. These contaminants enter soils through atmospheric deposition, wastewater irrigation, agrochemical applications, and direct industrial discharges [3].

Industrial activities, particularly non-ferrous metal smelting and mining, are the primary anthropogenic sources of this pollution, with metallurgical slag—a byproduct of ore processing—making a significant contribution [6,7]. Pb–Zn smelting generates vast quantities of slag, often disposed of in landfills or reused without adequate environmental safeguards, resulting in the leaching of Pb, Zn, Cd, and As into surrounding soils [8]. Slag from Pb–Zn operations typically contains 1–5% Pb, 10–30% Zn, and variable Cd levels, far exceeding natural soil background concentrations [9]. Globally, the annual production of Pb–Zn slag exceeds 10 million tons, stockpiled near smelters in China, India, Australia, and Central Asia [10]. In mining districts of southern China, soil Pb concentrations near slag heaps reach 2000 mg/kg—more than 100 times the regulatory limit—while Zn levels surpass 5000 mg/kg [11,12].

The geochemical instability of slag under varying environmental conditions exacerbates contamination. Acidic rainfall lowers soil pH and enhances metal solubilization [13], while organic matter increases metal bioavailability [14]. Redox fluctuations in waterlogged soils release bound metal ions into groundwater [15]. In arid regions, dust storms disperse fine slag particles over hundreds of kilometers, contaminating remote farmlands [16,17]. These processes create diffuse pollution plumes that infiltrate aquifers and river systems, extending contamination well beyond point sources.

Ref. [18] shows that environmental risks are multifaceted. In agroecosystems, elevated Pb and Cd levels inhibit seed germination and reduce crop yields by 20–50% [19]. Plants such as rice and wheat hyperaccumulate Zn, transferring it to edible parts and thereby posing dietary risks [20,21]. Soil microbial communities experience declines in enzyme activity of up to 70%, disrupting nutrient cycling [21,22]. Human exposure occurs through ingestion of contaminated produce, inhalation of dust, and dermal contact [23,24]. Children are particularly vulnerable, with blood Pb levels above 5 μg/dL linked to irreversible IQ deficits [25]. Chronic Cd exposure induces itai-itai disease, characterized by severe bone pain and kidney failure.

Pb–Zn slag pollution exemplifies these risks globally [26,27]. In Yunnan Province, China, decades of Pb–Zn smelting have contaminated over 1000 km^2 of farmland [28]. In Kabwe, Zambia, childhood blood Pb levels average 50 μg/dL—ten times the WHO thresholds—due to slag recycling in informal economies [29–31]. In Kazakhstan, the Shymkent lead plant has generated millions of tons of slag over several decades, with documented soil Pb concentrations exceeding 3000 mg/kg near the facility—more than 900 times the maximum permissible concentration—yet this site remains largely absent from the international peer-reviewed literature [32]. It should be noted that the soil Pb concentration of 3000 mg/kg reported for the Shymkent site [32] was determined using atomic absorption spectrometry (AAS) following GOST-standardized protocols, which are methodologically comparable to ICP-based international methods (ICP-OES, ICP-MS) for total metal determination in soils [33]. The background and reference values cited from South Korean study sites [33] were obtained using validated ICP-MS procedures consistent with ISO 17294 standards [34]. While minor procedural differences between GOST and ISO/US EPA extraction protocols may exist, these do not materially affect the order-of-magnitude comparison with international regulatory thresholds presented in this review. Climate change intensifies these threats: increased rainfall enhances leaching, while rising temperatures accelerate slag weathering and metal release [35–37].

Current environmental assessment methods include chemical analysis, GIS-based spatial mapping, bioindicators, and predictive modeling [38–40]. Sequential extraction procedures such as BCR differentiate metal fractions and inform bioavailability assessment [41,42]. Geostatistical tools, including kriging, interpolate contamination hotspots, while ecological risk indices quantify environmental threats [43–45]. However,

these methods face limitations: high costs restrict adoption in low-resource settings; site-specific variability requires calibration; and insufficient integration of multi-media exposure pathways leads to an underestimation of holistic risk [46,47]. Emerging tools such as diffusive gradients in thin films provide labile metal proxies, but standardization lags [48–50].

Despite extensive global research on heavy metal contamination near smelting areas, studies that specifically address Pb–Zn slag and employ systematic environmental assessment remain fragmented [9–11,51]. Existing research is concentrated in China, Europe, and parts of South America, with Central Asia—particularly Kazakhstan—entirely unrepresented in the peer-reviewed literature despite hosting major Pb–Zn smelting infrastructure [52]. Previous reviews have examined heavy metal contamination in soils near smelting areas in general terms [10], human health risks from heavy metals at industrial sites [53], and pollution indices as assessment tools [54]. However, none of these reviews have specifically focused on Pb–Zn slag as a distinct contamination source, nor have any systematically mapped and categorized the full range of environmental assessment methods applied across slag-contaminated sites globally. This gap limits methodological standardization and evidence synthesis for this particular class of industrial waste.

This review contributes three novel elements to the existing literature: (i) a slag-specific focus that distinguishes Pb–Zn slag from broader smelter-related contamination as a distinct geochemical source; (ii) a comprehensive categorization and evidence mapping of all environmental assessment methods applied in this context; and (iii) the first systematic identification of the Central Asian research gap in the peer-reviewed literature on Pb–Zn slag contamination.

This scoping review addresses these gaps by systematically mapping the global evidence base on soil contamination from Pb–Zn slag and the environmental assessment methods employed in primary studies. Following PRISMA-ScR 2018 guidelines [55], the review pursues three objectives: (1) to characterize the scope and distribution of soil contamination from Pb–Zn slag and smelting activities reported in the literature; (2) to identify and categorize environmental assessment and predictive modeling methods applied across study contexts; and (3) to identify geographic, methodological, and thematic research gaps with particular relevance to Kazakhstan and Central Asia.

2. Materials and Methods

2.1. Study Design

This scoping review was conducted in accordance with PRISMA-ScR 2018 guidelines [55]. The review process comprised four sequential stages: (1) Identification—three electronic databases were searched using a predefined Boolean string; (2) Screening—retrieved records were assessed by title and abstract against eligibility criteria; (3) Eligibility—full texts of potentially relevant records were retrieved and evaluated against inclusion and exclusion criteria; and (4) Inclusion—studies meeting all criteria were retained for data charting and evidence mapping. The review protocol is publicly registered at OSF: https://osf.io/ktg86 (registered 16 March 2026); accessed on 16 March 2026). A grant AP25795537 from the Science Committee of the Ministry of Science and Higher Education of the Republic of Kazakhstan funded the review. The PRISMA-ScR 2018 checklist is provided in Table S1.

2.2. Eligibility Criteria

Studies were selected using the Population, Concept, and Context (PCC) framework. The Population comprised soils contaminated by Pb–Zn slag or associated smelting and mining activities. The Concept encompassed ecological assessment methods and predictive

modeling approaches for evaluating soil contamination. The Context included industrial sites globally, with particular relevance to the Shymkent region of Kazakhstan.

Inclusion criteria were: (1) peer-reviewed journal articles published between January 2010 and March 2025; (2) studies reporting soil contamination directly linked to Pb–Zn slag, smelter emissions, or metallurgical waste; (3) studies employing at least one environmental assessment or predictive modeling method; and (4) publications available in English.

Exclusion criteria were: (1) studies focused exclusively on construction material applications of slag without environmental assessment; (2) wastewater treatment studies without soil contamination data; (3) pyrometallurgical metal recovery processes; (4) solidification/stabilization technology studies without field environmental data; and (5) publications prior to 2010.

2.3. Information Sources and Search Strategy

A systematic literature search was conducted on 16 March 2026 across three databases: Dimensions (n = 351), PubMed (n = 10), and OpenAlex (n = 49), yielding 410 records in total. Scopus and Web of Science were not included due to institutional access restrictions at the time of the search. The selected combination was chosen to maximize coverage: Dimensions indexes over 130 million publications and has demonstrated comparable or superior recall to Scopus and Web of Science for environmental science queries [56]; OpenAlex aggregates records from Crossref, PubMed, and institutional repositories, providing broad open-access coverage [57]; and PubMed ensures retrieval of biomedical and toxicological studies. This combination has been validated as methodologically appropriate for scoping reviews in environmental health [56]. The following Boolean search string was applied uniformly across all databases:

("Lead-Zinc Slag" OR "Pb–Zn slag" OR "zinc slag" OR "lead slag") AND ("soil contamination" OR "soil pollution" OR "heavy metals" OR "environmental assessment" OR "remediation")

2.4. Study Selection and Screening Process

All retrieved records were imported into Rayyan (Rayyan Systems Inc., Cambridge, MA, USA; http://rayyan.ai/, accessed on 16 March 2026) for systematic management [58]. After automated and manual duplicate removal (n = 27), a total of 383 records underwent title and abstract screening by one reviewer against the predefined eligibility criteria. Records that clearly did not meet the inclusion criteria were excluded (n = 253), yielding 130 records for full-text assessment. Following full-text screening, 56 studies met all inclusion criteria and were retained for data extraction and evidence mapping. The study selection process is illustrated in the PRISMA-ScR flow diagram (Figure 1).

2.5. Data Extraction and Evidence Mapping

Data were extracted from the 56 included studies using a standardized charting form implemented in Elicit (Elicit PBC, San Francisco, CA, USA; https://elicit.com/, accessed on 7 April 2026) and Microsoft Excel 2021 (Microsoft Corporation, Redmond, WA, USA). Extracted variables included: bibliographic details (authors, publication year, journal); geographic scope (country, region); contamination source (slag type, smelter, tailings, mine); heavy metals analyzed; environmental assessment methods employed; predictive or transport models used; number of soil samples collected; and key findings regarding contamination levels and risks.

The study selection process and the number of records included at each stage are illustrated in the PRISMA-ScR flow diagram.

Full data extraction is provided in Table S2 (Supplementary Materials).

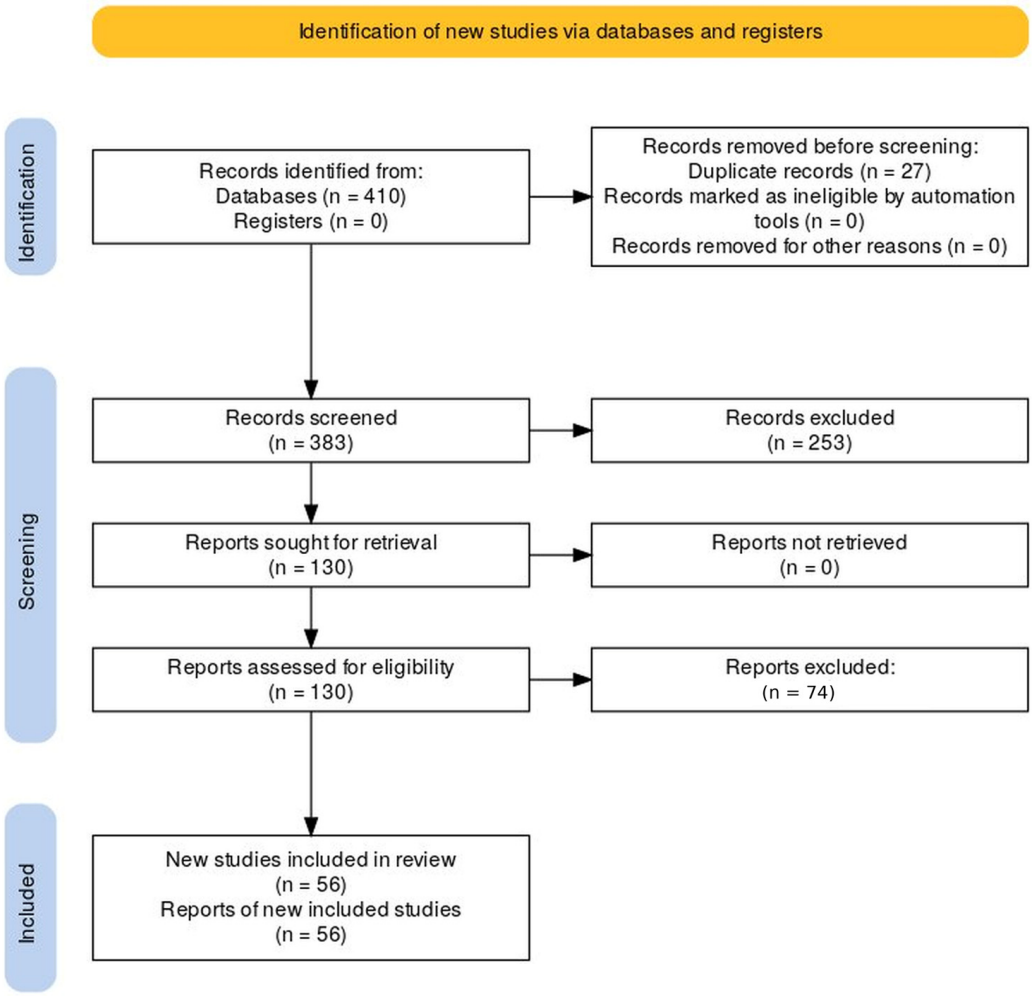


Figure 1. PRISMA-ScR 2018 flow diagram illustrating the identification, screening, eligibility assessment, and inclusion of studies in this scoping review.

2.6. Methodological Quality Appraisal

Consistent with the PRISMA-ScR 2018 guidelines, a formal risk-of-bias assessment is not required for scoping reviews, as their primary objective is to map the extent and nature of available evidence rather than to synthesize effect estimates [55]. Nevertheless, to strengthen the reliability of the findings, a basic methodological quality appraisal was conducted for all 56 included studies using four criteria adapted from established environmental research quality frameworks: (1) adequacy of sampling design (sample size $\geq$ 20, spatial coverage documented); (2) use of validated analytical methods (ICP-MS, ICP-OES, AAS, or pXRF with documented quality assurance/quality control procedures); (3) inclusion of reference or background samples for comparison; and (4) application of at least one standardized assessment framework (e.g., US EPA, Hakanson PER [59], Müller Igeo). Each criterion was scored as 'met', 'partially met', or 'not met'. Studies meeting all four criteria were classified as high methodological quality; those meeting two or three were classified as moderate; and those meeting fewer than two were classified as low.

2.7. AI-Assisted Tools

Several AI-assisted tools were used during the preparation of this review. Language editing and grammar checking of the manuscript text were performed using Claude (claude-3-5-sonnet, Anthropic, San Francisco, CA, USA). Literature organization and initial data extraction support were performed using Elicit (Elicit PBC, San Francisco, CA, USA;

https://elicit.com/, accessed on 7 April 2026), an AI-assisted research tool; all extracted data were subsequently verified manually by the authors against the original sources. The graphical abstract was created using Napkin AI (Napkin AI Inc., San Francisco, CA, USA; https://www.napkin.ai/, accessed on 7 April 2026). No AI tool was used for data analysis, statistical computations, interpretation of results, or drawing scientific conclusions. All AI-generated content was reviewed, verified, and edited by the authors, who take full responsibility for the accuracy and integrity of the submitted manuscript.

3. Results

3.1. Study Selection and PRISMA Flow

The study selection process followed the four-stage PRISMA-ScR protocol described in Section 2. The most common reasons for exclusion at the full-text stage were: a focus on construction-material applications of slag (n = 98), wastewater treatment without soil contamination data (n = 82), and pyrometallurgical metal recovery without a field environmental assessment (n = 73). The complete study selection flow is presented in Figure 1.

Methodological Quality of Included Studies

Of the 56 included studies, 34 (60.7%) met all four quality criteria and were classified as displaying high methodological quality. These studies employed validated analytical techniques with documented QA/QC procedures, collected ≥20 soil samples with adequate spatial coverage, included reference or background samples, and applied at least one standardized assessment framework. A further 18 studies (32.1%) were classified as moderate quality, most commonly lacking documented QA/QC procedures or reference samples. Four studies (7.1%) were classified as low quality due to small sample sizes (n < 20) and the absence of background comparisons. All four low-quality studies were published before 2018, suggesting that methodological rigor has improved over time. The key findings of this review—including the dominance of cadmium as an ecological risk driver and of lead as a health risk—were consistent across high- and moderate-quality studies, indicating that the overall conclusions are robust to variations in methodological quality.

3.2. Characteristics of Included Studies

The 56 included studies were published between 2010 and 2025, with a marked increase in publication frequency after 2020, reflecting growing global concern over the environmental impacts of metallurgical waste. Specifically, 15 studies were published between 2010 and 2017, compared with 41 between 2018 and 2025, representing a 2.7-fold increase. Study designs were predominantly empirical field investigations, with the majority collecting soil samples from sites adjacent to active or abandoned Pb–Zn smelters, slag heaps, or tailings deposits. Peer-reviewed journal articles constituted all included publications. The characteristics of included studies are summarized in Table 1. The country-level distribution of included studies is presented in Figure 2, annual publication trends are illustrated in Figure 3, the frequency of contamination source types is presented in Figure 4 and frequency of heavy metal(oid)s mentions analyzed in the included studies is presented in Figure 5.

Table 1. Characteristics of included studies (n = 56).

Publication Year	n	%
2010–2014	3	5.4
2015–2017	12	21.4
2018–2020	14	25.0
2021–2023	20	35.7
2024–2025	7	12.5
Contamination source		
Smelter (active or abandoned)	38	67.9
Pb–Zn slag heap	10	17.9
Tailings/mine waste	5	8.9
Mixed sources	3	5.4
Heavy metals studied		
Pb + Zn + Cd (all studies)	56	100
+As	42	75.0
+Cu	35	62.5
+Hg	18	32.1
+Tl	3	5.4
Study design		
Empirical field study	48	85.7
Modeling study	5	8.9
Combined field + modeling	3	5.4

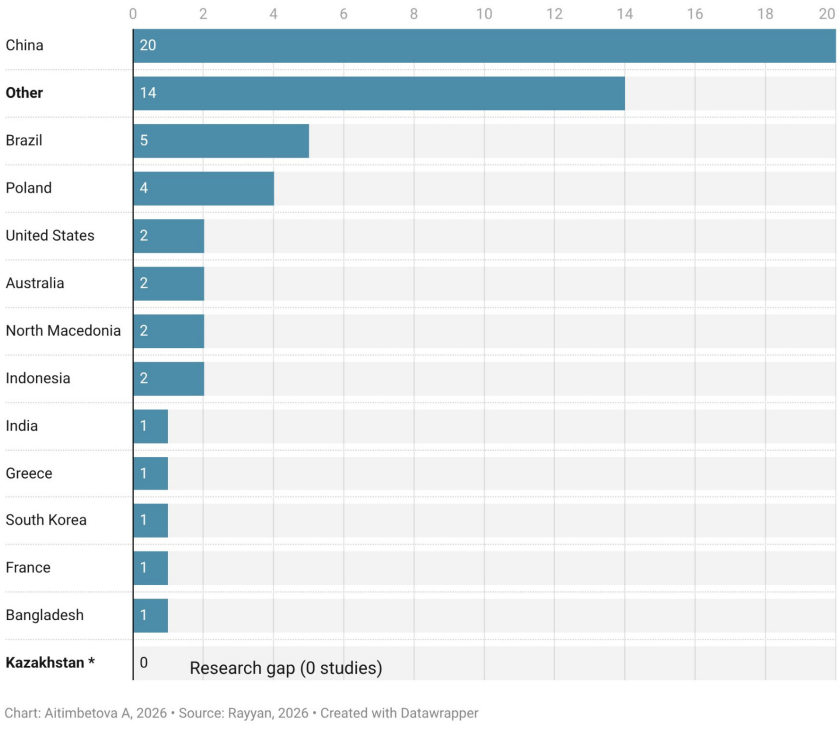


Figure 2. Country-level distribution of the included studies and identified research gaps. * Kazakhstan is marked as a research gap (0 studies identified in the peer-reviewed literature despite major Pb–Zn smelting operations in the Shymkent region). Chart created with Datawrapper (Datawrapper GmbH, Berlin, Germany; https://www.datawrapper.de/, accessed on 16 March 2026).

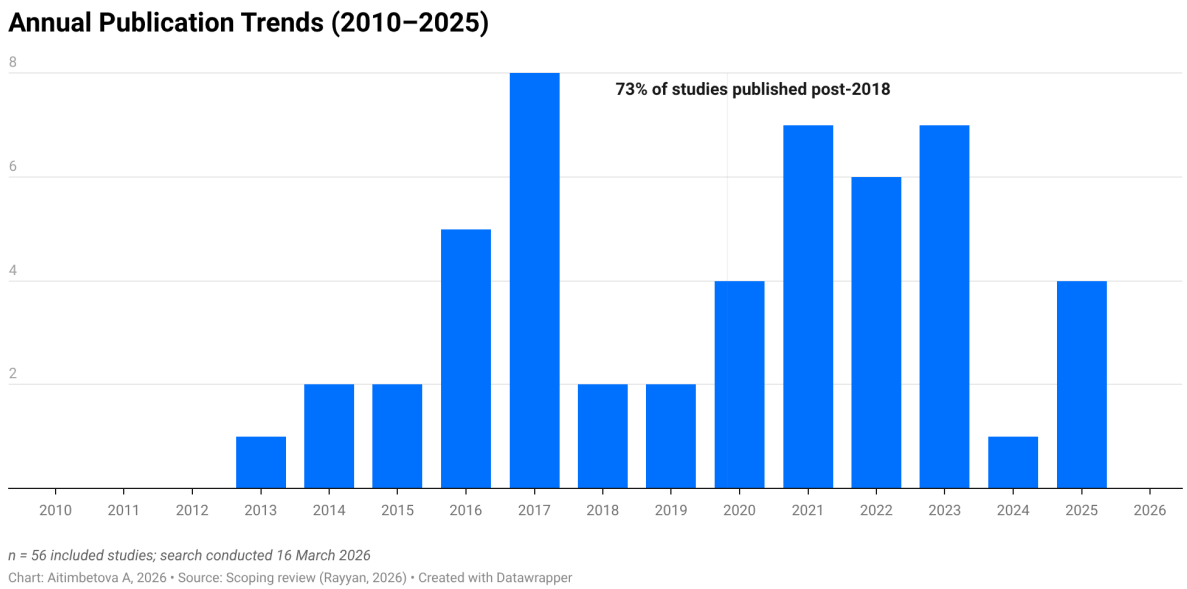


Figure 3. Annual distribution of included studies (2010–2025). Chart created by the authors based on data extracted from included studies using Rayyan [57]. Created with Datawrapper (Datawrapper GmbH, Berlin, Germany).

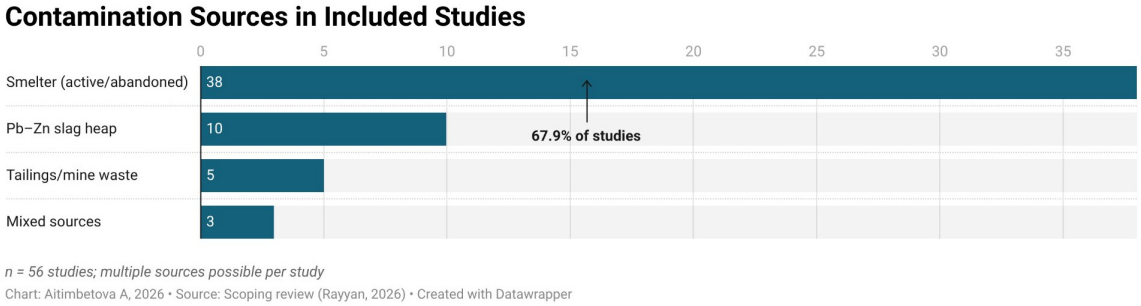


Figure 4. Frequency of contamination source types in the reviewed studies. Chart created by the authors based on data extracted from included studies using Rayyan [57]. Created with Datawrapper (Datawrapper GmbH, Berlin, Germany).

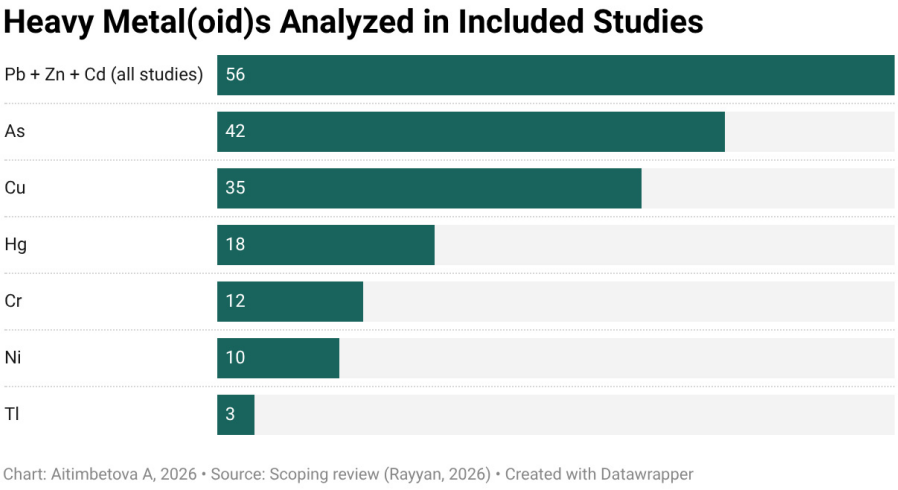


Figure 5. Frequency of heavy metal(oid)s analyzed in the included studies (n = 56). Chart created by the authors based on data extracted from included studies using Rayyan [57]. Created with Datawrapper (Datawrapper GmbH, Berlin, Germany).

3.3. Geographic Distribution of Studies

The 56 included studies exhibited a pronounced geographic concentration in regions with established Pb–Zn smelting histories. China dominated the literature, with 20 studies (35.7%) [28,60–65], reflecting the country's status as the world's largest producer of lead and zinc [66]. Poland contributed five studies (8.9%) [67,68], primarily examining legacy contamination from historical Pb–Zn mining districts. Brazil accounted for four studies (7.1%) [69,70], with a particular focus on the former Santo Amaro smelter site in Bahia state [63]. The United States and Australia each contributed two studies (3.6%), while Bangladesh [71], India [72], Indonesia [73,74], France, Greece [75,76], South Korea [33], and the Republic of Macedonia [77] each contributed 1–2 studies [65,78,79]. The geographic distribution is presented in Figure 6.

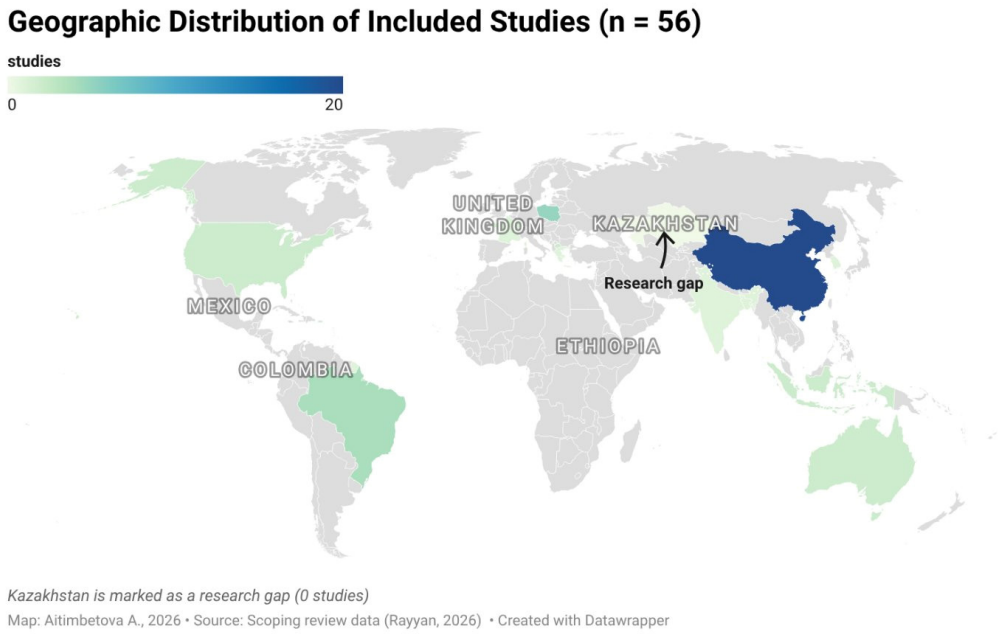


Figure 6. Geographical distribution of included studies [58].

Critically, no studies were identified from Kazakhstan despite the presence of one of Central Asia's largest Pb–Zn smelting complexes in the Shymkent region [80], representing a significant research gap with direct relevance to this review. Central Asia as a whole was absent from the identified literature, highlighting a major geographic underrepresentation in the global evidence base.

3.4. Environmental Assessment Methods Used in the Literature

The 56 included studies employed a diverse range of environmental assessment methods, which were categorized into five primary groups: pollution indices, ecological risk assessment, human health risk assessment, spatial analysis, and advanced analytical and modeling approaches. Many studies applied multiple methods simultaneously, reflecting a trend toward integrated assessment frameworks.

3.4.1. Pollution Indices

Pollution indices were the most frequently applied assessment tools, used in 41 studies (73.2%). The most common indices included the Single Factor Pollution Index (PI), the Nemerow Synthetic Pollution Index (NSPI), the Geoaccumulation Index (Igeo), and the Enrichment Factor (EF) [81]. These indices provide standardized quantitative measures of

contamination relative to background or regulatory threshold values, enabling comparison across study sites and metals.

3.4.2. Ecological Risk Assessment

Ecological risk assessment methods were applied in 38 studies (67.9%) [82]. The Potential Ecological Risk Index (PER/RI) [83,84], originally developed by Hakanson (1980) [59], was the most widely used approach, calculating risk based on metal toxicity response coefficients and contamination factors. Risk grades ranged from low to significantly high ecological risk, with cadmium (Cd) identified as the primary driver of high ecological risk in the majority of studies (34 of 38 studies reporting ecological risk, 89.5%), primarily due to its high toxicity response coefficient (Tr = 30) in the Hakanson (1980) [59] framework—the highest among the metals commonly assessed at Pb–Zn slag sites. However, it should be noted that this ranking is partly an artifact of the toxicity coefficient system, in which Cd receives a coefficient substantially higher than Pb (Tr = 5), Zn (Tr = 1), and As (Tr = 10) [85]. Where alternative toxicity coefficients were applied, the relative risk ranking of metals varied [86,87].

3.4.3. Human Health Risk Assessment

Human health risk assessment following the United States Environmental Protection Agency (US EPA) framework was applied in 29 studies (51.8%). These assessments calculated non-carcinogenic hazard quotients (HQ) and hazard indices (HI), as well as carcinogenic risk indices (CR/TCR) for adults and children separately, considering exposure pathways including ingestion, dermal contact, and inhalation [88,89]. Six studies employed Monte Carlo simulation for probabilistic risk assessment (10.7%) [66,90].

3.4.4. Spatial Analysis Methods

Geospatial analysis was employed in 32 studies (57.1%) [91,92]. Geographic Information Systems (GIS) with kriging interpolation were used for spatial distribution mapping [89,90] and for identifying contamination hotspots. Principal Component Analysis (PCA) and Cluster Analysis (CA) were applied in 28 studies (50.0%) [93] to identify sources and differentiate anthropogenic from geogenic metal contributions. Positive Matrix Factorization (PMF) [94] and APCS-MLR receptor models were used in 12 studies (21.4%) for quantitative source apportionment [95].

3.4.5. Advanced Analytical and Modeling Approaches

Advanced analytical techniques were applied across multiple studies. Portable X-ray fluorescence (pXRF) was used for rapid field screening in eight studies (14.3%) [96–98]. Lead isotope ratio analysis ($^{206}Pb/^{207}Pb$) for source tracing was applied [99]. Sequential extraction procedures (BCR, Tessier) for metal fractionation and bioavailability assessment were employed in 9 studies [100] (16.1%). Predictive transport modeling, including Hydrus-1D version 4.xx (PC-Progress, Prague, Czech Republic) simulations and multisurface geochemical modeling, was used in four studies (7.1%) [101–103]. Biological and ecotoxicological methods, including microbial community analysis (16S rRNA), phytotoxicity bioassays, and enzymatic biomarkers (dehydrogenase activity), were applied in 14 studies (25.0%) [104]. The distribution of assessment methods is summarized in Table 2.

Table 2. Distribution of environmental assessment methods applied in the included studies (n = 56), with example software and analytical tools.

Assessment Method	*n*	%	Example Software/Tools
Pollution indices (PI, Nemerow, Igeo, EF)	41	73.2	Microsoft Excel, R version 4.3.1 (EnvStats)
Ecological risk index (PER/RI)	38	67.9	Microsoft Excel, IBM SPSS STATISTICS V28
GIS + spatial mapping (kriging)	32	57.1	ArcGIS Pro 3.1 (Esri, Redlands, CA, USA), QGIS 3.32, Surfer 25 (Golden Software, Golden, CO, USA)
Human health risk (US EPA, HQ/HI)	29	51.8	EPA ExpoBox, RISC5, R
PCA + Cluster Analysis	28	50.0	IBM SPSS STATISTICS V28, R version 4.3.1 (FactoMineR), Origin
PMF source apportionment	12	21.4	EPA PMF VERSION 5.0 (US EPA, Washington, DC, USA), ME-2 (Paul Scherrer Institute, Villigen, Switzerland)
Sequential extraction (BCR/Tessier)	9	16.1	ICP-MS/OES (instrumental)
Microbial community (16S rRNA)	8	14.3	QIIME2 V2023.5, Mothur v1.48.0, R version 4.3.1 (vegan)
pXRF field screening	8	14.3	Olympus Vanta (Olympus Corporation, Tokyo, Japan), Bruker S1 TITAN (Bruker Corporation, Billerica, MA, USA)
Monte Carlo simulation	6	10.7	Oracle Crystal Ball (Oracle Corporation, Austin, TX, USA), @RISK version 8 (Palisade Corporation, Ithaca, NY, USA), R version 4.3.1 (mc2d)
Phytoremediation + BCF/TF	6	10.7	Microsoft Excel 2021
Pb isotope tracing	5	8.9	MC-ICP-MS (instrumental)
Predictive transport models (Hydrus-1D version 4.xx (PC-Progress, Prague, Czech Republic))	4	7.1	Hydrus-1D version 4.xx (PC-Progress, Prague, Czech Republic), PHREEQC v3.7 (US Geological Survey, Reston, VA, USA), MODFLOW 6 (US Geological Survey, Reston, VA, USA)
Ecotoxicology (PICT, bioassays)	4	7.1	EC50 calculators, R version 4.3.1 (drc)
Geophysical methods (GPR, radionuclides)	3	5.4	GSSI (Geophysical Survey Systems Inc., Nashua, NH, USA), Geosoft Oasis
LCA/Material flow analysis	2	3.6	SimaPro version 9 (PRé Sustainability, Amersfoort, The Netherlands), OpenLCA version 2.0 (GreenDelta, Berlin, Germany), GaBi v10 (Sphera Solutions, Stuttgart, Germany)

Note: PI = Pollution Index; Igeo = Geoaccumulation Index; EF = Enrichment Factor; PER/RI = Potential Ecological Risk Index; GIS = Geographic Information System; PCA = Principal Component Analysis; PMF = Positive Matrix Factorization; BCR = Bureau Communautaire de Référence; pXRF = portable X-ray fluorescence; BCF = Bioconcentration Factor; TF = Translocation Factor; GPR = Ground-Penetrating Radar; LCA = Life Cycle Assessment; PICT = Pollution-Induced Community Tolerance, HQ/HI = Hazard Quotient/Hazard Index, MC-ICP-MS = Multicollector Inductively Coupled Plasma Mass Spectrometry.

The comparative analysis (Table 3) reveals that each method category addresses a distinct dimension of contamination assessment. Pollution indices and ecological risk indices are most suitable for initial site screening due to their simplicity and low data requirements. However, they cannot capture metal bioavailability or ecosystem-level impacts. Human health risk frameworks provide regulatory-grade risk estimates but are limited by deterministic exposure assumptions unless supplemented with Monte Carlo simulation. Spatial methods (GIS, kriging) are essential for delineating contamination boundaries and identifying hotspots, but depend critically on sampling density. Source apportionment models (PMF, PCA) enable targeted remediation planning but require

sufficiently large datasets for statistical reliability. Sequential extraction and biological methods provide complementary information on metal mobility and ecological effects, respectively, that chemical indices alone cannot capture. The trend toward integrated multi-method frameworks observed in post-2018 studies (61% of publications) reflects growing recognition that no single method adequately characterizes the full complexity of Pb–Zn slag contamination. An optimal assessment strategy for slag-contaminated sites would combine rapid screening (pXRF, pollution indices) with confirmatory spatial analysis (GIS-kriging), risk quantification (US EPA + Monte Carlo), and ecosystem health evaluation (biological methods).

Table 3. Comparative analysis of environmental assessment methods for Pb–Zn slag-contaminated soils.

Method	Strengths	Limitations	Recommended Application
Pollution indices (PI, Igeo, EF)	Simple calculation; low data requirements; enables cross-site comparison using standardized thresholds	Does not assess bioavailability or ecological impact; results sensitive to choice of reference/background value [105]	Initial screening and baseline contamination characterization
Ecological risk index (PER/RI)	Integrates metal toxicity coefficients into a single composite score; enables comparative ranking across metals [106,107]	Relies on predefined toxicity coefficients (Hakanson, 1980) [59] that may not reflect site-specific bioavailability; does not account for metal speciation or synergistic effects	Comparative ecological risk ranking across metals and sites
Human health risk (US EPA HQ/HI/CR)	Internationally standardized framework; separates carcinogenic and non-carcinogenic risk; differentiates exposure for adults and children [82]	Deterministic by default; relies on generic exposure parameter assumptions; does not capture spatial variability of contamination.	Regulatory risk assessment and remediation prioritization
Monte Carlo simulation	Quantifies uncertainty in risk estimates; provides probability distributions rather than single point values [85]	Requires large input datasets for parameter distributions; computationally more demanding than deterministic approaches	Probabilistic refinement of health risk assessment
GIS + kriging interpolation	Spatial visualization of contamination gradients; identifies hotspots for targeted remediation [87,93]	Requires sufficient sample density for reliable interpolation; uncertainty increases with sparse or clustered sampling.	Spatial risk mapping and contamination boundary delineation
PCA/PMF source apportionment	Quantifies contributions of different pollution sources; distinguishes anthropogenic from geogenic inputs [92,93]	Requires large sample sizes (typically $n > 50$); results are sensitive to input data quality and the number of factors selected.	Source identification for targeted remediation strategies
Sequential extraction (BCR/Tessier)	Differentiates metal fractions by bioavailability; informs mobility under changing environmental conditions [40,41]	Operationally defined fractions; poor selectivity between phases; time-consuming and labor-intensive	Bioavailability assessment and leaching risk evaluation

Table 3. *Cont.*

Method	Strengths	Limitations	Recommended Application
pXRF field screening	Rapid, non-destructive, cost-effective; suitable for large-scale surveys in resource-limited settings [108,109]	Lower precision than ICP-MS for trace concentrations; matrix effects require site-specific calibration	Preliminary field screening prior to laboratory confirmation
Predictive transport models (Hydrus-1D version 4.xx (PC-Progress, Prague, Czech Republic))	Simulates metal migration under varying conditions; supports long-term risk forecasting [99]	Requires detailed site-specific hydraulic and geochemical parameters; limited field validation at slag sites	Long-term risk prediction and remediation planning
Biological methods (16S rRNA, PICT, bioassays)	Integrates ecosystem-level response; captures bioavailability effects missed by chemical methods [104,110]	High variability between sites; limited standardization of protocols; requires specialized equipment and expertise.	Complementary ecosystem health assessment

3.5. Evidence Mapping of Research Themes

Analysis of the 56 included studies revealed four dominant research themes: (1) contamination characterization and spatial distribution; (2) ecological and human health risk assessment; (3) environmental assessment methodology and validation; and (4) remediation and ecological restoration approaches.

Contamination characterization was the most prevalent theme, addressed in 45 studies (80.4%), with all studies reporting elevated concentrations of Pb, Zn, and Cd that exceeded national or international regulatory thresholds [111]. Ecological and human health risk assessment was addressed in 38 studies (67.9%) [73,78], with Cd consistently identified as the primary ecological risk driver and Pb as the dominant human health concern, particularly for children through soil ingestion [70,87,112]. Methodological studies validating or comparing assessment approaches appeared in 12 studies (21.4%), including comparisons of pXRF versus ICP-MS [109] and evaluations of different extraction schemes for bioavailability assessment [78]. Remediation-oriented studies, including phytoremediation, electrokinetic remediation, and geophysical contamination mapping, appeared in 14 studies (25.0%) [67,108].

A notable temporal trend was observed: studies published before 2018 predominantly focused on contamination characterization (88%), while post-2018 studies increasingly integrated multiple assessment methods and predictive modeling (61%), reflecting methodological maturation in the field [92].

To provide a quantitative summary of contamination severity, descriptive statistics were calculated for maximum soil Pb concentrations reported across the reviewed studies. Among studies reporting absolute concentration values (n = 32), Pb ranged from 58 to 59,000 mg/kg, with a mean of 9878 mg/kg and a median of 2397 mg/kg. The interquartile range was 503–16,038 mg/kg, reflecting substantial variability across sites. The Pb concentration of 3000 mg/kg reported at the Shymkent slag site [32] exceeds the global median by a factor of 1.3, placing it near the 53rd percentile of reported values globally. While this positions Shymkent within the mid-range of documented slag-contaminated sites, it is important to note that the Shymkent value represents a single published estimate, whereas more extensively studied sites (e.g., Santo Amaro, Brazil: up to 24,962 mg/kg; Upper Silesia, Poland: up to 31,200 mg/kg) have been characterized through multiple independent investigations. These statistics should be interpreted as indicative, as differences

in sampling depth, extraction protocols, and site selection across studies preclude formal meta-analytic pooling.

4. Discussion

This scoping review synthesizes evidence from 56 studies published between 2010 and 2025, mapping the global landscape of environmental assessment methods applied to soils contaminated by Pb–Zn slag and associated smelting activities. To our knowledge, this is the first scoping review to focus specifically on Pb–Zn slag as a source of contamination, to categorize assessment methods used in this context systematically, and to document the absence of Central Asian studies in the global evidence base. The findings reveal significant advances in methodological diversity, a pronounced geographic concentration of research in Asia, and critical knowledge gaps relevant specifically to Central Asia and Kazakhstan.

Figure 7 illustrates the integrated assessment framework.

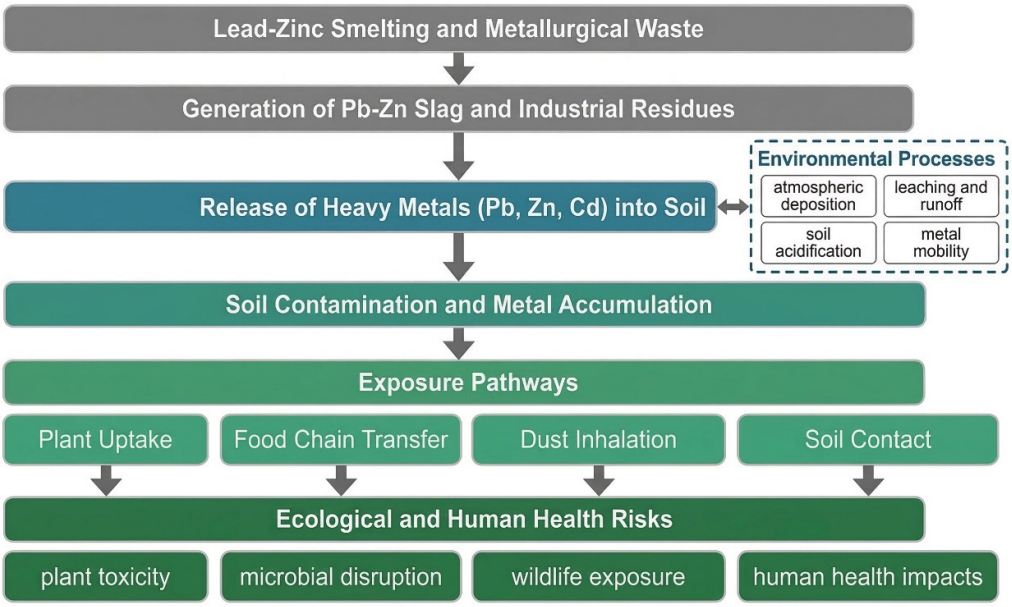


Figure 7. Conceptual framework for integrated environmental assessment of Pb–Zn slag-contaminated soils, illustrating pathways from contamination sources to risk assessment and policy response.

To contextualize contamination severity at the Shymkent site relative to global patterns, Table 4 summarizes the concentration ranges of Pb, Zn, and Cd reported across the most-represented study regions.

Table 4. Comparative heavy metal concentrations (mg/kg) at Pb–Zn slag and smelter sites across key study regions.

Region	Metal	Range (mg/kg)	Mean (mg/kg)	*n* Values	Regulatory Limit (mg/kg)
China	Pb	4–10,564	2968	11	400 (GB 36600) [113]
	Zn	152–41,833	9496	7	2000 (GB 36600)
	Cd	0.2–180	49.8	10	20 (GB 36600)
Poland	Pb	454–31,200	10,751	3	600 (Polish Reg.) [114]
	Zn	1037–11,800	4679	3	2000
	Cd	12.9–15.0	13.9	2	15
Brazil	Pb	17,862–37,460	26,761	3	300 (CONAMA 420) [115]
	Zn	8572–95,940	55,532	3	2000
	Cd	335–454	394.5	2	3

Table 4. *Cont.*

Region	Metal	Range (mg/kg)	Mean (mg/kg)	*n* Values	Regulatory Limit (mg/kg)
France	Pb	1050–5840	2647	3	300 (French std.) [116]
	Zn	1390–34,800	14,185	4	-
	Cd	20–202	80.7	3	-
Shymkent, Kazakhstan [32]	Pb	3000	-	1	32 (KZ MPC)

Note: Concentration ranges represent maximum values reported in individual studies within each region, extracted from study Abstracts section and Section 3 via Elicit (https://elicit.com/, accessed on 7 April 2026). Not all included studies reported absolute concentration values; *n* = number of studies with extractable numeric data per region. Regulatory limits: China—GB 36600-2018 (screening values, industrial land); Poland—Regulation of the Minister of Environment (2016); Brazil—CONAMA Resolution 420/2009; Kazakhstan—MPC for residential soils. Zn and Cd data for Shymkent are not available in the peer-reviewed literature.

4.1. Research Trends in Soil Contamination from Pb–Zn Slag

The marked increase in publications after 2018, with 41 of 56 studies (73.2%) published in this period, reflects growing global regulatory pressure and scientific concern over the environmental legacy of metallurgical waste [117]. Early studies predominantly focused on basic characterization of total heavy metal concentrations, whereas post-2018 research increasingly integrates multi-method frameworks combining spatial analysis, probabilistic risk modeling, and microbial assessment [53,118]. This methodological maturation aligns with international recognition that single-method approaches are insufficient to capture the dynamic, spatially heterogeneous nature of slag-derived contamination [119]. Unlike previous reviews that have examined heavy metal contamination broadly in the vicinity of smelters [53], this review is the first to isolate Pb–Zn slag as the specific contamination source and to provide a structured method-by-method evidence map across geographic contexts. The distinct geochemical properties of Pb justify the slag-specific focus–Zn slag—including high residual metal content (1–5% Pb, 10–30% Zn), alkaline pH buffering capacity, and long-term weathering behavior—which differentiate it from other metallurgical wastes such as copper slag or steelmaking slag and necessitate tailored assessment approaches [14,17].

The dominance of China in the literature (*n* = 20, 35.7%) reflects the country's position as the world's largest lead and zinc producer, with extensive documented contamination around smelting complexes in Hunan, Yunnan, and Guizhou [116], and in Henan [62,65,120]. European contributions, primarily from Poland and legacy sites in the Linares district of Spain [121], emphasize long-term historical contamination and remediation challenges [122]. The near-complete absence of studies from Central Asia, and Kazakhstan in particular, represents a critical evidence gap given the scale of Pb–Zn smelting operations in the Shymkent region, one of the largest in the former Soviet Union [105,123].

The quantitative data compiled in Table 4 enable a direct comparison: the soil Pb level of 3000 mg/kg documented at Shymkent [32] exceeds the global median Pb concentration reported across the reviewed slag sites (2397 mg/kg, *n* = 32) by a factor of 1.3. While this value falls below the extreme contamination levels documented at the Santo Amaro smelter in Brazil (up to 37,460 mg/kg) and historical Pb–Zn mining districts in Upper Silesia, Poland (up to 31,200 mg/kg), it substantially exceeds the mean Pb concentration reported across Chinese study sites (2968 mg/kg, *n* = 11), which represent the most extensively studied context in the global literature. The absence of any systematic environmental assessment at a site with this level of contamination—contrasted with decades of published research at comparably affected sites in China, Europe, and Brazil—underscores the urgency of the Central Asian research gap identified in this review.

4.2. Advances in Environmental Assessment Methods

The diversity of assessment methods identified across 56 studies reflects substantial progress in the field. Pollution indices, including the Single Factor Pollution Index, Nemerow Synthetic Pollution Index, and Geoaccumulation Index, were the most widely used tools (73.2%), providing standardized, comparable measures of contamination severity relative to background values [51,54,106,124,125]. Their widespread adoption across national regulatory contexts—including Chinese GB standards, US EPA thresholds, and European ANZECC guidelines—underscores their utility as universal screening tools. However, direct cross-study comparisons remain limited by differences in reference values [107,126].

Ecological risk assessment using the Potential Ecological Risk Index [85,127] was applied in 67.9% of studies, identifying cadmium as the primary ecological risk driver in most, attributable to its high toxicity response coefficient (Tr = 30) within the Hakanson [59] framework [66]. This finding should be interpreted with the caveat that the Hakanson [59] coefficients assign Cd a weight 30 times that of Zn and 6 times that of Pb, which may overestimate the relative ecological risk of Cd at sites where Pb concentrations exceed background values by a greater magnitude [85]. This finding has particular implications for slag-contaminated sites, where Cd co-occurs with Pb and Zn as a product of polymetallic ore processing and exhibits high mobility under acidic soil conditions [128,129].

Human health risk assessment following US EPA guidelines was conducted in 51.8% of studies, with children consistently identified as the most vulnerable population group due to higher rates of soil ingestion and developing physiological systems [130]. The adoption of Monte Carlo [66] simulation for probabilistic risk assessment in 10.7% of studies represents a methodological advance over deterministic approaches, providing uncertainty quantification essential for evidence-based remediation planning [131,132].

Geospatial methods, including GIS-based kriging interpolation and source apportionment models (PMF, PCA), were applied in over 50% of studies, enabling spatial visualization of contamination gradients and quantitative differentiation of anthropogenic versus geogenic metal sources [133]. The integration of portable XRF for rapid field screening, validated against ICP-MS [134] in multiple studies, demonstrates the potential for cost-effective, large-scale soil surveys in resource-limited settings [109].

Emerging approaches, including predictive transport modeling (Hydrus-1D version 4.xx (PC-Progress, Prague, Czech Republic)), multisurface geochemical modeling, lead isotope tracing, and biological assessment methods (16S rRNA microbial analysis, PICT ecotoxicology, enzymatic biomarkers), appeared in a smaller proportion of studies but represent important methodological frontiers [110]. Their limited application in slag-specific contexts highlights opportunities for methodological transfer from adjacent fields.

4.3. Research Gaps and Future Directions

Several critical research gaps emerge from this review. First, the absence of studies from Kazakhstan and Central Asia represents the most geographically significant gap. The Shymkent lead plant, one of the largest in Central Asia, has operated for decades, generating substantial slag deposits. However, no peer-reviewed environmental assessment studies meeting international methodological standards were identified [135]. This gap is particularly concerning given documented soil lead concentrations exceeding 3000 mg/kg near the plant—more than 900 times the maximum permissible concentration—and documented health impacts on local populations [136].

Second, predictive modeling approaches remain underrepresented in the slag-specific literature. Only four studies (7.1%) employed transport or fate models to forecast metal migration under varying environmental conditions, such as acid rain, climate variability, or land-use change [137,138]. This underrepresentation likely reflects several interrelated

factors: (i) high parameterization requirements—models such as Hydrus-1D version 4.xx (PC-Progress, Prague, Czech Republic) demand detailed site-specific data on soil hydraulic properties, metal speciation coefficients, and boundary conditions that are rarely available at slag sites and expensive to obtain [99]; (ii) geochemical complexity—Pb–Zn slag involves simultaneous dissolution of multiple mineral phases (e.g., willemite, anglesite, smithsonite) under variable pH and redox conditions, complicating model calibration beyond standard single-metal transport scenarios [14,17]; and (iii) disciplinary tradition—the heavy metal contamination literature has been dominated by empirical field-based research approaches, with predictive modeling more commonly applied in hydrogeology and contaminant transport fields than in soil science and environmental geochemistry [138]. Future research should address this gap through three specific directions. First, coupled reactive transport models that integrate slag dissolution kinetics with metal sorption and precipitation processes should be developed and validated at field-scale Pb–Zn slag sites, building on existing Hydrus-1D version 4.xx (PC-Progress, Prague, Czech Republic) applications [99]. Second, machine learning approaches, which have shown promise for predicting heavy metal migration under acid rain conditions [137], could provide computationally efficient alternatives to process-based models, particularly for sites where detailed geochemical parameterization is unavailable. Third, climate-scenario modeling is urgently needed for Central Asian slag sites, where projected increases in extreme precipitation events and temperature fluctuations are expected to accelerate slag weathering and metal leaching [35,36], yet no predictive assessments have been conducted. The semi-arid climate of southern Kazakhstan, characterized by low annual precipitation (300–400 mm), high evapotranspiration rates, and frequent dust storms, creates distinct metal transport dynamics that differ fundamentally from those under the humid conditions in which most existing Hydrus-1D version 4.xx (PC-Progress, Prague, Czech Republic) applications have been validated [35,36]. In arid environments, limited vertical leaching is offset by lateral dust-driven dispersal, surface runoff concentration during rare but intense precipitation events, and capillary rise of metal-laden solutions during dry periods. These processes require adapted parameterization of predictive models that incorporate wind erosion modules and episodic recharge functions, which are not typically included in standard Hydrus-1D version 4.xx (PC-Progress, Prague, Czech Republic) configurations. The application of such climate-adapted predictive modeling is therefore not merely desirable but essential for accurate risk forecasting at Central Asian slag sites.

Third, standardized multi-method assessment frameworks are lacking. The heterogeneity of methods, reference values, and reporting standards across studies severely limits cross-site comparability and policy translation [139]. Development of internationally harmonized protocols for slag-contaminated site assessment, analogous to existing frameworks for mine tailings, is warranted.

Fourth, biological and ecotoxicological assessment methods—including microbial community analysis, phytotoxicity bioassays, and enzymatic biomarkers—remain underutilized relative to chemical methods. These approaches provide integrative measures of ecosystem health that chemical indices alone cannot capture [140,141].

The identified research priorities are summarized in Figure 8. Figure 8 organizes the identified research gaps into a priority hierarchy. At the foundational level, the complete absence of peer-reviewed environmental assessments from Central Asia represents the most urgent gap, as it precludes any evidence-based environmental management at one of the region's most contaminated industrial sites. The intermediate level highlights methodological gaps—specifically, the underrepresentation of predictive transport modeling and biological assessment methods—that limit the capacity for forward-looking risk management. At the apex, the lack of internationally standardized assessment protocols for slag-contaminated

sites impedes cross-jurisdictional comparability and policy harmonization. This hierarchical framing suggests that research investments should prioritize foundational geographic gaps before addressing higher-order methodological and standardization challenges.

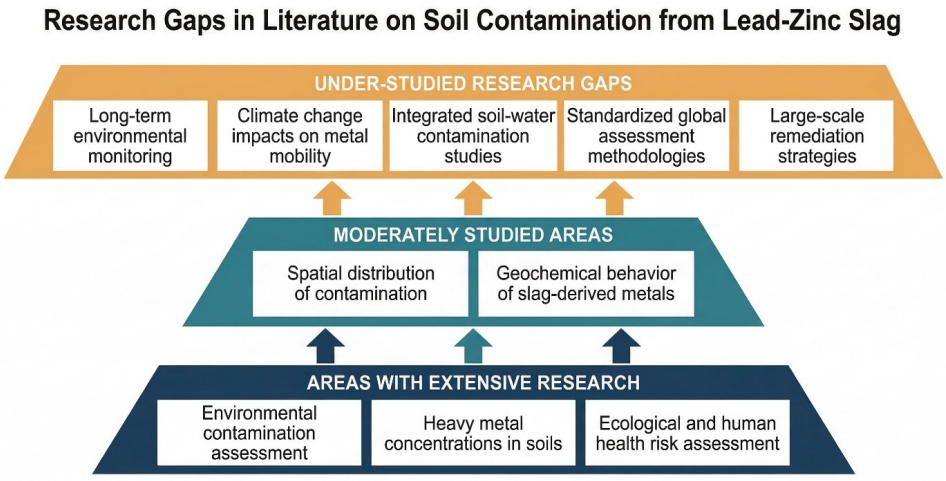


Figure 8. Research gaps pyramid for soil contamination assessment at Pb–Zn slag sites, organized by priority level from foundational geographic gaps to methodological and standardization priorities.

4.4. Relevance to Kazakhstan and Central Asia

The findings of this review have direct implications for environmental management in Kazakhstan. The Shymkent region hosts one of Central Asia's largest Pb–Zn smelting complexes, with slag deposits accumulated over several decades of intensive industrial activity [142]. However, the methodological toolkit used globally—including GIS-based spatial risk mapping, PMF source apportionment, US EPA health risk frameworks, and predictive transport modeling—has not been applied systematically in this context.

The geographic bias toward Chinese and European study sites, while reflecting genuine disparities in research capacity, also suggests that established assessment methods developed in these contexts may require adaptation to the specific soil types, climate conditions, and regulatory frameworks of Kazakhstan and Central Asia. The semi-arid climate of the Shymkent region, for example, differs substantially from the humid subtropical conditions prevalent in Chinese study sites [143–145], potentially affecting metal mobility, bioavailability, and remediation efficacy in ways not captured by existing models [146].

4.5. Limitations of the Review

This review has several limitations that should be acknowledged. The literature search was restricted to three databases—Dimensions, PubMed, and OpenAlex—which, while complementary, may have excluded relevant studies indexed in Russian-language databases such as eLIBRARY.ru (https://elibrary.ru/, accessed on 10 April 2026) or regional Central Asian repositories or regional Central Asian repositories. Although Dimensions and OpenAlex have demonstrated comparable bibliometric coverage to Scopus and Web of Science [56,57], excluding these two databases is a limitation, and future reviews should incorporate them to ensure comprehensive retrieval. This limitation is particularly relevant given the research gap identified in Kazakhstan, where substantial technical literature may exist in Russian but was not captured by the English-language search strategy employed.

The screening and data extraction process was conducted by a single reviewer, which introduces the possibility of selection bias despite the use of predefined eligibility criteria. Additionally, reliance on abstract-level assessment in studies without accessible full texts may have led to misclassification of borderline cases. Future reviews should employ dual-

reviewer screening and explicitly search Russian-language databases to improve coverage of Central Asian literature.

Although a basic methodological quality appraisal was conducted (Section 2.6), it does not constitute a formal risk-of-bias assessment as defined for systematic reviews. The appraisal criteria were adapted from general environmental research quality principles rather than a validated quality assessment tool specific to environmental contamination studies. Development of standardized quality appraisal instruments for environmental assessment studies remains a need in the field.

Additionally, bibliometric co-occurrence analysis (e.g., using VOSviewer version 1.6.20 (Leiden University, Leiden, The Netherlands)) was not conducted in this review, as the primary objective was evidence mapping of assessment methods rather than bibliometric network visualization. A keyword co-occurrence analysis linking terms such as "lead-zinc slag," "human health risk," and "Kazakhstan" would provide valuable insight into thematic clusters and emerging research fronts, and is recommended as a complementary analysis in future studies.

Regarding future research priorities, three directions emerge as most pressing from the evidence synthesized in this review. First, standardized protocols for environmental assessment specifically applicable to Pb–Zn slag-contaminated soils should be developed at the international level to enable cross-site comparability. Second, longitudinal monitoring of Pb, Zn, and Cd migration under arid and semi-arid conditions representative of Central Asia is critically needed, as dust-driven dispersal pathways remain poorly characterized in the global literature. Third, Kazakhstan-specific soil quality standards for slag-contaminated sites should be established, adapting international frameworks (e.g., Chinese GB 36600-2018, US EPA RSL) to regional geochemical and regulatory contexts.

4.6. Policy Implications

The findings of this scoping review carry several practical implications for environmental policy and governance, particularly in Kazakhstan and Central Asia. First, the documented absence of peer-reviewed environmental assessments for the Shymkent slag-contaminated area underscores the urgent need for nationally mandated baseline monitoring programs aligned with international standards. Regulatory authorities in Kazakhstan should prioritize developing soil quality standards specifically applicable to metallurgical slag sites, drawing on the Chinese GB 36600-2018 and European ANZECC frameworks identified in the included studies.

Second, the methodological diversity documented in this review suggests that a tiered assessment approach would be most appropriate for resource-limited Central Asian settings. Rapid screening using portable XRF, followed by confirmatory ICP-MS analysis and GIS-based spatial risk mapping, represents a cost-effective and internationally validated pathway for initial site characterization [147–149]. This approach has been successfully deployed in comparable industrial contexts in China, Poland, and Brazil [148,150,151].

Third, the consistent identification of children as the highest-risk population, absorbing significantly more lead than adults [152], across human health risk assessments reinforces the need for targeted public health interventions near slag-contaminated sites, including blood lead level surveillance programs [153] and restrictions on agricultural land use within defined contamination radii. Such measures are directly supported by the evidence synthesized in this review and align with WHO guidelines for preventing lead exposure, which recommend identifying and eliminating sources of exposure [154].

Specifically, the PMF (Positive Matrix Factorization) source apportionment model, identified as one of the most effective tools for distinguishing industrial from natural pollution sources (Section 3.4.4), should be prioritized by Kazakhstani environmental

agencies to quantify the relative contribution of the Shymkent lead plant versus natural geogenic background to current soil contamination levels. This distinction is critical for establishing legal liability and allocating remediation costs between the state and industrial operators. Furthermore, predictive transport models such as Hydrus-1D version 4.xx (PC-Progress, Prague, Czech Republic) should be applied to forecast long-term metal migration under the semi-arid climatic conditions specific to southern Kazakhstan, enabling proactive rather than reactive contamination management. The adoption of GIS-based spatial risk mapping would enable regulatory authorities to delineate exclusion zones around slag deposits and to establish evidence-based land-use restrictions, particularly for residential and agricultural development, within contamination radii identified through kriging interpolation.

Finally, the review highlights the importance of integrating environmental assessment data into remediation planning and land-use decision-making. Policymakers should require comprehensive multi-method environmental assessments—encompassing chemical, spatial, and biological indicators—to be completed prior to any residential, agricultural, or industrial development on or adjacent to former smelting sites.

5. Conclusions

This scoping review systematically mapped the global evidence base on soil contamination from Pb–Zn slag and associated smelting activities, identifying 56 peer-reviewed studies published between 2010 and 2025 that employed environmental assessment methods relevant to this context. The findings address three core objectives: characterizing the scope of contamination, mapping assessment methodologies, and identifying research gaps with particular relevance to Kazakhstan and Central Asia.

The review confirms that Pb–Zn slag and smelter emissions are persistent and widespread sources of soil contamination, with elevated concentrations of Pb, Zn, Cd, and As that consistently exceed national and international regulatory thresholds across all study regions. Cadmium was identified as the primary ecological risk driver in the majority of reviewed studies, largely attributable to its high toxicity response coefficient (Tr = 30) in the widely used Hakanson [59] framework and its elevated mobility under acidic soil conditions. However, this finding is partly dependent on the toxicity coefficient system employed, and site-specific risk rankings may vary when alternative weighting schemes are applied [85]. At the same time, lead posed the greatest human health risk, particularly for children, through soil ingestion. These findings align with global assessments of the hazards posed by metallurgical waste and underscore the urgency of systematic environmental monitoring at Pb–Zn slag-contaminated sites [155].

The methodological landscape has diversified substantially over the review period. Pollution indices, ecological risk assessment, human health risk frameworks, and GIS-based spatial analysis constitute the dominant assessment toolkit, applied in 50–73% of included studies. The increasing integration of source apportionment models (PMF, PCA), probabilistic risk assessment (Monte Carlo simulation) [66,156], and predictive transport modeling (Hydrus-1D version 4.xx (PC-Progress, Prague, Czech Republic)) reflects a maturation toward more holistic, policy-relevant assessment frameworks [157]. Emerging biological assessment methods—including microbial community analysis, phytotoxicity bioassays, and enzymatic biomarkers—complement chemical approaches by providing integrative measures of ecosystem health that indices alone cannot capture [140,158].

Despite this progress, three critical gaps were identified. First, Central Asia and Kazakhstan are absent from the peer-reviewed literature, despite hosting one of the region's largest Pb–Zn smelting complexes in Shymkent, with documented soil lead concentrations that exceed regulatory limits by orders of magnitude [52,105]. This represents both a sci-

entific gap and a public health concern requiring immediate attention. Second, predictive modeling of metal transport and fate under varying environmental conditions remains underrepresented in slag-specific contexts, limiting the capacity for evidence-based remediation planning and climate change adaptation. Third, the absence of standardized international protocols for slag-contaminated site assessment impedes cross-study comparability and policy translation across jurisdictions [117,159].

These findings carry direct implications for environmental governance in Kazakhstan. The methodological frameworks documented in this review—spanning spatial risk mapping, probabilistic health assessment, isotope-based source tracing, and biological monitoring—provide a validated toolkit that can be systematically applied to Pb–Zn contaminated sites in the Shymkent region. Future research should prioritize: (1) baseline environmental assessment of slag-contaminated soils in Kazakhstan using internationally standardized methods; (2) development of predictive models calibrated to the semi-arid climatic conditions of Central Asia; (3) integration of Russian-language literature and regional databases to capture existing but inaccessible evidence; and (4) establishment of long-term monitoring programs to track metal mobility and ecosystem recovery over time.

This scoping review provides a structured evidence map that can guide researchers, environmental managers, and policymakers in designing comprehensive assessment programs for Pb–Zn slag-contaminated sites, with particular relevance to the underserved Central Asian context.

Supplementary Materials: The following supporting information can be downloaded at: https://www.mdpi.com/article/10.3390/su18083934/s1, Table S1: PRISMA-ScR 2018 Checklist; Table S2: Full Data Extraction from Included Studies (n = 56).

Author Contributions: Conceptualization, Z.P. and A.A.; methodology, A.A.; investigation, Z.P. and A.A.; writing—original draft preparation, Z.P. and A.A.; writing—review and editing, A.A. All authors have read and agreed to the published version of the manuscript.

Funding: This research was funded by the Science Committee of the Ministry of Science and Higher Education of the Republic of Kazakhstan, grant number AP25795537.

Institutional Review Board Statement: Not applicable.

Informed Consent Statement: Not applicable.

Data Availability Statement: The data supporting the findings of this study are available from the corresponding author upon reasonable request.

Acknowledgments: The authors used AI-assisted tools during the preparation of this manuscript for the following purposes: (1) language editing and grammar checking of the manuscript text using Claude (claude-3-5-sonnet, Anthropic, San Francisco, CA, USA); (2) literature organisation and data extraction support using Elicit (Elicit PBC, San Francisco, CA, USA); (3) graphical abstract creation using Napkin AI (Napkin AI Inc., San Francisco, CA, USA). All AI-generated content was reviewed, verified, and edited by the authors. The authors take full responsibility for the accuracy and integrity of the submitted manuscript. No AI tool was used for data analysis, interpretation of results, or drawing scientific conclusions.

Conflicts of Interest: The authors declare no conflicts of interest.

References

1. Shomanova, Z.; Nossenko, Y.; Yerkibayeva, M.; Yessimova, D.; Kuspanova, A.; Aldasheva, A.; Kaimuldinova, K.; Safarov, R. Environmental Risk Assessment for Sustainable Industrial Urban Development: The Case of Northern Industrial Zone of Pavlodar, Kazakhstan. *PLoS ONE* **2025**, *20*, e0320835. [CrossRef]
2. Li, H.; Cui, X.; Sun, Y.; Zheng, P.; Wang, L.; Shi, X. Advances in Microbial Remediation of Heavy Metal-Contaminated Soils: Mechanisms, Synergistic Technologies, Field Applications and Future Perspectives. *Toxics* **2025**, *13*, 1069. [CrossRef]

3. Hou, D.; Jia, X.; Wang, L.; McGrath, S.P.; Zhu, Y.-G.; Hu, Q.; Zhao, F.-J.; Bank, M.S.; O'Connor, D.; Nriagu, J. Global Soil Pollution by Toxic Metals Threatens Agriculture and Human Health. *Science* **2025**, *388*, 316–321. [CrossRef] [PubMed]
4. Almotairy, H. Heavy Metal Contamination in Soil: Implications for Crop Resilience and Abiotic Stress Management. In *Abiotic Stress in Crop Plants—Ecophysiological Responses and Molecular Approaches*; Hasanuzzaman, M., Nahar, K., Eds.; IntechOpen: London, UK, 2024; ISBN 978-0-85014-006-4.
5. Gasparatos, D. Soil Contamination by Heavy Metals and Metalloids. *Environments* **2022**, *9*, 32. [CrossRef]
6. Machowski, R.; Rzetala, M.A.; Rzetala, M.; Solarski, M. Anthropogenic Enrichment of the Chemical Composition of Bottom Sediments of Water Bodies in the Neighborhood of a Non-Ferrous Metal Smelter (Silesian Upland, Southern Poland). *Sci. Rep.* **2019**, *9*, 14445. [CrossRef]
7. Azizi, M.; Faz, A.; Zornoza, R.; Martinez-Martinez, S.; Acosta, J.A. Phytoremediation Potential of Native Plant Species in Mine Soils Polluted by Metal(Loid)s and Rare Earth Elements. *Plants* **2023**, *12*, 1219. [CrossRef]
8. Nadłonek, W.; Cabała, J.; Szopa, K. Potentially Harmful Elements (As, Sb, Cd, Pb) in Soil Polluted by Historical Smelting Operation in the Upper Silesian Area (Southern Poland). *Minerals* **2024**, *14*, 475. [CrossRef]
9. Zhou, Z.; Peng, C.; Liu, X.; Jiang, Z.; Guo, Z.; Xiao, X. Pollution and Risk Assessments of Heavy Metal(Loid)s in the Soil around Lead-Zinc Smelteries via Data Integration Analysis. *Int. J. Environ. Res. Public Health* **2022**, *19*, 9698. [CrossRef] [PubMed]
10. Peng, Y.; Yang, R.; Jin, T.; Chen, J.; Zhang, J. Potentially Toxic Metal(Loid) Distribution and Migration in the Bottom Weathering Profile of Indigenous Zinc Smelting Slag Pile in Clastic Rock Region. *PeerJ* **2021**, *9*, e10825. [CrossRef] [PubMed]
11. Li, S.; Bi, X.; Li, Z.; Wang, H.; Li, X.; Feng, X.; Sun, G.; Chen, J.; Meng, B. Heavy Metal(Loid)s Contamination in Ground Dust and Associated Health Risks at a Former Indigenous Zinc Smelting Area. *Int. J. Environ. Res. Public Health* **2021**, *18*, 893. [CrossRef]
12. Cao, C.; Wang, L.; Li, H.; Wei, B.; Yang, L. Temporal Variation and Ecological Risk Assessment of Metals in Soil Nearby a Pb–Zn Mine in Southern China. *Int. J. Environ. Res. Public Health* **2018**, *15*, 940. [CrossRef] [PubMed]
13. Nowińska, K.; Kokowska-Pawłowska, M. Mineralogy of Zinc and Lead Metallurgical Slags in Terms of Their Impact on the Environment: A Review. *Minerals* **2024**, *14*, 852. [CrossRef]
14. Da Silva, J.A.G.F.; De Freitas, A.D.S.; Da Silva, V.S.G.; De Rosália E Silva Santos, C.E.; Fernandes Júnior, P.I.; De Melo, A.F.; Dos Santos Souza, P.A.; De Oliveira, A.S.; Dos Santos, N.M.; Do Nascimento, C.W.A. Assessing the Phytoextraction of Cd, Pb, and Zn from a Slag-Contaminated Soil by Legume Species Inoculated with Rhizobial Strains. *Environ. Process.* **2024**, *11*, 55. [CrossRef]
15. Saikia, N.; Borah, R.R.; Konwar, K.; Vandecastelee, C. pH Dependent Leachings of Some Trace Metals and Metalloid Species from Lead Smelter Slag and Their Fate in Natural Geochemical Environment. *Groundw. Sustain. Dev.* **2018**, *7*, 348–358. [CrossRef]
16. Rocchi, I.; Potysz, A.; Masotta, M.; Rocchi, S. Experimental Weathering of Historical Slags Exposed to Rhizosphere-like Organic Acids and Various pH Conditions. *J. Geochem. Explor.* **2022**, *243*, 107109. [CrossRef]
17. Pecina, V.; Juřička, D.; Hedbávný, J.; Klimánek, M.; Kynický, J.; Brtnický, M.; Komendová, R. The Impacts of Mining on Soil Pollution with Metal(Loid)s in Resource-Rich Mongolia. *Sci. Rep.* **2023**, *13*, 2763. [CrossRef]
18. Sasaki, T.; Horiguchi, H.; Matsukawa, T.; Kobayashi, M.; Omori, Y.; Oguma, E.; Komatsuda, A. A Suspected Case of "Itai-Itai Disease" in a Cadmium-Polluted Area in Akita Prefecture, Japan. *Environ. Health Prev. Med.* **2024**, *29*, 40. [CrossRef]
19. Csavina, J.; Field, J.; Taylor, M.P.; Gao, S.; Landázuri, A.; Betterton, E.A.; Sáez, A.E. A Review on the Importance of Metals and Metalloids in Atmospheric Dust and Aerosol from Mining Operations. *Sci. Total Environ.* **2012**, *433*, 58–73. [CrossRef] [PubMed]
20. Rajput, P.; Singh, A.; Agrawal, S.; Ghazaryan, K.; Rajput, V.D.; Movsesyan, H.; Mandzhieva, S.; Minkina, T.; Alexiou, A. Effects of Environmental Metal and Metalloid Pollutants on Plants and Human Health: Exploring Nano-Remediation Approach. *Stress Biol.* **2024**, *4*, 27. [CrossRef] [PubMed]
21. Yadav, K.; Kumar, D.; Gupta, A.K.; Gupta, B.; Tyagi, P.; Sharma, A.; Patra, P.K.; Patra, P.K.; Chaitanya, A.K. Heavy Metals Contamination and Their Phytoremediation in Soil and Water for Sustainable Environmental Restoration. *Discov. Environ.* **2025**, *3*, 201. [CrossRef]
22. Zhou, M.; Zheng, S. Multi-Omics Uncover the Mechanism of Wheat under Heavy Metal Stress. *Int. J. Mol. Sci.* **2022**, *23*, 15968. [CrossRef]
23. Rani, N.; Chauhan, A.; Sagar, N.A.; Kumar, V. Microbe-Mediated Regulation in Zinc-Contaminated Soils: The Synergistic Role of Hyperaccumulator Plants and Zinc-Tolerant Rhizobacteria. *Front. Agron.* **2025**, *7*, 1597149. [CrossRef]
24. DeLuca, N.M.; Angrish, M.; Wilkins, A.; Thayer, K.; Cohen Hubal, E.A. Human Exposure Pathways to Poly- and Perfluoroalkyl Substances (PFAS) from Indoor Media: A Systematic Review Protocol. *Environ. Int.* **2021**, *146*, 106308. [CrossRef]
25. Laidlaw, M.A.S.; Filippelli, G.M.; Brown, S.; Paz-Ferreiro, J.; Reichman, S.M.; Netherway, P.; Truskewycz, A.; Ball, A.S.; Mielke, H.W. Case Studies and Evidence-Based Approaches to Addressing Urban Soil Lead Contamination. *Appl. Geochem.* **2017**, *83*, 14–30. [CrossRef]
26. Kabata-Pendias, A.; Szteke, B. *Trace Elements in Abiotic and Biotic Environments*, 1st ed.; CRC Press: Boca Raton, FL, USA, 2015; ISBN 978-0-429-16151-3.
27. Satarug, S.; Gobe, G.C.; Vesey, D.A. Cadmium and Lead Exposure, Nephrotoxicity, and Mortality. *Toxics* **2020**, *8*, 86. [CrossRef]

28. Li, B.; Deng, J.; Li, Z.; Chen, J.; Zhan, F.; He, Y.; He, L.; Li, Y. Contamination and Health Risk Assessment of Heavy Metals in Soil and Ditch Sediments in Long-Term Mine Wastes Area. *Toxics* **2022**, *10*, 607. [CrossRef]
29. Nakata, H.; Nakayama, S.M.M.; Yabe, J.; Muzandu, K.; Kataba, A.; Ikenaka, Y.; Ishizuka, M. Interdisciplinary Approach to Addressing Lead Pollution Caused by Mining Activity in Kabwe, The Republic of Zambia. *Environ. Monit. Contam. Res.* **2022**, *2*, 94–111. [CrossRef]
30. Kříbek, B.; Nyambe, I.; Majer, V.; Knésl, I.; Mihaljevič, M.; Ettler, V.; Vaněk, A.; Penížek, V.; Sracek, O. Soil Contamination near the Kabwe Pb-Zn Smelter in Zambia: Environmental Impacts and Remediation Measures Proposal. *J. Geochem. Explor.* **2019**, *197*, 159–173. [CrossRef]
31. Chen, M.; Gazze, L.; DiTraglia, F.J.; Das, R.; Nriagu, J.; Erel, Y.; Boyle, E.A.; Taylor, C.M.; Weiss, D. Environmental Lead Risk in the 21st Century. *Commun. Earth Environ.* **2025**, *6*, 776. [CrossRef] [PubMed]
32. Salim, Y.; Issayeva, A.; Kidirbayeva, K.; Zhumadulayeva, A.I.; Dossybayeva, G.; Bozhbanbayeva, N.; Ashirbayeva, S. Influence of Lead-Zinc Slags of the Shymkent City on the Environment. *J. Ecol. Eng.* **2022**, *23*, 83–89. [CrossRef]
33. Yun, S.-W.; Baveye, P.C.; Kim, D.-H.; Kang, D.-H.; Lee, S.-Y.; Kong, M.-J.; Park, C.-G.; Kim, H.-D.; Son, J.; Yu, C. Analysis of Metal(Loid)s Contamination and Their Continuous Input in Soils around a Zinc Smelter: Development of Methodology and a Case Study in South Korea. *Environ. Pollut.* **2018**, *238*, 140–149. [CrossRef]
34. *ISO 17294-2:2016*; Water Quality—Application of Inductively Coupled Plasma Mass Spectrometry (ICP-MS)—Part 2: Determination of Selected Elements Including Uranium Isotopes. International Organization for Standardization: Geneva, Switzerland, 2016.
35. Riley, A.L.; Cameron, J.; Burke, I.T.; Onnis, P.; MacDonald, J.M.; Gandy, C.J.; Crane, R.A.; Byrne, P.; Comber, S.; Jarvis, A.P.; et al. Environmental Behaviour of Iron and Steel Slags in Coastal Settings. *Environ. Sci. Pollut. Res.* **2024**, *31*, 42428–42444. [CrossRef] [PubMed]
36. Visser, A.; Kroes, J.; Van Vliet, M.T.H.; Blenkinsop, S.; Fowler, H.J.; Broers, H.P. Climate Change Impacts on the Leaching of a Heavy Metal Contamination in a Small Lowland Catchment. *J. Contam. Hydrol.* **2012**, *127*, 47–64. [CrossRef]
37. Paltseva, A.A.; Neaman, A. An Emerging Frontier: Metal(Loid) Soil Pollution Threat Under Global Climate Change. *Environ. Toxicol. Chem.* **2020**, *39*, 1653–1654. [CrossRef]
38. Xiong, J.; Li, W.; Zhang, H.; Cheng, W.; Ye, C.; Zhao, Y. Selected Environmental Assessment Model and Spatial Analysis Method to Explain Correlations in Environmental and Socio-Economic Data with Possible Application for Explaining the State of the Ecosystem. *Sustainability* **2019**, *11*, 4781. [CrossRef]
39. Chen, L.; Mao, Y.; Zhao, R. GIS Application in Environmental Monitoring and Risk Assessment. In Proceedings of the 2022 3rd International Conference on Geology, Mapping and Remote Sensing (ICGMRS), Zhoushan, China, 22–24 April 2022; pp. 908–917.
40. Kross, A.; Kaur, G.; Jaeger, J.A.G. A Geospatial Framework for the Assessment and Monitoring of Environmental Impacts of Agriculture. *Environ. Impact Assess. Rev.* **2022**, *97*, 106851. [CrossRef]
41. Agnello, A.C.; Potysz, A.; Fourdrin, C.; Huguenot, D.; Chauhan, P.S. Impact of Pyrometallurgical Slags on Sunflower Growth, Metal Accumulation and Rhizosphere Microbial Communities. *Chemosphere* **2018**, *208*, 626–639. [CrossRef]
42. Rodgers, K.J.; McLellan, I.S.; Cuthbert, S.J.; Hursthouse, A.S. Enhanced Characterisation for the Management of Industrial Steel Processing by Products: Potential of Sequential Chemical Extraction. *Environ. Monit. Assess.* **2019**, *191*, 192. [CrossRef] [PubMed]
43. Li, X.; Liu, L.; Wang, Y.; Luo, G.; Chen, X.; Yang, X.; Gao, B.; He, X. Integrated Assessment of Heavy Metal Contamination in Sediments from a Coastal Industrial Basin, NE China. *PLoS ONE* **2012**, *7*, e39690. [CrossRef]
44. Lin, Y.-P.; Anthony, J.; Mukhtar, H.; Lin, C.-M. A Spatial Prioritization Method for Identifying Potential Eco-Risk Distributions of Heavy Metals in Soil and Birds. *Ecotoxicol. Environ. Saf.* **2021**, *220*, 112383. [CrossRef]
45. Enjavinejad, S.M.; Zahedifar, M.; Moosavi, A.A.; Khosravani, P. Integrated Application of Multiple Indicators and Geographic Information System-Based Approaches for Comprehensive Assessment of Environmental Impacts of Toxic Metals-Contaminated Agricultural Soils and Vegetables. *Sci. Total Environ.* **2024**, *926*, 171747. [CrossRef]
46. Rui, J.; Shabrina, Z.; Gong, W. Artificial Intelligence Applications in Urban Extreme Heat Management: A Systematic Review of Forecasting, Monitoring, Mitigation and Decision Support. *Environ. Impact Assess. Rev.* **2026**, *119*, 108363. [CrossRef]
47. Oldenkamp, R.; Hamers, T.; Wilkinson, J.; Slootweg, J.; Posthuma, L. Regulatory Risk Assessment of Pharmaceuticals in the Environment: Current Practice and Future Priorities. *Environ. Toxicol. Chem.* **2024**, *43*, 611–622. [CrossRef] [PubMed]
48. Senila, M. Metal and Metalloid Monitoring in Water by Passive Sampling—A Review. *Rev. Anal. Chem.* **2023**, *42*, 20230065. [CrossRef]
49. Liu, H.; Chi, L.; Shen, J.; Arandiyan, H.; Wang, Y.; Wang, X. Principles, Applications, and Limitations of Diffusive Gradients in Thin Films Induced Fluxed in Soils and Sediments. *Chemosphere* **2024**, *350*, 141061. [CrossRef]
50. Hedberg, J.; Fransson, K.; Prideaux, S.; Roos, S.; Jönsson, C.; Odnevall Wallinder, I. Improving the Life Cycle Impact Assessment of Metal Ecotoxicity: Importance of Chromium Speciation, Water Chemistry, and Metal Release. *Sustainability* **2019**, *11*, 1655. [CrossRef]

51. Gelly, R.; Fekiacova, Z.; Guihou, A.; Doelsch, E.; Deschamps, P.; Keller, C. Lead, Zinc, and Copper Redistributions in Soils along a Deposition Gradient from Emissions of a Pb-Ag Smelter Decommissioned 100 Years Ago. *Sci. Total Environ.* **2019**, *665*, 502–512. [CrossRef]
52. Baubekova, A.; Akindykova, A.; Mamirova, A.; Dumat, C.; Jurjanz, S. Evaluation of Environmental Contamination by Toxic Trace Elements in Kazakhstan Based on Reviews of Available Scientific Data. *Environ. Sci. Pollut. Res.* **2021**, *28*, 43315–43328. [CrossRef]
53. Han, Y.; Zhang, S.; Kang, D.; Hao, N.; Peng, J.; Zhou, Y.; Liu, K.; Chen, Y. A Decade Review of Human Health Risks from Heavy Metal Contamination in Industrial Sites. *Water Air Soil Pollut.* **2025**, *236*, 144. [CrossRef]
54. Kowalska, J.B.; Mazurek, R.; Gąsiorek, M.; Zaleski, T. Pollution Indices as Useful Tools for the Comprehensive Evaluation of the Degree of Soil Contamination–A Review. *Environ. Geochem. Health* **2018**, *40*, 2395–2420. [CrossRef]
55. Tricco, A.C.; Lillie, E.; Zarin, W.; O'Brien, K.K.; Colquhoun, H.; Levac, D.; Moher, D.; Peters, M.D.J.; Horsley, T.; Weeks, L.; et al. PRISMA Extension for Scoping Reviews (PRISMA-ScR): Checklist and Explanation. *Ann. Intern. Med.* **2018**, *169*, 467–473. [CrossRef]
56. Hook, D.W.; Porter, S.J.; Herzog, C. Dimensions: Building Context for Search and Evaluation. *Front. Res. Metr. Anal.* **2018**, *3*, 23. [CrossRef]
57. Visser, M.; Van Eck, N.J.; Waltman, L. Large-Scale Comparison of Bibliographic Data Sources: Scopus, Web of Science, Dimensions, Crossref, and Microsoft Academic. *Quant. Sci. Stud.* **2021**, *2*, 20–41. [CrossRef]
58. Ouzzani, M.; Hammady, H.; Fedorowicz, Z.; Elmagarmid, A. Rayyan—A Web and Mobile App for Systematic Reviews. *Syst. Rev.* **2016**, *5*, 210. [CrossRef]
59. Hakanson, L. An Ecological Risk Index for Aquatic Pollution Control.a Sedimentological Approach. *Water Res.* **1980**, *14*, 975–1001. [CrossRef]
60. Ge, W.; Gao, F.; Gao, J.; Ding, J.; Han, L.; Wang, J.; Zhang, T.; Li, H.; Yan, Y. The Synergistic Impact of Cadmium and the Wheat Rhizosphere on the Soil Bacterial Community in Alkaline Cropland in Northern China. *J. Soils Sediments* **2025**, *25*, 2420–2434. [CrossRef]
61. Lu, X.; Zhuang, S. Determining Environmental Risk and Source of Heavy Metal(Loid)s in the Surrounding Farmland Soil of a Zinc Smelter in Water Source Area, Northwest China. *Environ. Earth Sci.* **2022**, *81*, 67. [CrossRef]
62. Li, B.; Wang, Y.; Jiang, Y.; Li, G.; Cui, J.; Wang, Y.; Zhang, H.; Wang, S.; Xu, S.; Wang, R. The Accumulation and Health Risk of Heavy Metals in Vegetables around a Zinc Smelter in Northeastern China. *Environ. Sci. Pollut. Res.* **2016**, *23*, 25114–25126. [CrossRef]
63. Li, P.; Lin, C.; Cheng, H.; Duan, X.; Lei, K. Contamination and Health Risks of Soil Heavy Metals around a Lead/Zinc Smelter in Southwestern China. *Ecotoxicol. Environ. Saf.* **2015**, *113*, 391–399. [CrossRef]
64. Chen, Q.; Liu, Y.; Li, W.; Zhao, W.; Li, H.; Huang, Q.; Yang, Y.; Bi, T.; Long, J. Elevated Thallium Enrichment, Source, and Health Risks in Soils Surrounding a Lead–Zinc Smelter, Southwest China. *J. Hazard. Mater. Adv.* **2026**, *21*, 100968. [CrossRef]
65. Yang, L.; Ge, S.; Liu, J.; Iqbal, Y.; Jiang, Y.; Sun, R.; Ruan, X.; Wang, Y. Spatial Distribution and Risk Assessment of Heavy Metal(Oid)s Contamination in Topsoil around a Lead and Zinc Smelter in Henan Province, Central China. *Toxics* **2023**, *11*, 427. [CrossRef]
66. Zhou, Y.; Jiang, D.; Ding, D.; Wu, Y.; Wei, J.; Kong, L.; Long, T.; Fan, T.; Deng, S. Ecological-Health Risks Assessment and Source Apportionment of Heavy Metals in Agricultural Soils around a Super-Sized Lead-Zinc Smelter with a Long Production History, in China. *Environ. Pollut.* **2022**, *307*, 119487. [CrossRef]
67. Rachwał, M.; Wawer, M.; Magiera, T.; Steinnes, E. Integration of Soil Magnetometry and Geochemistry for Assessment of Human Health Risk from Metallurgical Slag Dumps. *Environ. Sci. Pollut. Res.* **2017**, *24*, 26410–26423. [CrossRef]
68. Szatyłowicz, E.; Rozpondek, R.; Rozpondek, K.; Kacprzak, M. Evaluation of Contamination of Zn-Pb Industry Degraded Areas Using Spatial Information. *Inż. Ekol.* **2017**, *18*, 106–113. [CrossRef]
69. Carvalho, F.M.; Tavares, T.M.; Lins, L. Soil Contamination by a Lead Smelter in Brazil in the View of the Local Residents. *Int. J. Environ. Res. Public Health* **2018**, *15*, 2166. [CrossRef]
70. Souza, L.Z.S.; De Andrade Lima, L.R.P. Risk Assessment for the Presence of Potentially Toxic Elements in the Vicinity of a Former Lead Smelter in Bahia, Brazil. *Environ. Earth Sci.* **2021**, *80*, 532. [CrossRef]
71. Akber, M.A.; Rahman, M.A.; Islam, M.A.; Islam, M.A. Potential Ecological Risk of Metal Pollution in Lead Smelter-Contaminated Agricultural Soils in Khulna, Bangladesh. *Environ. Monit. Assess.* **2019**, *191*, 351. [CrossRef] [PubMed]
72. Ray, P.; Datta, S.P.; Dwivedi, B.S. Long-Term Irrigation with Zinc Smelter Effluent Affects Important Soil Properties and Heavy Metal Content in Food Crops and Soil in Rajasthan, India. *Soil Sci. Plant Nutr.* **2017**, *63*, 628–637. [CrossRef]
73. Adventini, N.; Santoso, M.; Lestiani, D.D.; Syahfitri, W.Y.N.; Rixson, L. Lead Identification in Soil Surrounding a Used Lead Acid Battery Smelter Area in Banten, Indonesia. *J. Phys. Conf. Ser.* **2017**, *860*, 012006. [CrossRef]
74. Lestiani, D.D.; Syahfitri, W.Y.N.; Adventini, N.; Kurniawati, S.; Damastuti, E.; Santoso, M.; Biswas, B.; Mukhtar, R. Impacts of a Lead Smelter in East Java, Indonesia: Degree of Contamination, Spatial Distribution, Ecological Risk, and Health Risk Assessment of Potentially Toxic Elements in Soils. *Environ. Monit. Assess.* **2023**, *195*, 1165. [CrossRef]

75. Karachaliou, T.; Protonotarios, V.; Kaliampakos, D.; Menegaki, M. Using Risk Assessment and Management Approaches to Develop Cost-Effective and Sustainable Mine Waste Management Strategies. *Recycling* **2016**, *1*, 328–342. [CrossRef]
76. Douay, F.; Roussel, H.; Fourrier, H.; Heyman, C.; Chateau, G. Investigation of Heavy Metal Concentrations on Urban Soils, Dust and Vegetables Nearby a Former Smelter Site in Mortagne Du Nord, Northern France. *J. Soils Sediments* **2007**, *7*, 143–146. [CrossRef]
77. Pančevski, Z.; Stafilov, T.; Bačeva, K. Distribution of Heavy Metals in Some Vegetables Grown in the Vicinity of Lead And Zinc Smelter Plant. *Contrib. Sect. Nat. Math. Biotech. Sci.* **2017**, *35*, 25–36. [CrossRef]
78. Jafari, Y.; Jones, B.G.; Pacheco, J.C.; Umoru, S. Trace Element Soil Contamination from Smelters in the Illawarra Region, New South Wales, Australia. *Environ. Earth Sci.* **2020**, *79*, 372. [CrossRef]
79. Bérard, A.; Capowiez, L.; Mombo, S.; Schreck, E.; Dumat, C.; Deola, F.; Capowiez, Y. Soil Microbial Respiration and PICT Responses to an Industrial and Historic Lead Pollution: A Field Study. *Environ. Sci. Pollut. Res.* **2016**, *23*, 4271–4281. [CrossRef]
80. Nikolic, B.; Nikolic, S.; Vujacic, V.; Trajkovic, S. Development of the Production of Lead and Precious Metals in Central Asia. *Podzemni Rad.* **2014**, *22*, 73–79. [CrossRef]
81. Sutherland, R.A. Bed Sediment-Associated Trace Metals in an Urban Stream, Oahu, Hawaii. *Environ. Geol.* **2000**, *39*, 611–627. [CrossRef]
82. Shen, F.; Li, Y.; Zhang, M.; Awasthi, M.K.; Ali, A.; Li, R.; Wang, Q.; Zhang, Z. Atmospheric Deposition-Carried Zn and Cd from a Zinc Smelter and Their Effects on Soil Microflora as Revealed by 16S rDNA. *Sci. Rep.* **2016**, *6*, 39148. [CrossRef]
83. Niemeyer, J.C.; Nogueira, M.A.; Carvalho, G.M.; Cohin-De-Pinho, S.J.; Outeiro, U.S.; Rodrigues, G.G.; Da Silva, E.M.; Sousa, J.P. Functional and Structural Parameters to Assess the Ecological Status of a Metal Contaminated Area in the Tropics. *Ecotoxicol. Environ. Saf.* **2012**, *86*, 188–197. [CrossRef]
84. De Andrade Lima, L.R.P.; Bernardez, L.A. Characterization of the Soil Contamination around the Former Primary Lead Smelter at Santo Amaro, Bahia, Brazil. *Environ. Earth Sci.* **2017**, *76*, 470. [CrossRef]
85. Cao, Y.; Wang, R.; Liu, Y.; Li, Y.; Jia, L.; Yang, Q.; Zeng, X.; Li, X.; Wang, Q.; Wang, R.; et al. Improved Calculations of Heavy Metal Toxicity Coefficients for Evaluating Potential Ecological Risk in Sediments Based on Seven Major Chinese Water Systems. *Toxics* **2023**, *11*, 650. [CrossRef]
86. Xu, W.; Meng, K.; Du, W.; Cai, Z.; Li, Y.; Chen, X.; Zhang, Y. Cadmium Dominance in Heavy Metal Pollution: Ecological Risks and Human Health Implications in the Guan River Estuary, China. *Front. Mar. Sci.* **2025**, *12*, 1554838. [CrossRef]
87. Keizer, M.G.; Hooghiemstra-Tielbeek, M.; Haan, F.A.M.D. Contamination of Soil and Street Dust with Lead and Cadmium near a Lead Smelter at Arnhem, Netherlands. *Neth. J. Agric. Sci.* **1982**, *30*, 227–235. [CrossRef]
88. Gaurav, V.K.; Sharma, C. Estimating Health Risks in Metal Contaminated Land for Sustainable Agriculture in Peri-Urban Industrial Areas Using Monte Carlo Probabilistic Approach. *Sustain. Comput. Inform. Syst.* **2020**, *28*, 100310. [CrossRef]
89. Shetty, B.R.; Pai, B.J.; Salmataj, S.A.; Naik, N. Assessment of Carcinogenic and Non-Carcinogenic Risk Indices of Heavy Metal Exposure in Different Age Groups Using Monte Carlo Simulation Approach. *Sci. Rep.* **2024**, *14*, 30319. [CrossRef]
90. Custodio, M.; Peñaloza, R.; Ochoa, S.; De La Cruz, H.; Rodríguez, C.; Cuadrado, W. Microbial and Potentially Toxic Elements Risk Assessment in High Andean River Water Based on Monte Carlo Simulation, Peru. *Sci. Rep.* **2023**, *13*, 21473. [CrossRef] [PubMed]
91. Jin, H.; Zhihong, P.; Jiaqing, Z.; Chuxuan, L.; Lu, T.; Jun, J.; Xinghua, L.; Wenyan, G.; Junkang, G.; Binbin, S.; et al. Source Apportionment and Quantitative Risk Assessment of Heavy Metals at an Abandoned Zinc Smelting Site Based on GIS and PMF Models. *J. Environ. Manag.* **2023**, *336*, 117565. [CrossRef] [PubMed]
92. Hu, X.; Wang, J.; Lv, Y.; Liu, X.; Zhong, J.; Cui, X.; Zhang, M.; Ma, D.; Yan, X.; Zhu, X. Effects of Heavy Metals/Metalloids and Soil Properties on Microbial Communities in Farmland in the Vicinity of a Metals Smelter. *Front. Microbiol.* **2021**, *12*, 707786. [CrossRef]
93. Mihali, C.; Butean, C.; Michnea, A.; Pop, N. Application of Pollution Indexes, Cluster Analysis and Isocontent Chart to the Study of Soil Pollution. *Creat. Math. Inform.* **2013**, *22*, 207–214. [CrossRef]
94. Paatero, P.; Tapper, U. Positive Matrix Factorization: A Non-negative Factor Model with Optimal Utilization of Error Estimates of Data Values. *Environmetrics* **1994**, *5*, 111–126. [CrossRef]
95. Lv, H.; Lu, Z.; Fu, G.; Lv, S.; Jiang, J.; Xie, Y.; Luo, X.; Zeng, J.; Xue, S. Pollution Characteristics and Quantitative Source Apportionment of Heavy Metals within a Zinc Smelting Site by GIS-Based PMF and APCS-MLR Models. *J. Environ. Sci.* **2024**, *144*, 100–112. [CrossRef] [PubMed]
96. Wang, H.-L.; Shen, C.-Y.; Li, P.-L.; Faisal, M.; Zhu, S. Vertical Distribution Characteristics and Source Apportionment Of Heavy Metals in Urban Near-Surface Dust Based on Receptor Model. *Pol. J. Environ. Stud.* **2021**, *30*, 5811–5831. [CrossRef]
97. Gunchin, G.; Streli, C.; Darby, I.; Karydas, A.G.; Eleftheriadis, K.; Lodoysamba, S.; Shagjjamba, D.; Migliori, A.; Padilla-Alvarez, R.; Manousakas, M.; et al. Three-Year Long Source Apportionment Study of Airborne Particles in Ulaanbaatar Using X-Ray Fluorescence and Positive Matrix Factorization. *Aerosol Air Qual. Res.* **2019**, *19*, 1056–1067. [CrossRef]
98. Panqing, Y.; Abliz, A.; Xiaoli, S.; Aisaiduli, H. Human Health-Risk Assessment of Heavy Metal–Contaminated Soil Based on Monte Carlo Simulation. *Sci. Rep.* **2023**, *13*, 7033. [CrossRef]

99. Komárek, M.; Ettler, V.; Chrastný, V.; Mihaljevič, M. Lead Isotopes in Environmental Sciences: A Review. *Environ. Int.* **2008**, *34*, 562–577. [CrossRef]
100. Wang, L.; Jin, Y.; Weiss, D.J.; Schleicher, N.J.; Wilcke, W.; Wu, L.; Guo, Q.; Chen, J.; O'Connor, D.; Hou, D. Possible Application of Stable Isotope Compositions for the Identification of Metal Sources in Soil. *J. Hazard. Mater.* **2021**, *407*, 124812. [CrossRef] [PubMed]
101. Cipullo, S.; Prpich, G.; Campo, P.; Coulon, F. Assessing Bioavailability of Complex Chemical Mixtures in Contaminated Soils: Progress Made and Research Needs. *Sci. Total Environ.* **2018**, *615*, 708–723. [CrossRef] [PubMed]
102. Agrelli, D.; Caporale, A.G.; Adamo, P. Assessment of the Bioavailability and Speciation of Heavy Metal(Loid)s and Hydrocarbons for Risk-Based Soil Remediation. *Agronomy* **2020**, *10*, 1440. [CrossRef]
103. Li, G.; Chi, H.; Hou, Y.; Williams, P.N.; Liu, Z.; Cai, C. Accurate Bioaccessibility Assessment of Soil Heavy Metals by Combining Their Speciation and in Vitro Model with Human Gut Microbiota. *Environ. Sci. Eur.* **2024**, *36*, 209. [CrossRef]
104. Grassi, G.; Lamy, I.; Pucheux, N.; Ferrari, B.J.D.; Faburé, J. State of the Art of Triad-Based Ecological Risk Assessment: Current Limitations and Needed Implementations in the Case of Soil Diffuse Contamination. *Front. Environ. Sci.* **2022**, *10*, 878238. [CrossRef]
105. Ramazanova, E.; Lee, S.H.; Lee, W. Stochastic Risk Assessment of Urban Soils Contaminated by Heavy Metals in Kazakhstan. *Sci. Total Environ.* **2021**, *750*, 141535. [CrossRef]
106. Sharma, K.; Janardhana Raju, N.; Singh, N.; Sreekesh, S. Heavy Metal Pollution in Groundwater of Urban Delhi Environs: Pollution Indices and Health Risk Assessment. *Urban Clim.* **2022**, *45*, 101233. [CrossRef]
107. Yan, Z.-G.; Zheng, X.; Zhang, Y.-Z.; Yang, Z.-H.; Zhou, Q.; Men, S.-H.; Du, J.-Z. Chinese Technical Guideline for Deriving Water Quality Criteria for Protection of Freshwater Organisms. *Toxics* **2023**, *11*, 194. [CrossRef] [PubMed]
108. Jha, G.; Ulery, A.L.; Lombard, K.; VanLeeuwen, D.; Brungard, C.; Dari, B.; Sihi, D. Portable X-Ray Fluorescence (PXRF) Analysis of Total Metal(Loid)s and Sequential Extraction of Bioavailable Arsenic in Agricultural Soils of Animas Watershed. *Water Air Soil Pollut.* **2021**, *232*, 308. [CrossRef]
109. Al Maliki, A.; Al-lami, A.K.; Hussain, H.M.; Al-Ansari, N. Comparison between Inductively Coupled Plasma and X-Ray Fluorescence Performance for Pb Analysis in Environmental Soil Samples. *Environ. Earth Sci.* **2017**, *76*, 433. [CrossRef]
110. Skubała, K.; Styburski, J.; Chowaniec, K. Assessment of the Suitability of Dehydrogenase Activity as a Biomarker in the Plant Rhizosphere Soil and Lichen Thalli for Trace Element Pollution Around a Zinc Smelter—A Preliminary Research. *Rocz. Ochr. Śr.* **2025**, *27*, 361–372. [CrossRef]
111. Rieuwerts, J.; Farago, M. Heavy Metal Pollution in the Vicinity of a Secondary Lead Smelter in the Czech Republic. *Appl. Geochem.* **1996**, *11*, 17–23. [CrossRef]
112. Kachur, A.N.; Arzhanova, V.S.; Yelpatyevsky, P.V.; Von Braun, M.C.; Von Lindern, I.H. Environmental Conditions in the Rudnaya River Watershed—A Compilation of Soviet and Post-Soviet Era Sampling around a Lead Smelter in the Russian Far East. *Sci. Total Environ.* **2003**, *303*, 171–185. [CrossRef]
113. *GB 36600-2018*; Soil Environmental Quality—Risk Control Standard for Soil Contamination of Development Land. Ministry of Ecology and Environment of China: Beijing, China, 2018.
114. *Dz.U. 2016 poz. 1395*; Regulation of the Minister of the Environment on Soil Quality Standards. MIN. ŚRODOWISKA: Warsaw, Poland, 2016.
115. *CONAMA Resolution No. 420/2009*; Conselho Nacional do Meio Ambiente Criteria and Guiding Values for Soil Quality Regarding the Presence of Chemical Substances. Conselho Nacional do Meio Ambiente: Brasília, Brazil, 2009.
116. Agence de l'Environnement et de la Maîtrise de l'Énergie. *ADEME/BRGM; Valeurs de Constat d'Impact (VCI) Pour les Sols*; Agence de l'Environnement et de la Maîtrise de l'Énergie: Angers, France, 2007.
117. Godbole, P.; Meshram, P.; Jawadand, S.; Meshram, T.; Randive, K. A Critical Analysis of Industrial Slags, Their Hazard Potential and Remediation with Reference to Sustainable Development Goals (SDGs). *Discov. Civ. Eng.* **2025**, *2*, 117. [CrossRef]
118. Montes-Montes, G.; Muñoz-Ramírez, Z.Y.; Cortes-Palacios, L.; Carrillo-Campos, J.; Ramírez-Sánchez, O.; Ortiz-Aguirre, I.; Muñoz-Castellanos, L.N.; González-Escobedo, R. Microbial Diversity and Heavy Metal Resistome in Slag-Contaminated Soils from an Abandoned Smelter in Chihuahua, Mexico. *Soil Syst.* **2025**, *9*, 30. [CrossRef]
119. Zhang, X.; Cao, L.; Ge, J.; Feng, R.; Han, W.; Huang, X.; Wang, S.; Wang, Y. Hyperspectral Unmixing-Based Remote Sensing Inversion of Multiple Heavy Metals in Mining Soils: A Case Study of the Lengshuijiang Antimony Mine, Hunan Province. *Remote Sens.* **2026**, *18*, 767. [CrossRef]
120. Zang, Z.; Li, Y.; Li, H.; Guo, Z.; Zhang, R. Spatiotemporal Variation and Pollution Assessment of Pb/Zn from Smelting Activities in China. *Int. J. Environ. Res. Public Health* **2020**, *17*, 1968. [CrossRef]
121. Ordóñez, A.; Loredo, J.; De Miguel, E.; Charlesworth, S. Distribution of Heavy Metals in the Street Dusts and Soils of an Industrial City in Northern Spain. *Arch. Environ. Contam. Toxicol.* **2003**, *44*, 160–170. [CrossRef]
122. Kupczak, K.; Warchulski, R.; Ettler, V.; Mihaljevič, M. The Impact of Buried Historical Copper Slags on Contemporary Soil Contamination. *J. Geochem. Explor.* **2025**, *273*, 107743. [CrossRef]

123. Lu, N.; Luo, Y.; Wang, N.; Zhang, B.; Li, G.; Sun, Y.; Liu, Y. Analysis of Heavy Metal Content Characteristicsin Topsoil of Wasteland in the Industrial andMining Areas of Shenmu, Shaanxi Province, China. *Pol. J. Environ. Stud.* **2025**, *34*, 263–273. [CrossRef]
124. Swain, C.K. Environmental Pollution Indices: A Review on Concentration of Heavy Metals in Air, Water, and Soil near Industrialization and Urbanisation. *Discov. Environ.* **2024**, *2*, 5. [CrossRef]
125. Gayathri, S.; Krishnan, K.A.; Krishnakumar, A.; Maya, T.M.V.; Dev, V.V.; Antony, S.; Arun, V. Monitoring of Heavy Metal Contamination in Netravati River Basin: Overview of Pollution Indices and Risk Assessment. *Sustain. Water Resour. Manag.* **2021**, *7*, 20. [CrossRef]
126. Reinikainen, J.; Bouhoulle, E.; Sorvari, J. Inconsistencies in the EU Regulatory Risk Assessment of PFAS Call for Readjustment. *Environ. Int.* **2024**, *186*, 108614. [CrossRef]
127. Hamid, E.; Payandeh, K.; Karimi Nezhad, M.T.; Saadati, N. Potential Ecological Risk Assessment of Heavy Metals (Trace Elements) in Coastal Soils of Southwest Iran. *Front. Public Health* **2022**, *10*, 889130. [CrossRef]
128. Kasemodel, M.C.; Lima, J.Z.; Sakamoto, I.K.; Varesche, M.B.A.; Trofino, J.C.; Rodrigues, V.G.S. Soil Contamination Assessment for Pb, Zn and Cd in a Slag Disposal Area Using the Integration of Geochemical and Microbiological Data. *Environ. Monit. Assess.* **2016**, *188*, 698. [CrossRef]
129. Woszczyk, M.; Spychalski, W.; Boluspaeva, L. Trace Metal (Cd, Cu, Pb, Zn) Fractionation in Urban-Industrial Soils of Ust-Kamenogorsk (Oskemen), Kazakhstan—Implications for the Assessment of Environmental Quality. *Environ. Monit. Assess.* **2018**, *190*, 362. [CrossRef]
130. Liu, J.; Ma, Y.; Zhang, S.; Yao, Y.; Wang, X.; Chen, T.; He, Y.; Qi, J. Health Risk Assessment of Heavy Metal Pollution in Farmland Downstream of Lead-Zinc Smelter. *IOP Conf. Ser. Earth Environ. Sci.* **2021**, *687*, 012057. [CrossRef]
131. Xing, W.; Zhang, H.; Scheckel, K.G.; Li, L. Heavy Metal and Metalloid Concentrations in Components of 25 Wheat (Triticum Aestivum) Varieties in the Vicinity of Lead Smelters in Henan Province, China. *Environ. Monit. Assess.* **2016**, *188*, 23. [CrossRef] [PubMed]
132. Sun, Z.; Chen, J.; Wang, X.; Lv, C. Heavy Metal Accumulation in Native Plants at a Metallurgy Waste Site in Rural Areas of Northern China. *Ecol. Eng.* **2016**, *86*, 60–68. [CrossRef]
133. Liang, X.; Wang, C.; Song, Z.; Yang, S.; Bi, X.; Li, Z.; Li, P. Soil Metal(Loid)s Pollution around a Lead/Zinc Smelter and Source Apportionment Using Isotope Fingerprints and Receptor Models. *Appl. Geochem.* **2021**, *135*, 105118. [CrossRef]
134. Maxim, A.; Bain, D.J.; Burgess, J. Urban Soils in a Historically Industrial City: Patterns of Trace Metals in Pittsburgh, Pennsylvania. *Environ. Res. Commun.* **2022**, *4*, 075004. [CrossRef]
135. Romanov, V.I.; Merkulov, V.V.; Kabiyeva, S.K.; Bestembek, E.S.; Zhaslan, R.K.; Zhumanazarova, G.M. Investigation of the Chemical and Mineralogical Composition of Metallurgical Slags of Jsc "Qarmet" Temirtau. *КазУТБ* **2024**, *2*, 290–295. [CrossRef]
136. Lameck, A.S.; Mlelwa, D.; Chagu, J.; Sanga, V.; Tsere, M.H.; Malunguja, G.K.; Mwakalesi, A.J. Unveiling the Hidden Risks: Heavy Metal Concentrations in Soil and Vegetables Irrigated with Kalobe Wastewater Stabilization Ponds, Mbeya, Tanzania. *J. Food Prot.* **2025**, *88*, 100653. [CrossRef]
137. Yao, J.; Qian, J.; Ji, D. Machine Learning-Based Analysis of Heavy Metal Migration Under Acid Rain: Insights from the RF and SVM Algorithms. *Minerals* **2025**, *15*, 663. [CrossRef]
138. Hollander, A.; Peijnenburg, W.; Breure, T. Fate and Transport of Contaminants. In *Ecological Impacts of Toxic Chemicals (Open Access)*; Mansuripur, F., Ed.; BENTHAM SCIENCE PUBLISHERS: Singapore, 2011; pp. 13–42. ISBN 978-1-60805-121-2.
139. Izah, S.C.; Ogwu, M.C.; Alum, E.U.; Poyeri, W.R.; Kari, A. Rethinking Data Presentation in Trace Metal Studies of Food and Environmental Matrices: Consequences for Statistical Inference, Reproducibility, and Risk Assessment. *J. Trace Elem. Miner.* **2026**, *16*, 100289. [CrossRef]
140. Martinez-Haro, M.; Acevedo, P.; Pais-Costa, A.J.; Neto, J.M.; Vieira, L.R.; Ospina-Alvarez, N.; Taggart, M.A.; Guilhermino, L.; Ribeiro, R.; Marques, J.C. Ecotoxicological Tools in Support of the Aims of the European Water Framework Directive: A Step towards a More Holistic Ecosystem-Based Approach. *Ecol. Indic.* **2022**, *145*, 109645. [CrossRef]
141. Hook, S.E.; Gallagher, E.P.; Batley, G.E. The Role of Biomarkers in the Assessment of Aquatic Ecosystem Health. *Integr. Environ. Assess. Manag.* **2014**, *10*, 327–341. [CrossRef]
142. Alipuly, M.; Rysbekov, K.; Begentayev, M.; Lee, J.; Azat, S. Mine Waste and Its Recycling in Kazakhstan. *Energy Environ.* **2026**, 0958305X261425530. [CrossRef]
143. Zhen, Z.; Wang, S.; Luo, S.; Ren, L.; Liang, Y.; Yang, R.; Li, Y.; Zhang, Y.; Deng, S.; Zou, L.; et al. Significant Impacts of Both Total Amount and Availability of Heavy Metals on the Functions and Assembly of Soil Microbial Communities in Different Land Use Patterns. *Front. Microbiol.* **2019**, *10*, 2293. [CrossRef]
144. Naimanova, A.; Akhmetova, S.; Issayeva, A.; Vyrakhmanova, A.; Alipbekova, A. Phytoaccumulation of Heavy Metals in South Kazakhstan Soils (Almaty and Turkestan Regions): An Evaluation of Plant-Based Remediation Potential. *Int. J. Des. Nat. Ecodyn.* **2024**, *19*, 451–464. [CrossRef]
145. Cui, J.; Luo, C.; Tang, C.W.; Chan, T.; Li, X. Speciation and Leaching of Trace Metal Contaminants from E-Waste Contaminated Soils. *J. Hazard. Mater.* **2017**, *329*, 150–158. [CrossRef] [PubMed]

146. Mench, M.; Vangronsveld, J.; Didier, V.; Clijsters, H. Evaluation of Metal Mobility, Plant Availability and Immobilization by Chemical Agents in a Limed-Silty Soil. *Environ. Pollut.* **1994**, *86*, 279–286. [CrossRef] [PubMed]
147. Suh, J.; Lee, H.; Choi, Y. A Rapid, Accurate, and Efficient Method to Map Heavy Metal-Contaminated Soils of Abandoned Mine Sites Using Converted Portable XRF Data and GIS. *Int. J. Environ. Res. Public Health* **2016**, *13*, 1191. [CrossRef] [PubMed]
148. Barago, N.; Pavoni, E.; Floreani, F.; Crosera, M.; Adami, G.; Lenaz, D.; Larese Filon, F.; Covelli, S. Portable X-Ray Fluorescence (pXRF) as a Tool for Environmental Characterisation and Management of Mining Wastes: Benefits and Limits. *Appl. Sci.* **2022**, *12*, 12189. [CrossRef]
149. Ran, J.; Wang, D.; Wang, C.; Zhang, G.; Yao, L. Using Portable X-Ray Fluorescence Spectrometry and GIS to Assess Environmental Risk and Identify Sources of Trace Metals in Soils of Peri-Urban Areas in the Yangtze Delta Region, China. *Environ. Sci. Process. Impacts* **2014**, *16*, 1870. [CrossRef]
150. Alqattan, Z.A.; Artiola, J.F.; Walls, D.; Ramírez-Andreotta, M.D. Evaluating the Portable X-Ray Fluorescence Reliability for Metal(Loid)s Detection and Soil Contamination Status. *Env. Monit. Assess* **2024**, *196*, 765. [CrossRef]
151. Xia, F.; Hu, B.; Zhu, Y.; Ji, W.; Chen, S.; Xu, D.; Shi, Z. Improved Mapping of Potentially Toxic Elements in Soil via Integration of Multiple Data Sources and Various Geostatistical Methods. *Remote Sens.* **2020**, *12*, 3775. [CrossRef]
152. Mulyati, T.A.; Pujiono, F.E.; Indah, I. The Exposure of Pb to Hair and Nails in Children Around "X" Coal Mines Using Atomic Absorption Spectroscopy (AAS) Method. *J. Kesehat. Lingkung.* **2021**, *13*, 174. [CrossRef]
153. Egan, K.B.; Tsai, R.J.; Chuke, S.O. Integrating Childhood and Adult Blood Lead Surveillance to Improve Identification and Intervention Efforts. *J. Public Health Manag. Pract.* **2019**, *25*, S98–S104. [CrossRef] [PubMed]
154. Needleman, H. Lead Poisoning. *Annu. Rev. Med.* **2004**, *55*, 209–222. [CrossRef] [PubMed]
155. Zhang, Q.; Chen, Y.; Du, L.; Zhang, M.; Han, L. Accumulation and Subcellular Distribution of Heavy Metal in *Paulownia fortunei* Cultivated in Lead-Zinc Slag Amended with Peat. *Int. J. Phytoremediat.* **2019**, *21*, 1153–1160. [CrossRef]
156. Li, J.; Li, X.; Tai, X.-S.; Tuo, X.-Y.; Zhou, F.-Y.; Rong, Y.-J.; Zang, F. Machine Learning-Assisted Source Identification and Probabilistic Ecological-Health Risk Assessment of Heavy Metal(Loid)s in Urban Park Soils. *Sci. Rep.* **2025**, *15*, 17451. [CrossRef]
157. Fu, X.; Geng, G.; Hopke, P.K.; Shen, H. Advances in Emissions, Modeling, and Source Apportionment. *Environ. Sci. Technol.* **2026**, *60*, 5927–5933. [CrossRef]
158. Blasco, C.; Picó, Y. Prospects for Combining Chemical and Biological Methods for Integrated Environmental Assessment. *TrAC Trends Anal. Chem.* **2009**, *28*, 745–757. [CrossRef]
159. Das, S.; Kim, G.W.; Hwang, H.Y.; Verma, P.P.; Kim, P.J. Cropping With Slag to Address Soil, Environment, and Food Security. *Front. Microbiol.* **2019**, *10*, 1320. [CrossRef]

Disclaimer/Publisher's Note: The statements, opinions and data contained in all publications are solely those of the individual author(s) and contributor(s) and not of MDPI and/or the editor(s). MDPI and/or the editor(s) disclaim responsibility for any injury to people or property resulting from any ideas, methods, instructions or products referred to in the content.

An Environmental Assessment of the Heavy Metal Impact on the Soil Cover: The Case Study of Shymkent

Zhaksylyk Pernebayev
Limited Liability Company "Centre for Scientific Research and Ecological Expertise KazEcoHolding", Shymkent, Kazakhstan
pernebaev.zh.d@mail.ru

Gulmira Kenzhibayeva
Mukhtar Auezov South Kazakhstan University, Shymkent, Kazakhstan
sovetovna.g7272@gmail.com (corresponding author)

Akmaral Issayeva
Limited Liability Company "Centre for Scientific Research and Ecological Expertise KazEcoHolding", Shymkent, Kazakhstan
akissayeva@mail.ru

Ayaulym Tileuberdi
Mukhtar Auezov South Kazakhstan University, Shymkent, Kazakhstan
17tile@gmail.com

Sabyr Balybek
Mukhtar Auezov South Kazakhstan University, Shymkent, Kazakhstan
ecology_uko@mail.ru

Kural Nurseiit
Limited Liability Company "Centre for Scientific Research and Ecological Expertise KazEcoHolding", Shymkent, Kazakhstan
kuralnurik15@gmail.com

Received: 4 April 2026 | Revised: 27 April 2026 | Accepted: 15 May 2026

Licensed under a CC-BY 4.0 license | Copyright (c) by the authors | *DOI: https://doi.org/10.48084/etasr.19108*

ABSTRACT

Soil contamination by heavy metals is a significant environmental problem that adversely affects soil systems and human health. However, integrated assessments that combine spatial distribution analysis, microstructural characterization, and economic damage evaluation remain limited for industrial cities such as Shymkent. This study aims to provide a comprehensive environmental assessment of heavy metal contamination in urban soils through a combined geochemical, microscopic, and economic approach. Soil and slag samples were collected along a transect at distances of 0–1000 m from a metallurgical waste source and analyzed using Scanning Electron Microscopy (SEM), X-Ray Diffraction (XRD), and Atomic Absorption Spectroscopy (AAS). The results revealed elevated concentrations of Pb, Zn, Cu, and Fe exceeding regulatory limits, with a clear decrease in concentration with increasing distance from the pollution source. Strong positive correlations among heavy metal concentrations indicate a common anthropogenic origin and synchronous migration within the soil profile. The economic assessment, based on a standardized national methodology, showed that the total environmental damage exceeds 750 million KZT per year, with iron and lead contributing most significantly to the overall impact. The novelty of this study lies in the integration of spatial analysis, microstructural investigation, and economic evaluation, providing new insights into the relationship among contamination distribution, migration processes, and

economic consequences. The results provide a scientific basis for environmental risk assessment, soil remediation planning, and sustainable urban land management in industrial regions.

Keywords-soil cover; sustainable development; heavy metals; environmental assessment; soil pollution; economic damage assessment

I. INTRODUCTION

Soil contamination from anthropogenic waste has a significant negative impact on the environment, leading to soil quality degradation and reduced biological productivity [1]. In this study, soil cover refers to the upper layer of the Earth's crust composed of mineral particles, organic matter, water, and air, which functions as a dynamic system supporting ecosystems and regulating pollutant migration. Long-term exposure to industrial activities, particularly metallurgical operations, results in the accumulation of heavy metals in soils, suppressing vegetation growth and increasing the risk of secondary contamination through leaching and pollutant transport processes [2]. Previous studies have reported average heavy metal concentrations reaching 27.9 ± 0.7 times the Maximum Permissible Concentration (MPC), mainly due to the historically intensive development of lead–zinc metallurgy and the use of outdated industrial technologies [3]. Rapid expansion of metallurgical production in the region occurred during periods when environmental regulations were limited or absent, contributing substantially to present-day contamination levels [4]. Heavy metals such as cadmium (Cd) and lead (Pb) are of environmental concern because of their toxicity, persistence, and ability to accumulate in soils and food chains [5, 6]. Continuous accumulation of metallurgical waste further increases the environmental burden on soil systems and intensifies the risk of secondary pollution through alkalization and migration of contaminants [7]. Among the most hazardous pollutants are Pb, Cd, Zn, and Cu due to their high mobility and ecological toxicity. Mineralogical investigations have shown that metallurgical slags mainly consist of fayalite (Fe_2SiO_4), magnetite (Fe_3O_4), olivine-group minerals, zinc ferrite ($ZnFe_2O_4$), sulfides, and Pb- and Zn-bearing phases, together with both crystalline and amorphous components [8].

X-Ray Diffraction (XRD) research has indicated that the amorphous phase content in slag materials ranges from 20% to 40% [9, 10]. In pyrometallurgical lead production, slag generated during concentrate smelting typically contains 0.3%–3% Pb, 3%–12% Zn, 25%–45% Fe, and 20%–35% SiO_2, with formation temperatures ranging between 1200°C and 1400°C [11]. Gas-cleaning systems associated with metallurgical operations also produce dust-rich wastes containing volatile Pb and Zn compounds, with Zn concentrations ranging from 20%–60% and Pb concentrations from 5%–25% [12]. In hydrometallurgical processes, zinc slag leaching with sulfuric acid produces residues enriched with insoluble Pb, Ag, and Fe compounds, typically containing 8%–15% Pb and 1%–5% Zn. Additional by-products, such as gypsum cake, are formed during zinc solution purification and contain calcium sulfate mixed with heavy metal impurities [13]. Globally, metallurgical industries generate approximately 2–2.5 billion tons of waste annually. Ferrous metallurgy contributes around 1.8 billion tons per year, while non-ferrous metallurgy accounts for approximately 0.2–0.3 billion tons [14]. Asia is responsible for nearly 60% of global metallurgical waste production, followed by Europe (20%) and North America (15%). China alone contributes approximately 40% of global metallurgical waste generation due to the rapid expansion of its metallurgical industry [15].

Despite the extensive body of research on heavy metal contamination, previous studies have primarily focused either on assessing pollutant concentrations or on developing remediation techniques. However, integrated approaches that combine spatial distribution analysis, microstructural characterization, and economic damage assessment remain limited, particularly for industrial cities such as Shymkent. Therefore, this study aims to provide a comprehensive environmental assessment of heavy metal contamination in the soil cover of Shymkent by integrating geochemical analysis, microstructural characterization, and economic evaluation. Specifically, the study investigates heavy metal concentrations at different distances from a metallurgical waste source, examines their spatial distribution and migration patterns, analyzes the microstructural properties of slag and soil samples, evaluates relationships among heavy metal concentrations, and estimates the associated environmental and economic damage. The novelty of this work lies in the application of an integrated methodological framework that combines field observations, laboratory analyses, and economic assessment to achieve a holistic understanding of heavy metal pollution in an industrial urban environment. The findings contribute to the development of scientifically grounded strategies for soil remediation, environmental monitoring, and sustainable urban land management.

II. MATERIALS AND METHODS

The study was conducted in the industrial zone of Shymkent, which is historically associated with lead–zinc metallurgical activities (Figure 1). Sampling was carried out in May–June 2024 in the zone affected by metallurgical waste (slag dumps).



Fig. 1. Map of the study area with sampling locations (adapted from Google Maps).

TABLE I. CHARACTERISTICS OF SAMPLES

Sample code	Sampling places from sources	DMS coordinates		Sampling size	pH
		N	E		
A 1	0 m	42°18′43″	69°31′29″	50 mm-150 mm	7.5-8
A 2	50 m	42°18′40″	69°31′39″	50-150 mm	7.6-8.1
A 3	100 m	42°18′39″	69°31′41″	10 mm-30 mm	7.6-8.2
A 4	200 m	42°18′37″	69°31′47″	10 mm-30 mm	7.7-8.3
A 5	500 m	42°18′35″	69°31′51″	5 mm-20 mm	7.7-8.4
A 6	1000 m	42°18′33″	69°31′59″	5 mm-20 mm	7.8-8.5

Sample preparation was carried out in accordance with [16]. The samples were pre-dried in drying cabinets at 105°C and then ground to a size of 0.1 mm in a grinding mill. Measurements were carried out at element-specific wavelengths (e.g., Pb: 217 nm; Zn: 213.9 nm; Cu: 324.8 nm). The Limits of Detection (LOD) for the analyzed elements ranged from 0.001 to 0.01 mg/kg, depending on the element. The concentrations of heavy metals (Pb, Zn, Cu, Fe) were determined using AAS (ContrAA 300). Measurements were carried out at element-specific wavelengths (Pb: 217 nm; Zn: 213.9 nm; Cu: 324.8 nm). The LOD ranged from 0.001 to 0.01 mg/kg depending on the element. Microstructural analysis of slag and soil samples was performed using SEM (JSM-6490LV, JEOL, Japan). The analysis was conducted at an accelerating voltage of 15 kV–20 kV in Backscattered Electron (BSE) mode. The obtained images were used to evaluate the morphology, porosity, and phase distribution of the samples. Quality control procedures included the analysis of Certified Reference Materials (CRM), procedural blanks, and duplicate samples. All measurements were performed in five replicates. The recovery rates for heavy metals ranged from 92% to 105%, indicating acceptable analytical accuracy. The Relative Standard Deviation (RSD) did not exceed 5%, confirming good precision of the measurements. Statistical processing of the data was performed using descriptive statistics (mean and standard deviation) and Pearson correlation analysis to assess the relationships between heavy metal concentrations. The significance of the correlations was evaluated at a confidence level of $p < 0.05$. In addition, the obtained concentrations were compared with MPC to assess the level of soil contamination.

The economic damage caused by environmental pollution is estimated using a standardized calculation method that combines pollutant emissions and regulatory coefficients. The calculation is performed in accordance with the methodology approved by the Government of the Republic of Kazakhstan for environmental damage assessment [17]. The model incorporates parameters such as pollutant mass, regulatory limits, emission duration, and environmental risk coefficients. All variables used in the calculation are defined in:

$$U = (C_{fact} - C_{norm}) \cdot 3600/1000000 \cdot A_i \cdot T \cdot 2.2MCI \cdot 10 \cdot K_1 \cdot K_2 \quad (1)$$

where U is the economic damage indicator, C_{fact} is the actual emission rate of pollutants, C_{norm} is the regulatory emission rate, A_i is the hazard coefficient of pollutant i (1/MPC), T is the operating time (h/year), MCI is the monthly calculation index (KZT), 10 is the increasing coefficient, K_1 is the coefficient accounting for environmental conditions, and K_2 is the coefficient of possibility of environmental consequences. All parameters were selected in accordance with national regulatory guidelines, ensuring the consistency and comparability of the obtained results.

III. RESULTS AND DISCUSSION

The chemical compositions of the samples are outlined in Table II.

TABLE II. CHEMICAL COMPOSITION OF THE SAMPLES

Average amount of slag components		Average content of oxide and sulfide compounds in slag	
Formula	*%*	*Formula*	*%*
Na	2.28±0.11	Na_2O	2.58±0.18
Mg	1.88±0.02	MgO	3.45±0.085
Al	2.89±0.02	Al_2O_3	5.56±0.13
Si	0.85±0.0002	SiO_2	25.12±1.21
K	0.89±0.001	K_2O	1.17±0.04
Ca	9.94±0.24	CaO	12.80±0.31
Ti	014±0.0001	TiO_2	0.29±0.005
Cr	0.05±0.0	Cr_2O_3	0.07±0.0003
Mn	0.46±0.001	MnO_2	0.76±0.002
Fe	26.98±1.11	Fe_2O_3	37.9±1.22
Cu	1.16±0.0035	CuO	0.55±0.003
Zn	3.95±0.18	ZnO	3.65±0.004
Pb	0.27±0.003	ZnS	1.48±0.003

The main metal content of lead-zinc residues, as depicted in Table II, is Pb 2%-8%, Zn 3%-12%, Cu 0.5%-3%, Fe 15%-25%, Ag 10 g/t-150 g/t, Bi 0.01%-0.5%, Sb 0.1-2%, Sn 0.05%-0.3%, and Cd 0.01%-0.1%. It was found that non-metallic components include: SiO_2 25%-40%, Al_2O_3 8-15%, CaO 10%-20%, MgO 2%-6%, Fe_2O/FeO 20%-35%, SO2 1%-5%, and P_2O_5 0.1%-0.8%. Physical properties include density from 2.8 g/cm^3 to 3.5 g/cm^3, particle sizes from 0.1 mm to 50 mm, dark grey to black color, sometimes metallic luster, vitreous or crystalline or a mix of both, and a porosity of 15-40%. Figure 2 illustrates the microstructure and elemental composition of the obtained samples.

According to the obtained results, the residual minerals identified in the samples included pyroxenes, olivine, melilite, magnesioferrite, zincoferrite, galena (PbS), sphalerite (ZnS), magnetite, hematite, and zinc.

Figure 3 presents the analysis of the sample matrix and its mineralogical composition. Correlation analysis revealed an extremely high positive linear relationship between the concentrations of Pb, Zn, Cu, Ni, As, Hg, Cr, and Cd at 0-1000 m from the source of contamination. This indicates the almost synchronous nature of the change in the content of all studied elements within the considered zone. The distribution profile of the elements was derived from the obtained correlation coefficients. The highest correlation coefficient values ($r \approx 0.9998–1$) were found for the Pb–Cd, Cd–Cu, Ni–As, and Zn–As pairs.

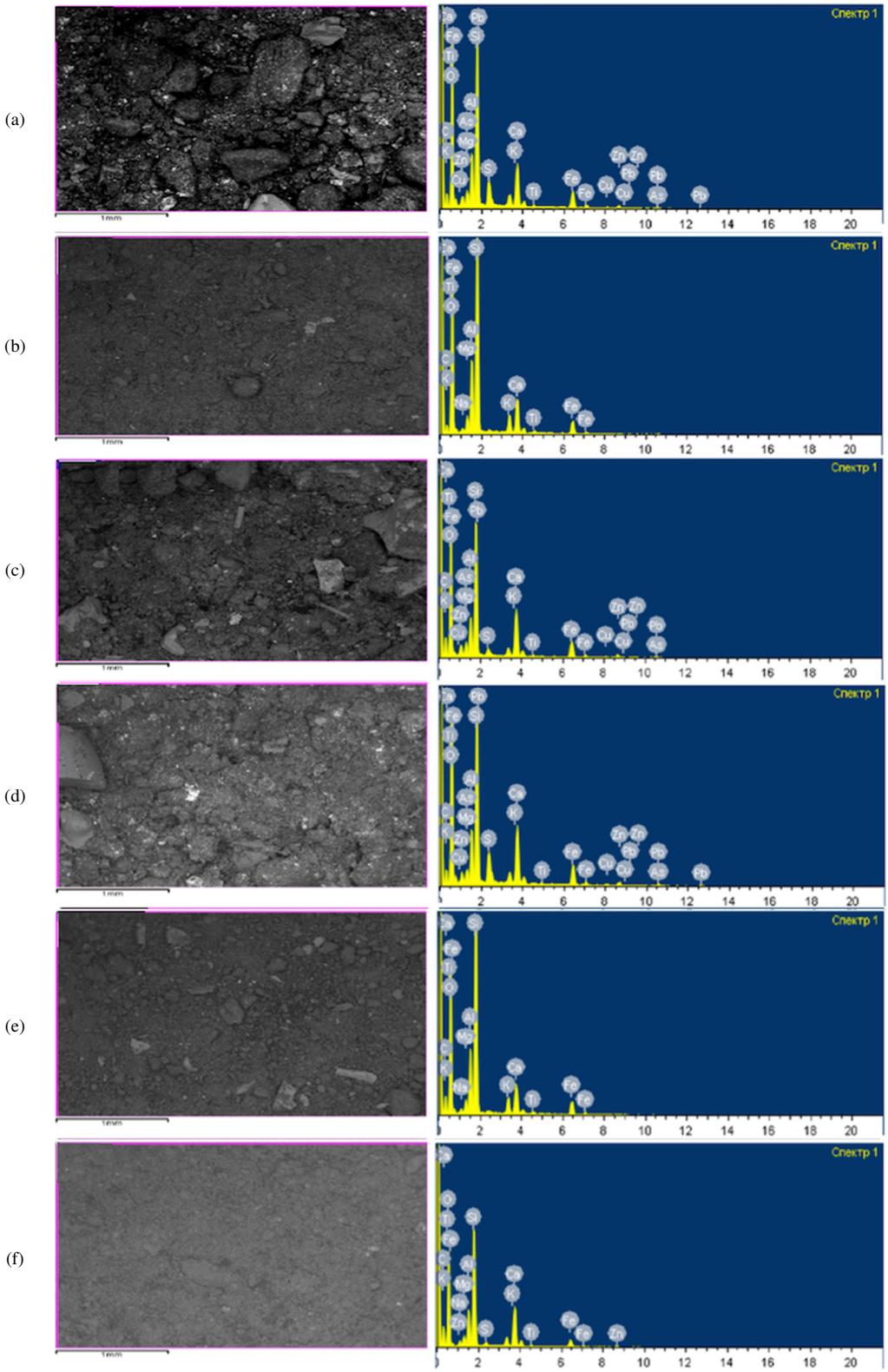


Fig. 2. Mineralogical and elemental composition of the samples: (a) – A1 sample, (b) – A2 sample, (c) – A3 sample, (d) – A4 sample, (e) – A5 sample, and (f) – A6 sample.

The minimum values (r ≈ 0.9982–0.9988) recorded for combinations of Hg–Cr, Cr–Cd, and Pb–Cr also remain statistically significant. They are extremely high and do not reflect significant geochemical differentiation. The extremely high correlation coefficients (r ≈ 0.999–1) can be explained by the common anthropogenic source of contamination (metallurgical waste), leading to synchronous deposition and migration of heavy metals in the soil. In 2022, the institution had to pay the state a fine of 1322762.3 tenge for 52.664358912 tons of harmful emissions into the environment allocated from the technological process. This amount is the cost of environmental damage caused to the atmosphere in financial terms. According to the previous service of the institution for this number of fines, Standard Steel KZ LLP would have to pay 144716685.8 tenge per year for 5761.7 tons. The economic assessment of environmental damage (U) is portrayed in Table III.

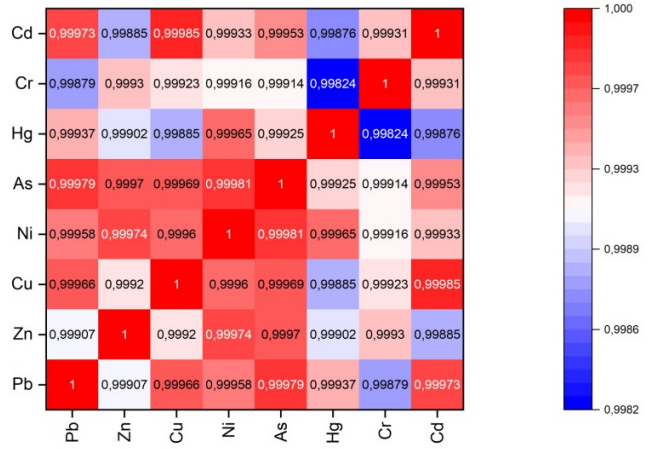


Fig. 3. Correlation matrix of heavy metal intake.

TABLE III. CHARACTERISTICS OF SAMPLES

The pollutant	C_{fact} (t/year)	C_{norm} (t/year)	Difference (t/year)	U (million tenge/year)
Pb	5761,7	0	5761,7	87.3
Zn	3785	0	3785	57.3
Cu	1475	0	1475	22.3
Fe	38560	0	38560	584.6

IV. CONCLUSIONS

This study provides a comprehensive environmental assessment of heavy metal contamination in the soil cover of Shymkent, synthesizing geochemical analysis, microstructural characterization, and economic evaluation. The findings demonstrate that metallurgical waste creates a distinct geochemical anomaly, where heavy metals such as Pb, Zn, Cu, and Fe are distributed synchronously within a 1000 m radius of the pollution source. The obtained data confirm elevated concentrations of heavy metals in the topsoil layer, exceeding permissible limits and indicating a strong anthropogenic impact associated with long-term industrial activity. Correlation analysis revealed a high positive relationship between the studied elements, suggesting a common source of contamination and similar migration mechanisms in the soil profile. The economic assessment indicates that environmental damage from heavy metal pollution is substantial, exceeding 750 million KZT per year, with iron and lead contributing the most significantly to the total impact. These findings highlight the importance of prioritizing the specific elements in remediation and monitoring strategies. The novelty of this study lies in the integration of spatial analysis, microstructural investigation, and economic evaluation, providing a holistic understanding of contamination processes in an industrial urban environment. Finally, these outcomes have practical implications for environmental management, including the development of targeted soil remediation strategies, optimization of monitoring systems, and support for decision-making in urban land use planning.

DECLARATION OF COMPETING INTERESTS

The authors declare no competing interests.

ACKNOWLEDGMENT

This research is supported by the Ministry of Science and Higher Education of the Republic of Kazakhstan, under grant number AP25795537 "Ecological assessment of the locations of lead on environmental objects and the development of technology for the reclamation of slag heap lands."

DATA AVAILABILITY

The data that support the findings of this study are available from the corresponding author upon reasonable request.

AI USE AND DECLARATION OF GENERATIVE AI USE

The authors did not use Generative AI in the preparation of this manuscript.

REFERENCE LIST STYLE AND EXAMPLES

[1] C. J. Bronick and R. Lal, "Soil structure and management: a review," *Geoderma*, vol. 124, no. 1, pp. 3–22, Jan. 2005, https://doi.org/10.1016/j.geoderma.2004.03.005.

[2] C. Huang, H. Huang, and P. Qin, "In-situ immobilization of copper and cadmium in contaminated soil using acetic acid-eggshell modified diatomite," *Journal of Environmental Chemical Engineering*, vol. 8, no. 4, Aug. 2020, Art. no. 103931, https://doi.org/10.1016/j.jece.2020.103931.

[3] Y. Wang, J. Zhang, Y. Gao, Y. Fu, S. Ma, and A. Zhang, "Impact of Saline Water Irrigation on Soil Carbon Pool Composition and the Response of Carbon Emissions to Water Regulation," *Journal of Agronomy and Crop Science*, vol. 211, no. 6, 2025, Art. no. e70120, https://doi.org/10.1111/jac.70120.

[4] J. Xiong, L. An, H. Lu, and C. Zhu, "Exogenous nitric oxide enhances cadmium tolerance of rice by increasing pectin and hemicellulose contents in root cell wall," *Planta*, vol. 230, no. 4, pp. 755–765, Sept. 2009, https://doi.org/10.1007/s00425-009-0984-5.

[5] B. Ren, W. Wei, M. Wei, and G. Zhao, "Combined Application of Commercial Hydroxyapatite and a Straw-Derived Organic Fertilizer Immobilizes Cadmium in an Alkaline-Contaminated Soil," *Environments*, vol. 13, no. 2, Feb. 2026, https://doi.org/10.3390/environments13020110.

[6] Z. Youcai and Z. Chenglong, "Amphoteric Metal Hazardous Wastes and Hydrometallurgical Processes of Zinc and Lead," in *Pollution Control and Resource Reuse for Alkaline Hydrometallurgy of Amphoteric Metal Hazardous Wastes*, Z. Youcai and Z. Chenglong, Eds. Cham: Springer International Publishing, 2017, pp. 1–11.

[7] R. Hesami, A. Salimi, and S. M. Ghaderian, "Lead, zinc, and cadmium uptake, accumulation, and phytoremediation by plants growing around Tang-e Douzan lead–zinc mine, Iran," *Environmental Science and Pollution Research*, vol. 25, no. 9, pp. 8701–8714, Mar. 2018, https://doi.org/10.1007/s11356-017-1156-y.

[8] R. Di Cagno, L. Guidi, L. De Gara, and G. F. Soldatini, "Combined cadmium and ozone treatments affect photosynthesis and ascorbate-dependent defences in sunflower," *New Phytologist*, vol. 151, no. 3, pp. 627–636, 2001, https://doi.org/10.1046/j.1469-8137.2001.00217.x.

[9] K. Khaskhoussy, B. Kahlaoui, B. M. Nefzi, O. Jozdan, A. Dakheel, and M. Hachicha, "Effect of Treated Wastewater Irrigation on Heavy Metals Distribution in a Tunisian Soil," *Engineering, Technology & Applied Science Research*, vol. 5, no. 3, pp. 805–810, June 2015, https://doi.org/10.48084/etasr.563.

[10] A. Rashid *et al.*, "Heavy Metal Contamination in Agricultural Soil: Environmental Pollutants Affecting Crop Health," *Agronomy*, vol. 13, no. 6, May 2023, https://doi.org/10.3390/agronomy13061521.

[11] C. Shi and J. Qian, "High performance cementing materials from industrial slags — a review," *Resources, Conservation and Recycling*, vol. 29, no. 3, pp. 195–207, June 2000, https://doi.org/10.1016/S0921-3449(99)00060-9.

[12] R. Naz *et al.*, "Assessment of phytoremediation potential of native plant species naturally growing in a heavy metal-polluted industrial soils," *Brazilian Journal of Biology*, vol. 84, 2024, Art. no. e264473, https://doi.org/10.1590/1519-6984.264473.

[13] B. Gorai, R. K. Jana, and Premchand, "Characteristics and utilisation of copper slag—a review," *Resources, Conservation and Recycling*, vol. 39, no. 4, pp. 299–313, Nov. 2003, https://doi.org/10.1016/S0921-3449(02)00171-4.

[14] A. Pooladi and R. Bazargan-Lari, "Simultaneous removal of copper and zinc ions by Chitosan/Hydroxyapatite/nano-Magnetite composite," *Journal of Materials Research and Technology*, vol. 9, no. 6, pp. 14841–14852, Nov. 2020, https://doi.org/10.1016/j.jmrt.2020.10.057.

[15] D. M. Abdulah, A. H. A. Al-Dosky, and A. H. Mohammed, "Lead and zinc exposure in the blood of workers in municipal waste management," *Environmental Science and Pollution Research*, vol. 27, no. 10, pp. 11147–11154, Apr. 2020, https://doi.org/10.1007/s11356-020-07722-7.

[16] ISO 11464:2006 Soil quality — Pretreatment of samples for physico-chemical analysis. Switzerland: International Standard, 2006.

[17] "On approval of the Rules for economic assessment of damage from environmental pollution - IPS 'Adilet.'" https://adilet.zan.kz/rus/docs/P070000535_.

sustainability

MDPI

Article

Integrated Geochemical, Vegetation, and Risk Assessment of a Pb–Zn Slag Reprocessing Site in Southern Kazakhstan: Implications for Sustainable Remediation Prioritization

Zhaksylyk Pernebayev [1], Akbota Aitimbetova [2,*] and Azhar Abubakirova [3,*]

[1] LLP Centre for Scientific Research and Ecological Expertise KazEcoHolding, Shymkent 160012, Kazakhstan; ecocentre2018@mail.ru
[2] Department of Ecology Shymkent, M. Auezov South Kazakhstan University, Shymkent 160012, Kazakhstan
[3] Department of Biology, Zhanibekov University, Shymkent 160012, Kazakhstan
* Correspondence: akbota.askarkyzy@auezov.edu.kz (A.A.); azhar.baikal79@mail.ru (A.A.)

Abstract

Reprocessing historical lead–zinc (Pb–Zn) slag offers a circular-economy pathway for secondary metal recovery, yet it can remobilize legacy contaminants where containment is inadequate, transferring risk to the surrounding land. Sustainable management of such sites requires frameworks that link contamination assessment to actionable remediation. We integrated ICP-OES geochemistry, native-plant biomonitoring, and US EPA RAGS-based risk modeling at an active Pb–Zn slag reprocessing site in Shymkent, Southern Kazakhstan. Twenty-four soil samples along four cardinal transects, two reference samples, and four composite plant samples (*Centaurea pseudosquarrosa* + *Plantago lanceolata*) were analyzed for ten metals by ICP-OES. UCC-referenced indices classified six metals as geoaccumulation Class 6 at most points (enrichment factors up to 90,871, confirming an exclusively anthropogenic origin). Peak concentrations reached 9350 mg·kg^{-1} Pb, 290 mg·kg^{-1} Cd, and 10,900 mg·kg^{-1} As—exceeding Kazakhstan MPC by 72×, 290×, and 5450×. Worst-case carcinogenic risk reached 4.3 × 10^{-3} (43× above the US EPA threshold), driven almost entirely by arsenic (93%); ecosystem risk (RCR_{total} = 223) was dominated by cadmium (43%), arsenic (27%), and mercury (16%)—a disconnect between mass-based and toxicity-based prioritization. On this basis we propose a three-tier remediation framework (engineered containment, phytostabilization, monitored attenuation) that couples resource recovery with contamination control, is transferable to analogous Pb–Zn legacy sites, and supports sustainable land use, urban resilience, and responsible secondary-resource use.

Keywords: heavy metal contamination; circular economy; contaminated site management; risk assessment; phytostabilization; ecological risk; arsenic; cadmium; slag reprocessing; Central Asia

Check for updates

Academic Editor: Malgorzata Kacprzak

Received: 22 May 2026
Revised: 11 June 2026
Accepted: 17 June 2026
Published: 2 July 2026

Copyright: © 2026 by the authors. Licensee MDPI, Basel, Switzerland. This article is an open access article distributed under the terms and conditions of the Creative Commons Attribution (CC BY) license.

1. Introduction

Reprocessing historical lead–zinc (Pb–Zn) slag remains a globally significant environmental challenge. Slag heaps and tailings impoundments, accumulated over decades of pyrometallurgical operations, act as persistent metal reservoirs, releasing Pb, Zn, Cd, As, and Hg into surrounding soils via wind-driven particle transport, surface runoff, and slow leaching into groundwater [1–3]. Although secondary recovery of residual metals from such slags is increasingly recognized as a circular-economy opportunity [4,5], reprocessing operations can remobilize legacy contaminants if dust suppression, runoff control, and

surface stabilization are inadequate [6,7]. This duality—slag as both a valuable secondary raw material and a chronic source of soil-borne metal release—underscores the need for site-specific environmental assessment as an integral component of any reprocessing program. Where engineered containment, dust control, and runoff management are absent or insufficient, the same operations that close the metal loop can paradoxically extend the contamination footprint of the original smelting legacy, transferring risk from the heap itself to surrounding agricultural and residential land.

Southern Kazakhstan, specifically the Turkestan Region, hosts the Achisai polymetallic ore field and the Shymkent lead–zinc processing complex, together forming one of the largest concentrations of Pb–Zn metallurgical legacy in Central Asia [8]. The former Shymkent lead plant operated for about seven decades before Yuzhpolymetal JSC closed in 2012, leaving an uncontained slag heap that remains subject to aeolian dispersion under the semi-arid climate [6,8]. For regional context, the neighboring single-industry town of Kentau, 60 km to the south, which shares the same Pb–Zn ore–processing legacy, still had elevated soil Pb and Cd levels after more than two decades of passive recovery [9], underscoring the persistence of smelter contamination across the Turkestan Region. Recent assessments across Kazakhstan have likewise documented elevated soil heavy-metal burdens at industrial and urban sites [10,11], and Monte Carlo-based health risk modeling in comparable Pb–Zn mining areas confirms cadmium and arsenic as dominant carcinogenic risk drivers despite the conventional emphasis on lead [12].

To contextualize analytical data from such legacy sites, six complementary normalized indices are conventionally used. The contamination factor (*CF*) and the geoaccumulation index (*Igeo*) express contamination relative to a geochemical background; the enrichment factor (*EF*) distinguishes anthropogenic enrichment from lithogenic input; the pollution load index (*PLI*) and the modified degree of contamination (*mCd*) summarize multi-element loading; and the potential ecological risk index (RI) translates these into an integrated ecosystem-hazard score [13]. In situ phytoindication, based on tissue concentrations in native vegetation, provides independent biological validation of geochemical findings and identifies candidate species for phytostabilization [14].

Existing assessments of the Achisai–Kentau metallurgical corridor have examined individual aspects—soil chemistry, atmospheric deposition, or human exposure—in isolation. The present study integrates ICP-OES geochemistry along four cardinal-direction transects, a six-index pollution framework referenced to the upper continental crust (UCC), composite plant-tissue biomonitoring of two native species (*Centaurea pseudosquarrosa* and *Plantago lanceolata*), and US EPA RAGS-based health and ecosystem risk modeling into a single, site-specific analysis. To our knowledge, this combination has not been applied previously at the Shymkent slag reprocessing site, and the resulting framework is directly transferable to analogous Pb–Zn legacy reprocessing sites across Central Asia and globally. By translating contamination evidence into a tiered remediation strategy that reconciles secondary-resource recovery with contamination control, the study addresses the sustainability dimension of slag reprocessing and contributes directly to the United Nations Sustainable Development Goals on good health and well-being (SDG 3), sustainable cities and communities (SDG 11), responsible consumption and production (SDG 12), and life on land (SDG 15).

The specific objectives of this study were therefore to: (i) quantify Pb, Zn, Cd, Cu, As, Hg, Cr, Ni, Mn, and Fe concentrations in soils along four cardinal-direction transects (0–100 m) and at two distal reference points (300 m and 1.5 km) at an active Pb–Zn slag reprocessing site in Shymkent, Southern Kazakhstan; (ii) classify the resulting contamination using six complementary geochemical indices (*CF*, *Igeo*, *EF*, *PLI*, *mCd*, RI) referenced to the upper continental crust; (iii) characterize community-level metal uptake in two na-

tive species (*Centaurea pseudosquarrosa* and *Plantago lanceolata*) via the bioconcentration factor; (iv) quantify human-health and ecosystem risks using US EPA RAGS and REACH PNEC-based *RCR* frameworks; and (v) translate the integrated evidence into a site-specific, three-tier remediation prioritization framework transferable to analogous Pb–Zn legacy reprocessing sites in Central Asia and globally.

Comparable site-resolved assessments of Pb–Zn smelter and slag-reprocessing legacy contamination have been reported across multiple continents. Yang et al. [15] characterized the distribution of heavy metals in topsoil around a Pb–Zn smelter in Henan Province (Central China), reporting Pb, Cd, and As enrichment levels that consistently exceeded national risk-screening thresholds. Ettler et al. [16] used Pb isotopic evidence to trace the dispersal of contamination in stream sediments from the Příbram mining and smelting district (Czech Republic), demonstrating that smelter-derived Pb persists in the fluvial environment decades after operational closure. Angelovičová et al. [17] documented suppression of soil enzymatic activity in the Middle Spiš mining area (Slovakia), and Tembo et al. [18] quantified Cu–Pb–Cd–Zn contamination around the Kabwe smelter (Zambia)—a site that consistently ranks among the world's most polluted urban environments. More recently, Wang et al. [19] applied Monte Carlo simulation to characterize health risks in the Xicheng Pb–Zn mining area (China), identifying Cd and as dominant carcinogenic drivers despite a smaller absolute Pb burden. In post-Soviet Central Asia, Junusbekov et al. [9] documented elevated heavy-metal levels in soils around the Kentau Pb–Zn complex (~150 km north of Shymkent), Tleuova et al. [20] reported hydrogeological controls on heavy-metal mobility in Southern Kazakhstan, and Faurat et al. [10] characterized snow–soil–vegetation transfer of heavy metals in an industrial city in Kazakhstan. Across these geographically diverse cases, three recurring patterns emerge: (i) the spatial footprint of contamination consistently extends well beyond the immediate slag-deposit perimeter; (ii) Cd and As, rather than the more abundant Pb and Zn, often dominate human-health and ecosystem risk; and (iii) integrated assessments combining geochemistry, plant biomonitoring, and quantitative risk modeling remain rare relative to single-component studies. The present study addresses this last gap for the Achisai–Shymkent corridor of Central Asia, which to date has been examined only through fragmented single-aspect assessments [11].

2. Materials and Methods

2.1. Study Area

The study was conducted at and around an active lead–zinc slag reprocessing facility in Shymkent, Southern Kazakhstan (42.30° N, 69.58° E; Figure 1). The site lies within the semi-arid Turkestan Region (Köppen BSk), which has a strongly continental climate with a mean annual precipitation of about 400 mm and prevailing easterly and westerly winds that control the directional dispersion of contaminated dust from the slag heap [6,8].

The slag heap occupies a substantial fraction of the former Shymkent lead-smelting site and consists primarily of fine-grained (0.5–15 mm), dark gray to black, granular particles. Non-ferrous smelting slags of this type are characterized by complex mineralogy (pyroxenes, olivine, melilite, magnetite, residual galena, and sphalerite) and by the capacity to release Pb, Zn, and Cd upon weathering, with release rates sensitive to particle size and pH [21]. SEM-EDS analysis (JEOL JSM-6490LV, Tokyo, Japan) confirmed the presence of PbS, ZnS, ZnO, PbO, and Fe_2O_3 phases. Slag pH ranged from 7.5 to 8.5. The Badam River flows approximately 20 m west of the facility boundary, providing a potential pathway for metal transport into the aquatic environment [20]. In the reach adjacent to the slag-reprocessing site, the Badam River is a shallow mid-order stream characteristic of the semi-arid Turkestan piedmont, with seasonally variable hydrology typical of foothill rivers in Southern Kazakhstan [20]. Water depth and channel width vary substantially between

the dry season and the spring snowmelt freshet (April–May), with deeper and wider flow conditions during the freshet that increase the river's capacity to mobilize and transport fine particulate material delivered from adjacent upland surfaces. Hydrogeologically, the site overlies a shallow Quaternary alluvial aquifer hosted in poorly sorted gravels and sands of relatively high effective porosity, which provides limited natural attenuation capacity for dissolved metal species [20]. Two principal pathways for heavy-metal migration from the slag heap to the aquatic environment are therefore operative: (i) episodic high-intensity precipitation events generate surface runoff that can transport fine slag particulates and metal-bearing leachate across the unprotected slag-heap perimeter toward the riverbank within hours; and (ii) slow vertical infiltration through the vadose zone may deliver dissolved Cd, Zn, and other mobile species to the underlying shallow aquifer, with subsequent baseflow discharge to the river over longer timescales. These hydrogeological conditions, combined with the absence of an engineered containment liner beneath the slag heap, define the principal exposure pathways for off-site metal migration and provide the geomorphological rationale for the riverbank-directed (westward) component of the transect sampling design used in this study.

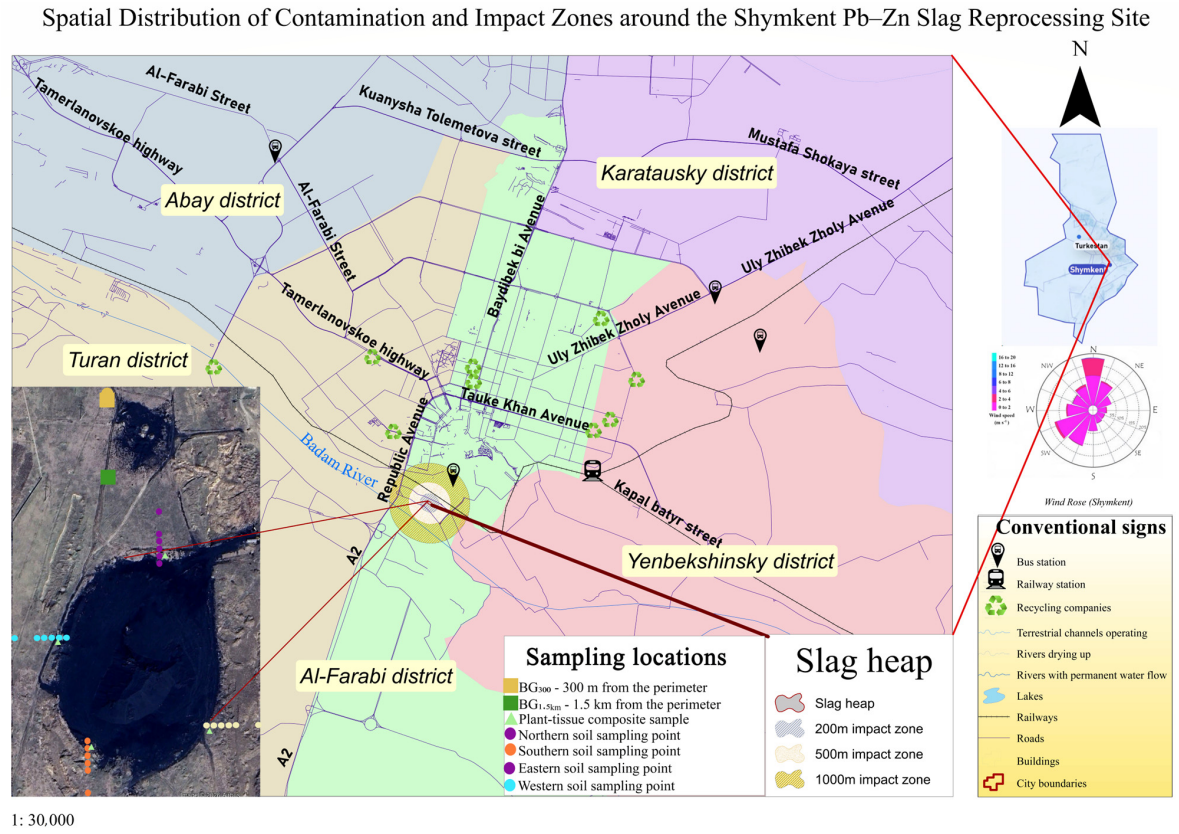


Figure 1. Location of the Pb–Zn slag reprocessing site in Shymkent, Southern Kazakhstan (42.30° N, 69.58° E). The main map (1:30,000) shows: (a) soil sampling locations along four cardinal-direction transects at 0, 1, 5, 10, 50, and 100 m from the slag heap perimeter, color-coded by direction (blue = north, green = east, orange = south, magenta = west); (b) reference soil samples at 300 m and 1.5 km distance (white squares); (c) plant-tissue sampling locations (white triangles); (d) impact zones delineated by estimated contamination extent (200 m, 500 m, 1000 m buffer rings); (e) key infrastructure including the Badam River, roads, and administrative district boundaries. The inset photograph (lower left) documents slag heap surface morphology and sampling access points. The location inset (upper right) indicates the site position within Kazakhstan. District names (Abay, Turán, Al-Farabi, Yenbekshinsky, Karatausky) and administrative landmarks provide geographic context. See Section 2.2 for detailed sampling-design rationale and Section 2.1 for site hydrogeological and geomorphological context.

2.2. Soil and Vegetation Sampling

Soil and plant tissue samples were collected on 24 April 2026 in accordance with GOST R 58595-2019 (soil sampling) [22], GOST 17.4.3.01-2017 [23] (general sampling requirements), and GOST 17.4.4.02-2017 (sample preparation) [24]. Twenty-four soil samples (0–50 cm depth) were collected along four cardinal-direction transects (north, south, east, west) at six distances from the slag heap perimeter: 0 m (transect origin at the heap edge), 1, 5, 10, 50, and 100 m (see Figure 1). Two reference soil samples were collected to characterize the local background: one at a 300 m radius outside the immediate slag-impact zone (sample 267, hereafter Bg_{300}), and one at a 1.5 km radius from the heap boundary.

Four composite plant-tissue samples were collected adjacent to each cardinal-direction transect, comprising above-ground biomass of the two dominant native species—*Centaurea pseudosquarrosa* Mikheev ex Gabrieljan et Mikheev (*Asteraceae*) and *Plantago lanceolata* L. (*Plantaginaceae*)—pooled in approximately equal proportions to represent community-level uptake. Plants were sampled within 1–10 m of the slag-heap perimeter in each direction. This community-level composite design characterizes the bulk above-ground canopy burden but, by construction, does not resolve species-specific uptake; biological interpretation of the plant data is therefore restricted to descriptive bulk-canopy observations (Sections 4.3 and 4.5). The dataset thus comprised 26 soil samples (24 transect points + 2 reference points) and 4 composite plant-tissue samples.

Immediately after collection, soil and plant samples were placed in pre-cleaned, double-bagged polyethylene containers, sealed, and individually labeled with sample identifier, date, GPS coordinates, transect direction, and distance from the slag-heap perimeter. Samples were transported from the field to the accredited Analytical Laboratory of LLP "KazEcoAnaliz" (Almaty, Kazakhstan) in insulated cooler boxes maintained at 4–8 °C using frozen ice packs to prevent microbial alteration of organic matter and minimize redistribution of mobile metal species between the sample and container surfaces during transit. Samples were transferred to the laboratory under a documented chain of custody and registered, weighed, and placed in temperature-controlled sample storage within 48 h of collection. Field handling, packaging, and transport procedures complied with the soil sampling requirements of GOST 17.4.4.02-2017 [24] and were consistent with the soil sample storage and transport guidance of ISO 18512:2007 [25].

All samples were air-dried at 20–25 °C in a dust-free, dark environment to constant mass (24–48 h), in accordance with the standard preparation protocol for total-element determination of plant and soil matrices by ICP-OES (ISO 17294-2; EPA Method 3050B) [26,27]. After drying, samples were sieved to <2 mm following removal of coarse debris and root material, and stored at +4 °C in sealed pre-cleaned containers pending acid digestion and analysis. The same air-drying protocol was applied to both soil and plant matrices to ensure analytical consistency; this approach is methodologically appropriate for total-metal determination and does not introduce volatilization losses at the applied temperature range, with the exception of trace mercury, for which a small loss cannot be excluded—however, mercury concentrations in plant tissue were below the analytical detection limit at all sampling locations (Section 3.3), so this constraint does not affect the reported results.

2.3. Chemical Analysis

Concentrations of As, Cd, Cr, Cu, Fe, Hg, Mn, Ni, Pb, and Zn in soil samples were determined by inductively coupled plasma optical emission spectrometry (ICP-OES; Shimadzu ICPE-9000, Kyoto, Japan) after acid digestion, in accordance with method M 02-902-157-10. Concentrations of the same elements in composite plant-tissue samples were determined according to method PND F 16.1:2.3:3.11-98 after wet mineralization. All analyses were performed during the period 27 April–5 May 2026 at the accredited Analytical Laboratory

of LLP «KazEcoAnaliz» (accreditation certificate KZ.T.02.1017, issued 25 February 2026, valid for both methods and all ten target elements), Almaty, Kazakhstan, under Order N°23-26 (Test Protocols N°23-01 and N°23-02 dated 5 May 2026; reference background protocol for the 1.5 km sample dated 5 May 2026, analyzed in the same calibration batch). Analytical quality control was implemented in accordance with the laboratory's ISO/IEC 17025-compliant internal procedures, including procedural blanks, analysis of certified reference materials within each batch with element-wise recoveries falling within the accreditation-defined acceptance limits (typically 80–120% for ICP-OES determinations), and replicate determinations on selected samples with relative standard deviations below 10% for major elements and below 20% for trace elements near the limit of quantification. Method detection limits were 0.2 $mg \cdot kg^{-1}$ for As and 0.1 $mg \cdot kg^{-1}$ for Hg in the plant matrix; values below detection were assigned half the detection limit for downstream calculations. Soil sample 260 (eastern transect, 100 m) returned matrix Fe (104 $mg \cdot kg^{-1}$) and Zn (7.79 $mg \cdot kg^{-1}$) values one to two orders of magnitude below those of adjacent samples on the same transect, most plausibly reflecting localized lithological heterogeneity (e.g., a quartz- or carbonate-dominated micro-substrate); this sample was retained in concentration means but excluded from Fe-normalized enrichment factor calculations to avoid artefactually inflated *EF* ratios.

2.4. Geochemical Pollution Indices

Six complementary indices were calculated to characterize single-element and aggregate contamination; their formulas, classification thresholds, and the reference values used in their calculation are consolidated in Table 1. The upper continental crust (UCC) compilation of Rudnick and Gao [28] was selected as the primary geochemical reference (Bn) over locally collected soils because both reference samples in the present study—at 300 m (Bg_{300}) and 1.5 km ($Bg_{1.5km}$)—showed elevated concentrations of at least one priority element (Section 3.1), and were therefore treated as distance-resolved exposure references rather than as a pristine geochemical baseline. Sample exceedance is reported against Kazakhstan's maximum permissible concentrations (MPC) for typical soils (Table 1), and ecosystem risk in Section 2.6 against REACH-derived PNEC values for soil [29].

Table 1. Pollution indices, classification thresholds, and regulatory reference values applied in this study.

Index/Reference	Formula or Values	Classification Thresholds	Source
Contamination factor (*CF*)	$CF = Cn/Bn$	<1 low; 1–3 moderate; 3–6 considerable; >6 very high	Hakanson [30]
Geoaccumulation index (*Igeo*)	$Igeo = \log_2(Cn/1.5 \cdot Bn)$	Class 0 ($\leq$0) unpolluted → Class 6 (>5) extreme	Müller [31]
Enrichment factor (*EF*)	$EF = (Cn/CFe)sample/(Bn/BFe)bg$	<2 minimal; 2–5 moderate; 5–20 significant; 20–40 very high; >40 exclusively anthropogenic	Sutherland [32]
Pollution load index (*PLI*)	$PLI = (CF_1 \times CF_2 \times \ldots \times CF_n)\hat{}(1/n)$	<1 unpolluted; >1 polluted	Tomlinson et al. [33]
Modified degree of contamination (*mCd*)	$mCd = (\Sigma CF_i)/n$	<1.5 nil; 1.5–2 low; 2–4 moderate; 4–8 high; 8–16 very high; 16–32 extremely high; >32 ultra-high	Abrahim & Parker [34]

Table 1. *Cont.*

Index/Reference	Formula or Values	Classification Thresholds	Source
Potential ecological risk index (*RI*)	$RI = \Sigma Eri$; $Eri = Tri \times CFi$	<150 low; 150–300 moderate; 300–600 considerable; >600 very high	Hakanson [30]
Toxic response factors (*Tri*)	Pb = 5; Zn = 1; Cd = 30; Cu = 5; As = 10; Hg = 40; Cr = 2; Ni = 5	—	Hakanson [30]
Upper continental crust (UCC) values used as Bn ($mg \cdot kg^{-1}$)	Pb = 17; Zn = 67; Cd = 0.09; Cu = 28; As = 4.8; Hg = 0.05; Cr = 92; Ni = 47; Mn = 774; Fe = 39,200	Geochemical baseline	Rudnick & Gao [28]
Kazakhstan MPC for typical soils ($mg \cdot kg^{-1}$)	Pb = 130; Zn = 220; Cd = 1.0; Cu = 33; As = 2.0; Hg = 2.1; Cr = 100; Ni = 85	Regulatory exceedance threshold	Sanitary Rules, Republic of Kazakhstan [35]
REACH PNEC for soil ($mg \cdot kg^{-1}$)	Pb = 212; Zn = 123; Cd = 0.56; Cu = 65; As = 29; Hg = 0.22; Ni = 15; Cr = 21	$RCR = PEC/PNEC$; >1 unacceptable ecosystem risk	ECHA [29]

2.5. Vegetation Biomonitoring and Bioconcentration Factor

Above-ground biomass concentrations of each metal in the composite plant samples (*C*plant) were related to the mean concentration of the same metal in soil along the corresponding transect (*C*soil) by computing the ratio *C*plant/*C*soil. Because each composite plant sample combined approximately equal biomass proportions of two phylogenetically and physiologically distinct species (*Centaurea pseudosquarrosa*, *Asteraceae*, and *Plantago lanceolata*, *Plantaginaceae*), this ratio is reported here as a *bulk vegetative canopy ratio*—that is, as a descriptive index of the combined above-ground metal burden of the two species—rather than as a species-resolved Bioconcentration Factor. The conventional excluder/accumulator/hyperaccumulator classification of Baker [36] requires species-level measurements and cannot be applied to composite samples; it is therefore not invoked here. The major implications of this composite-sampling design for biological interpretation are addressed in Sections 4.3 and 4.5.

2.6. Human-Health and Ecosystem Risk Assessment

Human health risk was assessed for an adult occupational worker scenario using the deterministic framework of the US EPA RAGS [37], with exposure factors taken from the US EPA Exposure Factors Handbook (2011 Edition) [38]. Three principal exposure pathways were integrated: incidental ingestion of soil, inhalation of resuspended particulates, and dermal contact. For each metal and each exposure pathway, the chronic daily intake (*CDI*, $mg \cdot kg^{-1} \cdot d^{-1}$) was calculated as:

$$CDI = (C \times IR \times EF \times ED \times CF)/(BW \times AT), \quad (1)$$

where C is the metal concentration in soil ($mg \cdot kg^{-1}$), *IR* is the pathway-specific intake rate (soil ingestion rate, inhalation rate, or dermal contact factor), *EF* is the exposure frequency ($d \cdot yr^{-1}$), *ED* is the exposure duration (yr), *CF* is a unit-conversion factor, *BW* is the body weight (kg), and *AT* is the averaging time (d). Exposure-factor values followed the US EPA standard adult-worker defaults: body weight 70 kg, soil ingestion 50 $mg \cdot d^{-1}$, inhalation rate 20 $m^{3} \cdot^{-1}$, exposed skin area 3300 cm^2, adherence factor 0.2 $mg \cdot cm^{-2}$, particulate emission factor 1.36×10^9 $m^3 \cdot kg^{-1}$, exposure frequency 250 $d \cdot yr^{-1}$, exposure duration

25 yr, and averaging time 70 yr (for carcinogenic endpoints) or 25 yr (for non-carcinogenic endpoints). The implications of using these defaults without site-specific localization are discussed in Section 4.5.

The carcinogenic risk (*CR*) for each metal–pathway combination was calculated by multiplying *CDI* by the slope factor (SF, $(mg \cdot kg^{-1} \cdot d^{-1})^{-1}$) obtained from the US EPA IRIS database [39], accessed on 5 May 2026:

$$CR_i = CDI_i \times SF_i, \quad (2)$$

Total carcinogenic risk was obtained by summing across metals and pathways. CR values below 10^{-6} are conventionally considered negligible; values between 10^{-6} and 10^{-4} are considered acceptable; and values above 10^{-4} are considered unacceptable [39].

Non-carcinogenic risk was assessed through the hazard quotient (*HQ*) and the hazard index (*HI*), using reference doses (*R*fD, $mg \cdot kg^1 \cdot d^1$) from the US EPA IRIS database:

$$HQ_i = CDI_i / RfD_i \quad (3)$$

$$HI = \Sigma_i \, HQ_i, \quad (4)$$

HI values exceeding 1.0 indicate potential non-carcinogenic risk to the receptor.

Ecosystem risk was assessed via the risk characterization ratio (*RCR*), defined as the ratio of the measured site-mean soil concentration (predicted environmental concentration, PEC) to the element-specific predicted no-effect concentration in soil (*PNEC*):

$$RCR_i = PEC / PNEC_i, \quad (5)$$

The element-specific *PNEC* values for soil ($mg \cdot kg^{-1}$ dry weight) were taken from REACH-registered substance dossiers compiled in the ECHA database [29]: Pb = 212, Zn = 123, Cd = 0.56, Cu = 65, As = 29, Hg = 0.22, Ni = 15, Cr = 21 (also reported in Table 1). The total ecosystem-risk score was computed as $RCR_{total} = \Sigma_i \, RCR_i$; $RCR > 1$ for any individual metal indicates an unacceptable risk to soil organisms for that metal at the site.

2.7. Statistical Analysis

Data are reported as mean ± standard deviation (SD). Differences in metal concentrations across cardinal-direction transects were assessed using one-way ANOVA with Tukey HSD post hoc ($\alpha = 0.05$). Spatial decay of Pb along each transect was examined for monotonicity; given the observed non-monotonic pattern with secondary peaks at intermediate distances (Section 3.1), no single-source dispersion model was fitted. All calculations were performed in Python 3.11 using the pandas (version 2.0.3), NumPy (version 1.24.3), and SciPy (version 1.11.1) libraries. No inferential statistical test was performed for the soil-to-plant relationship: the composite-sampling design yielded only one plant sample per cardinal direction ($n = 4$), and rank-based or parametric correlations across such a small biologically heterogeneous dataset would carry no statistical power; the directional pattern in plant tissue concentrations is therefore reported as a descriptive observation only (Sections 3.3 and 4.5).

3. Results

3.1. Heavy Metal Concentrations and Spatial Distribution

Soil concentrations of As, Cd, Cu, Hg, Pb, and Zn at the slag reprocessing site substantially exceeded both the upper continental crust geochemical background and Kazakhstan MPC values across all four cardinal-direction transects (Table 1, Figure 2). The site-mean ± SD concentrations across the 24 transect samples were 1754 ± 2447 $mg \cdot kg^{-1}$

Pb, 1254 ± 873 mg·kg^{-1} Zn, 53.7 ± 80 mg·kg^{-1} Cd, 684 ± 886 mg·kg^{-1} Cu, 1753 ± 2832 mg·kg^{-1} As, and 8.0 ± 16 mg·kg^{-1} Hg. The high standard deviations relative to the means reflect substantial directional and spatial heterogeneity rather than a smooth concentration gradient (see below).

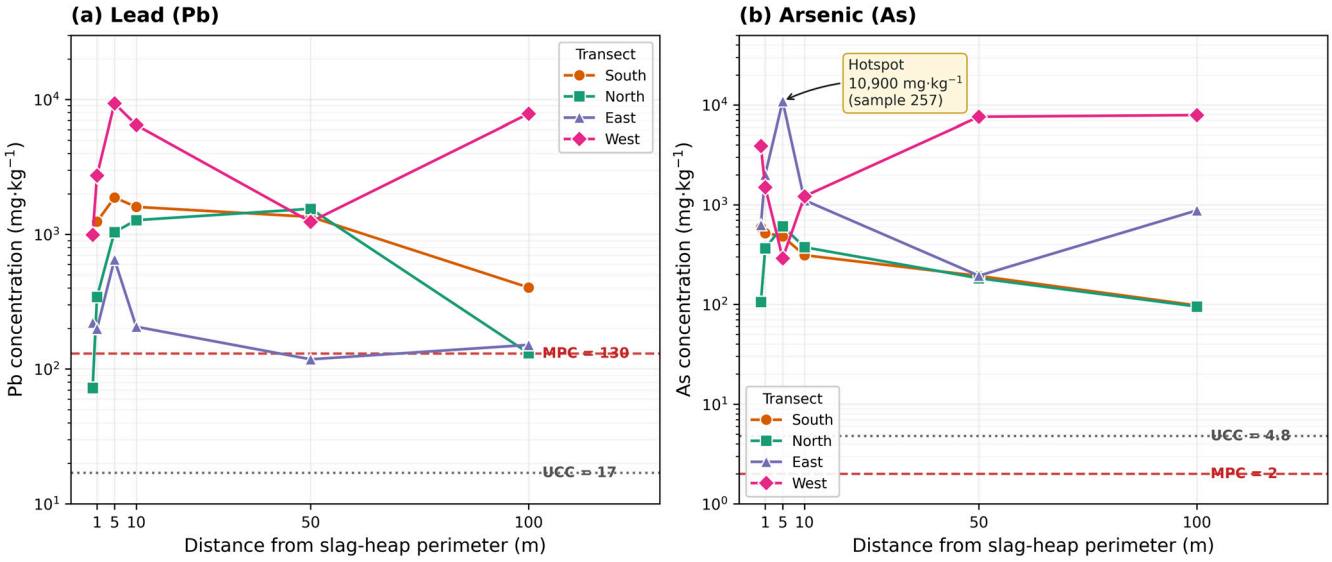


Figure 2. Heavy-metal concentrations along four cardinal-direction transects (south, north, east, west) from the slag heap perimeter at distances 0, 1, 5, 10, 50, and 100 m. (**a**) Lead (Pb): horizontal dashed line indicates the Kazakhstan MPC for Pb (130 mg·kg^{-1}); horizontal dotted line indicates the upper continental crust geochemical baseline for Pb (17 mg·kg^{-1}, Rudnick & Gao [28]). (**b**) Arsenic (As): horizontal dashed line indicates the Kazakhstan MPC for As (2 mg·kg^{-1}); horizontal dotted line indicates the upper continental crust geochemical baseline for As (4.8 mg·kg^{-1}). The y-axis is logarithmic in both subplots. The arsenic hotspot of 10,900 mg·kg^{-1} at the eastern transect 5 m point (sample 257) is annotated.

The highest single-sample concentrations were observed at 5 m on the western transect (sample 263): 9350 mg·kg^{-1} Pb (72× MPC), 290 mg·k^{-1} Cd (290× MPC), 2870 mg·kg^{-1} Zn (13× MPC), and 47.4 mg·kg^{-1} Hg (23× MPC), all co-occurring in a single soil aliquot. Arsenic peaked at 5 m on the eastern transect (sample 257) at 10,900 mg·kg^{-1}, exceeding the Kazakhstan MPC by 5450-fold and forming a discrete hotspot likely associated with arsenopyrite-bearing slag fragments (Section 4.5). Copper reached 4230 mg·kg^{-1} at 5 m on the southern transect (128× MPC), a finding not previously reported at this site. Chromium, nickel, and manganese remained at or below their respective MPCs at all transect points and showed *CF* and *EF* values consistent with a lithogenic origin (Table 2); these elements were therefore excluded from subsequent risk discussion.

The spatial distribution of metal concentrations was strongly asymmetric across cardinal directions, and the transect with the highest absolute single-sample peak was not always the transect with the highest mean concentration (Table 2). The western transect carried the highest mean values for Pb (4777 ± 3272 mg·kg^{-1}), Cd (165 ± 94), Hg (30 ± 18), and As (3735 ± 3044), and contained the absolute peak concentrations of Pb (9350 mg·kg^{-1} at West 5 m, sample 263), Cd (290 at the same point), Zn (2870 at the same point), and Hg (47.4 at the same point), all four metals co-occurring in a single soil aliquot.

Arsenic showed a contrasting spatial pattern. The absolute peak (10,900 mg·kg^{-1} at East 5 m, sample 257) occurred on the eastern transect, but the mean As concentration on the eastern transect (2621 ± 3743 mg·kg^{-1}) was lower than that on the western transect (3735 ± 3044 mg·kg^{-1}), because the eastern signal is dominated by a single extreme hotspot (10,900 mg·kg^{-1}) flanked by markedly lower concentrations at the other five

eastern sampling distances (630, 2010, 1113, 194, and 879 mg·kg^{-1} at 0, 1, 10, 50, and 100 m respectively), whereas the western transect exhibits broadly elevated As across multiple distances (3890 at 0 m, 7610 at 50 m, 7900 at 100 m), without any single extreme outlier. This pattern is consistent with two different contamination processes operating on the two transects: a discrete arsenopyrite-bearing slag fragment producing a localized point hotspot at East 5 m, versus broadly distributed atmospheric deposition and surface-runoff redistribution producing diffusely elevated As across the entire western transect.

Table 2. Mean ± SD and maximum-sample heavy-metal concentrations (mg·kg^{-1}) by cardinal-direction transect (n = 6 sampling distances per transect: 0, 1, 5, 10, 50, 100 m), reference samples, UCC, and Kazakhstan MPC. The "Maximum sample" row reports the absolute single-sample maximum measured anywhere at the site; the sampling location of each maximum is indicated in Section 3.1. UCC values from Rudnick and Gao [28].

Transect/Reference	Pb	Zn	Cd	Cu	As	Hg	Ni	Cr
South	1248 ± 466	1711 ± 808	27 ± 11	1387 ± 1377	366 ± 179	0.81 ± 0.81	17 ± 8	8 ± 4
North	735 ± 578	726 ± 481	14 ± 10	297 ± 195	289 ± 182	0.47 ± 0.16	9 ± 5	4 ± 2
East	258 ± 179	512 ± 301	8.5 ± 1.9	220 ± 72	2621 ± 3743	0.48 ± 0.30	6.7 ± 1.3	13 ± 13
West	4777 ± 3271	2066 ± 616	165 ± 94	832 ± 564	3735 ± 3043	30 ± 18	17 ± 6	12 ± 6
Site mean (n = 24)	1754 ± 2447	1254 ± 873	54 ± 80	684 ± 886	1753 ± 2832	8.0 ± 16	12 ± 7	9 ± 8
Bg_{300} (n = 1)	111	290	5.73	116	259	1.18	3.97	2.71
$Bg_{1.5\ km}$ (n = 1)	205	79	0.30	37.6	4.8	<0.1	29.9	98.2
UCC [28]	17	67	0.09	28	4.8	0.05	47	92
Kazakhstan MPC	130	220	1.0	33	2.0	2.1	85	100
Maximum sample	9350	2870	290	4230	10,900	48	n.d. *	n.d. *
Max sample/MPC	72×	13×	290×	128×	5450×	23×	<1×	<1×

Note: * Indicates values below detection limit (n.d.). The symbol × indicates fold-excess of Kazakhstan Maximum Permissible Concentration (e.g., 72× = 72-fold the MPC). Sample 260 (East 100 m) returned anomalously low Fe and Zn and was retained in concentration means but excluded from *EF* calculations. MPC = maximum permissible concentration for typical soils, Republic of Kazakhstan; UCC = upper continental crust.

Copper showed a third distribution pattern: although its mean was highest at the southern transect (1387 ± 1508 mg·kg^{-1}), the absolute peak (4230 mg·kg^{-1} at South 5 m, sample 245) was substantially higher than any value recorded on the western transect, indicating that Cu, like As, exhibits localized hotspot behavior rather than smooth radial decay. Pb concentrations did not decline monotonically with distance from the slag heap on either the western or northern transects: a secondary Pb maximum of 7850 mg·kg^{-1} was recorded at 100 m on the western transect, demonstrating that a simple radial dispersion model does not adequately describe the contamination plume around the heap. Together, these directional asymmetries—different mean-peak relationships across metals, secondary off-perimeter maxima, and the co-occurrence of multiple priority metals in a single West-transect aliquot—are consistent with patchy deposition controlled by the prevailing easterly–westerly wind regime, by topographic gradients, and by the discrete redistribution of arsenopyrite- and galena-bearing slag fragments during episodic surface-runoff events.

The two background reference samples revealed an instructive contrast (Table 2). The 300 m sample (Bg300) still showed clearly elevated As (259 mg·kg^{-1}), Cd (5.73), Hg (1.18), and Cu (116)—values 30–60× the UCC background—confirming that the impact zone of this site extends beyond 300 m. The 1.5 km sample (Bg1.5 km), in contrast, returned As, Cd, and Hg values close to UCC; however, its Pb concentration of 205 mg·kg^{-1} (12× UCC) indicates that aerial Pb deposition from the heap, or from related historical operations within the Achisai–Shymkent corridor, extends to at least 1.5 km. For this reason, all pollution indices reported here use UCC as the geochemical reference; the local 1.5 km sample is reported alongside for context but is not used as *B*n in *CF* and *Igeo* calculations.

The persistence of elevated As, Cd, Hg, and Cu at 300 m and of elevated Pb at 1.5 km most plausibly reflects three superimposed processes acting on overlapping timescales. First, long-range aeolian deposition of fine slag particulates (predominantly <10 µm aero-

dynamic diameter) accumulated during the multi-decadal operational period of the former Shymkent lead plant (c. 1940–2012) under the prevailing easterly and westerly wind regime [8]; particles in this size class can remain airborne over kilometre-scale distances under semi-arid conditions and account for the broad spatial footprint of the contamination signal documented at the 300 m reference point. Second, the site lies within the broader Achisai–Shymkent metallurgical corridor, which has hosted Pb–Zn extraction and processing since the early 20th century; the elevated Pb concentration of 205 mg·kg^{-1} at the 1.5 km reference point (12× UCC), in contrast to the near-UCC Cd, As, and Hg values at the same point, is consistent with a cumulative regional Pb-deposition signal that cannot be attributed to the present slag heap alone [9]. Third, episodic high-intensity precipitation events generate surface runoff that redistributes coarser arsenopyrite- and galena-bearing slag fragments along topographic gradients toward downslope catchment areas, producing localized off-perimeter hotspots inconsistent with a smooth radial decay model. Together, these three mechanisms—atmospheric dispersion, cumulative regional emissions, and runoff-mediated particulate redistribution—account for the observed extension of the impact zone well beyond 300 m and provide the methodological rationale for the use of UCC, rather than locally collected reference soils, as the geochemical baseline (Bn) in all index calculations reported below.

3.2. Geochemical Pollution Indices

All six pollution indices placed the site in the highest contamination categories for Pb, Cd, Zn, As, and Hg, while confirming that Cr, Ni, and Mn were within the lithogenic range (Table 3). Mean *CF* values were Cd = 597, As = 365, Hg = 160, Pb = 103, Cu = 24, and Zn = 19—all greatly exceeding the threshold of 6 for very high contamination [13,31]. Mean *Igeo* values placed Cd (7.4), As (6.5), Pb (4.9), Hg (4.0), and Zn (3.0) in the heavily-to-extremely contaminated range; the corresponding maxima (Cd 11.1, As 10.6, Hg 9.3, Pb 8.5, Cu 6.7) all reached *Igeo* Class 6 (extreme contamination, *Igeo* > 5). Of the 24 transect samples, Class 6 was reached by 22 samples for Cd, 18 for As, 14 for Pb, 6 for Hg, and 3 for Cu.

Table 3. Geochemical pollution indices for individual heavy metals at the Shymkent Pb–Zn slag reprocessing site, referenced to the upper continental crust [28]. Values are mean (max) across 24 transect samples; *EF* based on n = 23 after exclusion of sample 260.

Metal	*CF* Mean (Max)	I_{geo} * Mean (Max)	*EF* Mean (Max)	I_{geo} Cl. 6 (n/24)	Classification
Pb	103 (550)	4.93 (8.52)	2369 (15,511)	14	Extreme
Zn	19 (43)	3.03 (4.84)	391 (1208)	0	Heavily contaminated
Cd	597 (3222)	7.37 (11.07)	11,501 (90,871)	22	Extreme
Cu	24 (151)	3.27 (6.65)	526 (3117)	3	Extreme
As	365 (2271)	6.51 (10.56)	5066 (30,008)	18	Extreme
Hg	160 (948)	3.99 (9.30)	3654 (26,735)	6	Extreme
Cr	0.10 (0.40)	−4.33 (−1.90)	1.7 (6.4)	0	Lithogenic
Ni	0.26 (0.58)	−2.79 (−1.38)	5.2 (16.3)	0	Lithogenic

CF—contamination factor; *Igeo* *—geoaccumulation index; EF—Fe-normalized enrichment factor. EF > 40 indicates exclusively anthropogenic origin [34]. Aggregate indices: PLI mean = 9.6 (max 35.5); mCd mean = 141 (max 652); RI mean = 28,605 (max 138,355). See Section 3.2 for classifications and interpretations.

Enrichment factors (Fe-normalized) far exceeded the conventional threshold of 40, taken to indicate an exclusively anthropogenic origin [34]: mean *EF* values reached 11,501 for Cd, 5066 for As, 3654 for Hg, 2369 for Pb, and 526 for Cu, with sample-level maxima of 90,871 (Cd), 30,008 (As), and 26,735 (Hg). *EF* values for Cr (mean 1.7), Ni (5.2), and Mn (5.9) remained below 10, confirming a lithogenic origin for these elements and supporting the choice of Fe as the normalizing element. The combined indices *PLI* (mean 9.6, max

35.5), *mCd* (mean 141, max 652), and *RI* (mean 28,605, max 138,355) all classified the site as ultra-high multi-element contamination, with *RI* exceeding the conventional very-high threshold of 600 by approximately two orders of magnitude. Among individual element contributions to the Hakanson *RI*, mercury and cadmium dominated (mean Er for Hg = 6396; for Cd = 5370; for As = 3652) owing to their high toxic-response factors of 40 and 30, respectively [30]; lead, despite the highest absolute concentrations, contributed proportionally less (mean Er = 516).

The fold-excess values of all indices relative to Kazakhstan MPC are presented in Table 4.

Table 4. Heavy-metal concentrations (mg·kg^{-1} dry weight) in composite above-ground plant tissue at the four cardinal-direction transects, listed in order of increasing mean soil Cd concentration. Each composite comprised approximately equal biomass of *Centaurea pseudosquarrosa* and *Plantago lanceolata*.

Transect	Soil Cd Mean (mg·kg^{-1})	Pb (Plant)	Zn (Plant)	Cd (Plant)	Cu (Plant)	As (Plant)	Hg (Plant)
East	8.5	93.7	1120	44.8	337	<0.2	<0.1
North	14.0	221	1080	38.8	300	<0.2	<0.1
South	26.7	134	426	17.5	156	<0.2	<0.1
West	165	206	932	18.6	288	<0.2	<0.1

All plant concentrations in mg·kg^{-1} dry weight. As <0.2 and Hg < 0.1 mg·kg^{-1} are method detection limits in the plant matrix, values are reported as half the detection limit for downstream calculations.

3.3. Vegetation Tissue Analysis and Bulk Canopy Ratios

The bulk vegetative canopy ratio (C_{plant}/C_{soil}-mean) calculated for each cardinal-direction composite is reported in Table 5.

The ratio varied substantially across directions: on the eastern transect, where mean soil contamination was moderate, the ratios for Cd (5.24), Zn (2.19), and Cu (1.53) exceeded 1, indicating that the combined above-ground tissue burden of the two species exceeded the corresponding mean soil concentration. On the northern transect, the ratios for Cd (2.76) and Zn (1.49) also exceeded 1, while at the southern and western transects, where mean soil contamination was intermediate to extreme, all ratios were below 1 (e.g., Cd 0.66 south, 0.11 west; Pb 0.11 south, 0.04 west). Across the four directional composites, the bulk canopy ratio for Cd, Pb, and Zn decreased visually with increasing mean soil contamination.

Table 5. Bulk vegetative canopy ratios (C_{plant}/C_{soil}-mean) for composite plant tissue (combined *Centaurea pseudosquarrosa* and *Plantago lanceolata*, approximately equal biomass proportions) at the four cardinal-direction transects. The ratios are reported as a descriptive index of combined above-ground metal burden across the two species, not as a species-resolved Bioconcentration Factor; uptake-strategy classification is not invoked here because composite samples do not permit species-level physiological interpretation (see Section 4.3).

Transect	*BCF* Pb	*BCF* Zn	*BCF* Cd	*BCF* Cu
East	0.36	2.19	5.24	1.53
North	0.30	1.49	2.76	1.01
South	0.11	0.25	0.66	0.11
West	0.04	0.45	0.11	0.35

Ratios are unitless. As and Hg were excluded from the ratio calculation because plant concentrations were below detection limits at all four directional composites (Table 4). The Baker [36] excluder/accumulator/hyperaccumulator framework requires species-level measurements and is not applied to these composite values.

These ratios are reported here as descriptive bulk-canopy observations only. They do not support inference about the metal-uptake strategy of either constituent species,

because each composite combined approximately equal biomass proportions of *Centaurea pseudosquarrosa* (*Asteraceae*) and *Plantago lanceolata* (*Plantaginaceae*), and the resulting signal averages potentially divergent species-level uptake, translocation, and detoxification patterns into a single value (Section 4.3). For the same reason, no inferential statistical test (rank-based or parametric correlation) is reported across these four composite values: with a single observation per cardinal direction and biologically heterogeneous composites, such tests would have negligible statistical power and would not constitute meaningful evidence for a soil-to-plant relationship. The directional pattern is noted here as a visual observation that motivates expanded, species-resolved, replicated sampling in the next phase of the project (Section 4.5).

3.4. Human-Health and Ecosystem Risk

Health and ecosystem risk metrics for the adult occupational scenario are summarized in Table 6. The total carcinogenic risk at the worst-case sampling point reached CR = 4.3×10^{-3}, exceeding the US EPA acceptable threshold of 10^{-4} by 43-fold and the negligible threshold of 10^{-6} by 4310-fold. Arsenic was the dominant contributor (92.7% of CR), followed by cadmium (7.3%); chromium and nickel together contributed less than 0.01%. Across the 24 transect samples, the site-mean carcinogenic risk was $CR = 7.0 \times 10^{-4}$, still 7-fold above the US EPA acceptable limit. The non-carcinogenic hazard index reached $HI = 26.6$ at the worst-case sampling point (As-driven, 93%; Pb 5%; Cd 1%) and $HI = 4.3$ at the site mean—both far above the threshold of 1, indicating adverse non-carcinogenic effects.

Ecosystem risk, based on PEC/PNEC ratios, reached $RCR_{total} = 223$ at the site mean, with cadmium as the dominant component ($RCR_{Cd} = 96$, 43% of total), followed by arsenic ($RCR_{As} = 60$, 27%), mercury ($RCR_{Hg} = 36$, 16%), copper ($RCR_{Cu} = 11$), zinc ($RCR_{Zn} = 10$), and lead ($RCR_{Pb} = 8$). Although Pb dominated the absolute mass loading and the individual ecological risk index in the Hakanson framework (mean $Er_{Pb} = 516$), Cd emerged as the dominant ecological-risk driver in the *PEC/PNEC* framework, owing to its extremely low PNEC (0.56 mg·kg^{-1}) and high bioavailability under the site's neutral-to-alkaline soil conditions (pH 7.5–8.5). Arsenic contributed comparably high ecosystem risk in absolute terms—a finding not captured by the Hakanson framework alone and one that motivates the dual As + Cd priority-contaminant designation argued in Section 4.

Table 6. Summary of human-health and ecosystem risk at the Shymkent slag reprocessing site. Worst-case = sampling point with highest single-metal concentration (As: East 5 m, sample 257; other metals: West 5 m, sample 263). Site mean = mean across 24 transect samples.

Risk Metric	Worst Case	Site Mean	Threshold	Interpretation
Carcinogenic risk (*CR*)	4.3×10^{-3}	7.0×10^{-4}	10^{-6} negligible; 10^{-4} acceptable	Unacceptable
Non-carcinogenic hazard index (*HI*)	26.6	4.3	1.0	Adverse effects expected
RCR_{total}	—	223	1.0	Critical ecosystem risk
RCR_{Cd}	—	96	1.0	Dominant ecological driver
RCR_{As}	—	60	1.0	Critical
RCR_{Hg}	—	36	1.0	Critical
RCR_{Cu}	—	11	1.0	Very high
RCR_{Zn}	—	10	1.0	Very high
RCR_{Pb}	—	8.3	1.0	High

4. Discussion

The geochemical, plant-tissue, and risk evidence presented above place the Shymkent Pb–Zn slag reprocessing site among the most severely contaminated metallurgical legacy sites documented in Central Asia and globally. In the following sections, we develop the implications of this evidence for contaminant prioritization, vegetation-mediated containment, and site management.

4.1. Contamination Context

Peak soil concentrations at Shymkent (Pb 9350, Zn 2870, Cd 290, Cu 4230, As 10,900, Hg 47.4 mg·kg^{-1}) substantially exceed both Kazakhstan MPC values and concentrations reported for analogous Pb–Zn smelter-affected soils on three continents (Table 7). Among published comparator sites, only the Kabwe mine–smelter complex in Zambia approaches the Pb maximum recorded here, whereas the Cd, Cu, As, and Hg maxima at Shymkent exceed all listed comparators by factors of 4–100×. Notably, the 10,900 mg·kg^{-1} maximum at the eastern transect 5 m point is unprecedented at Pb–Zn smelter sites globally and is a defining feature of this site, warranting its independent recognition as an As-priority contamination zone. This designation is supported by three additional lines of evidence within our dataset. First, the high *Igeo* class 6 frequency for As (18 of 24 transect samples; Table 3) shows that extreme As contamination is not confined to the 10,900 mg·kg^{-1} hotspot but extends across most of the impact zone. Second, the As enrichment factor (mean 5066; maximum 30,008; Table 3) exceeds the conventional threshold for exclusive anthropogenic origin [34] by two to three orders of magnitude, confirming that the As burden cannot be attributed to natural lithogenic variability [28]. Third, As dominates the site's carcinogenic risk profile (92.7% of *CR* at the worst-case point and the dominant contributor to site-mean *CR*; Table 6), elevating the human-health relevance of the As signal above that of any other detected metal at this site. Together with the unprecedented maximum concentration, these spatial, geochemical, and toxicological lines of evidence justify the independent recognition of this site as an As-priority contamination zone.

The hierarchy $EF_{Cd} > EF_{As} > EF_{Hg} >$ EFPb $> EF_{Zn}$ differs from the $EF_{Pb} > EF_{Zn} > EF_{Cd}$ ranking commonly reported at Western European and Chinese Pb–Zn smelter sites [15,16], reflecting the unusually heavy contribution of Cd and As to the Shymkent contamination signature. This is consistent with the polymetallic ore feed of the Achisai deposit, in which arsenopyrite, sphalerite, and Cd-bearing sulfides constitute a larger proportion of the original ore than at most monometallic Pb–Zn operations.

Table 7. Comparison of peak concentrations (mg·kg^{-1}) of priority metals in soils at the Shymkent slag reprocessing site with published values from representative Pb–Zn smelter-affected soils worldwide.

Site	Country	Pb	Zn	Cd	As	Source
Shymkent slag site	Kazakhstan	9350	2870	290	10,900	Present study
Henan Pb–Zn smelter	China	up to ~8000	1526–6812	4.5–28.3	n.d.	[15]
Příbram smelter	Czech Republic	1200–5600	410–2800	3.2–18	20–80	[16]
Kentau–Aksu corridor	Kazakhstan	300–1500	180–620	0.4–1.65	n.d.	[17]
Middle Spiš Pb–Zn–Cu–Hg mining area	Slovakia	340–1850	290–960	1.2–6.8	n.d.	[18]
Kabwe mine/smelter	Zambia	780–14,100	n.d.	2.1–48	n.d.	[9]

n.d. = not determined/not reported in the cited study.

4.2. Arsenic and Cadmium as Co-Priority Contaminants

The risk-assessment results (Section 3.4) reveal a striking disconnect between mass-based and toxicity-based contaminant prioritization at this site [37]. By mass, Pb dominates the soil burden at most sampling points and is the contaminant most readily addressed by

conventional regulatory frameworks. However, the human-health risk assessment identifies arsenic as the dominant driver of carcinogenic and non-carcinogenic risk (92.7% of CR; 93% of *HI* at the worst-case point), reflecting both the extreme As hotspot of 10,900 mg·kg^{-1} on the eastern transect and the high IRIS slope factor for inorganic As (SFinh = 15.1 (mg·kg^{-1}·d^{-1})$^{-1}$). The ecosystem risk assessment, in turn, identifies cadmium as the dominant driver (RCR_{Cd} = 96, 43% of the total) owing to its extremely low PNEC (0.56 mg·kg^{-1}) and high bioavailability under the neutral-to-alkaline soil conditions documented at this site (pH 7.5–8.5).

Three structural causes explain the disconnect between mass-based and toxicity-based prioritization and clarify why the contaminant with the largest absolute soil burden need not be the dominant driver of risk at the same site. First, the IRIS inhalation slope factor for inorganic arsenic (SFinh = 15.1 (mg·kg^{-1}·d^{-1})$^{-1}$) is approximately three orders of magnitude higher than that of lead and four orders of magnitude higher than that of zinc, so that [37] even a moderately elevated As concentration produces a far larger contribution to *CR* than a much higher Pb concentration at the same point. Second, the REACH-derived *PNEC* for soil cadmium (0.56 mg·kg^{-1}) is the lowest among the eight priority metals assessed here—roughly 400× lower than the *PNEC* for Pb (212 mg·kg^{-1}) [29]—so that even modest Cd enrichment produces a disproportionately large RCR_{Cd} in the ecosystem risk framework. Third, the neutral-to-alkaline soil conditions documented at this site (pH 7.5–8.5) preferentially mobilize Cd^{2+} relative to Pb^{2+}, because Pb^{2+} is strongly retained by carbonate and Fe-oxide surfaces under these conditions, whereas Cd^{2+} is comparatively more bioavailable to plant roots and soil organisms [40]. The combined effect of these three factors—differential toxicological potency, differential PNEC stringency, and differential pH-dependent bioavailability—is that absolute mass loading and toxicity-weighted risk identify different priority contaminants at the same site, even when measured concentrations and risk frameworks are both internally consistent.

These three lines of evidence—mass loading, human-health risk, and ecosystem risk—therefore identify three priority contaminants (Pb, As, and Cd, respectively). A defensible management framework for this site must address all three simultaneously rather than treating Pb in isolation. Approaches that reduce Pb mobility without addressing Cd or As—such as phosphate amendments that form stable pyromorphite [$Pb_5(PO_4)_3Cl$] but leave Cd and As in exchangeable form—would fail to reduce the principal ecosystem and human-health risk drivers. Conversely, a strategy targeting only the As hotspot would overlook the broadly distributed Cd and Pb burden across the impact zone. The implication is clear: Pb–Zn smelter legacy sites should not be classified or prioritized based on Pb concentration alone, particularly at sites with polymetallic ore feeds.

4.3. Vegetation Biomonitoring: Bulk Canopy Metal Burden

Composite aboveground plant tissue (a mixture of *Centaurea pseudosquarrosa* and *Plantago lanceolata*, with approximately equal biomass proportions) was analyzed along the four cardinal-direction transects to characterize the bulk metal burden carried by the dominant native vegetation canopy at the site. Tissue Cd concentrations ranged from 17.5 mg·kg^{-1} DW (south) to 44.8 mg·kg^{-1} DW (east); tissue Zn from 426 to 1120 mg·kg^{-1} DW; and tissue Pb from 93.7 to 221 mg·kg^{-1} DW (Table 4). Arsenic and mercury concentrations in plant tissue were below detection limits in all four directions, despite very high soil concentrations of these elements on the western and eastern transects.

The bulk canopy ratio Cplant/Csoil (Table 5) exceeded 1 for several metals at the eastern and northern transects (Cd 5.24 and 2.76; Zn 2.19 and 1.49) and was consistently below 1 across all metals at the southern and western transects, where soil contamination was most severe. These ratios reflect the combined aboveground burden of the two species;

they do not allow either species to be classified as an excluder or an accumulator in the sense of Baker [36], because the underlying composite samples conflate species-specific uptake, translocation, and detoxification patterns into a single signal. *C. pseudosquarrosa* (*Asteraceae*) and *P. lanceolata* (*Plantaginaceae*) belong to phylogenetically distinct families that can exhibit opposite uptake strategies at the same site [14,41,42]; the composite design therefore averages potentially divergent species-level behaviors into an undifferentiated bulk signal that lacks a straightforward physiological interpretation.

For the same reason, the apparent inverse rank ordering between mean soil Cd, Pb, or Zn and the corresponding bulk canopy ratio across the four directional composites is interpreted here as a descriptive observation only. No mechanistic inference about physiological down-regulation of root uptake, selective mortality of accumulator phenotypes, or rhizosphere biogeochemical immobilization can be drawn from these four data points: each direction yielded a single composite sample combining two species, and species-resolved tissue concentrations, paired root–shoot transfer factors, and rhizosphere chemistry would all be required to support any such interpretation. The data presented here, therefore, document the combined metal burden in the dominant above-ground vegetation at this site but do not provide evidence of the metal-uptake strategy of either constituent species.

Species-resolved tissue analysis, with paired root and shoot sampling of *C. pseudosquarrosa* and *P. lanceolata* analyzed independently and replicated within each cardinal direction, is mandatory before any uptake-strategy interpretation can be supported. This species-resolved campaign is scheduled within the 2026–2028 continuation of the AP25795537 project (Section 4.6). Pending those data, no recommendation regarding the phytostabilization or phytoremediation potential of either species can be drawn from the present bulk-canopy results, and any such recommendation in the present manuscript has been removed.

4.4. Implications for Site Management

Integrating geochemical severity, plant biomonitoring, and risk-assessment data supports a preliminary three-tier zonation for remediation prioritization. Framed as a sustainable management strategy, this zonation is designed to reconcile two objectives often treated separately at legacy sites: recovering residual value from the slag as a secondary raw material and arresting the off-site migration of contaminants that threaten adjacent agricultural land, the Badam River, and the residential districts of Shymkent. The three tiers are:

Zone 1 (0–10 m perimeter; $PLI > 20$; $RCR_{total} > 100$): Active engineered intervention is essential. Options include (i) physical containment of the slag heap with a multilayer cover and surface stabilization; (ii) selective pyrometallurgical reprocessing of the slag, which has been shown to recover >70% of residual Zn and Pb from comparable feedstock while fixing Cd in stable gangue phases [4,5]; and (iii) hotspot excavation and off-site treatment of the highest As-bearing zones (e.g., East 5 m). Selective pyrometallurgical reprocessing, in particular, not only reduces the residual metal burden at this site but also offers a circular-economy pathway for resource recovery from secondary metallurgical materials, simultaneously addressing contamination and resource-recovery opportunities. The Badam River, located 20 m west of the facility, makes runoff control a particular priority for this zone; direct quantification of fluvial metal transport through dedicated sediment sampling is scheduled for the next phase of the project (Section 4.6).

Zone 2 (10–100 m; PLI 5–20; RCR_{total} 10–100): Phytostabilization using *C. pseudosquarrosa* and *P. lanceolata*, potentially combined with mycorrhizal inoculation and biochar amendment, is a cost-effective intervention pending the confirmatory studies outlined in Section 4.3. Concurrent monitoring of plant tissue concentrations, soil pH, and DTPA-extractable Cd should accompany any pilot-scale deployment.

Zone 3 (>100 m; $PLI < 5$; $RCR_{total} < 10$): Monitored natural attenuation with periodic resampling is appropriate, with priority attention to the west, where elevated concentrations were detected at 100 m and the 1.5 km background sample also showed elevated Pb. The persistence of measurable Pb deposition at 1.5 km has direct implications for residential exposure risk in the western and southwestern districts of Shymkent and warrants integration with city-level air-quality monitoring data.

4.5. Limitations

Several limitations of this study should be acknowledged. The most important is the composite vegetation-sampling design: as noted in Section 2.2, each directional plant sample pooled two phylogenetically distinct species—*Centaurea pseudosquarrosa* (*Asteraceae*) and *Plantago lanceolata* (*Plantaginaceae*)—in approximately equal proportions, so the resulting C_{plant}/C_{soil} ratios reflect a bulk canopy burden and cannot be interpreted in terms of species-level uptake strategy or the excluder/accumulator categories of Baker [36]; the four-direction design also precludes inferential statistics on the plant data (Section 3.3). Second, the study rests on a single April 2026 topsoil (0–50 cm) campaign and therefore does not capture seasonal variability in metal mobility under the episodic moisture regime of the semi-arid Turkestan Region; in particular, the As hotspot at sample 257 (East 5 m, 10,900 $mg \cdot kg^{-1}$) is likely associated with discrete arsenopyrite-bearing slag fragments rather than a smooth concentration gradient, which finer-resolution sampling along the eastern transect would resolve. Third, the human-health risk estimates (Section 2.6) are deterministic single-point values calculated from US EPA RAGS default exposure factors for an adult occupational scenario, without adjustment for site-specific conditions; given the arid, high-wind, dust-prone climate of Shymkent, the reported worst-case CR of 4.3×10^{-3} and *HI* of 26.6 should be regarded as conservative screening estimates rather than best-estimate central tendencies. These limitations directly define the priority directions for follow-up research set out in Section 4.6.

4.6. Future Research Directions

Priority directions for follow-up research are outlined in the 2026–2028 continuation of the AP25795537 research project and comprise five interlinked work packages. First, seasonal resampling of the impact zone is planned for spring, summer, and autumn 2026–2027 to capture temporal variability in metal mobility, dust deposition, and surface runoff under contrasting moisture regimes. Second, BCR sequential extraction [43] is scheduled for the 2027 analytical campaign on archived and freshly collected soil samples to determine operationally defined speciation of Pb, Zn, Cd, and As and to refine bioavailability estimates beyond the total-concentration measurements reported here. Third, species-resolved tissue analysis with paired root and shoot sampling of *Centaurea pseudosquarrosa* and *Plantago lanceolata* is planned for the 2026–2027 vegetation campaign to compute species-level transfer factors, distinguish the physiological and ecological mechanisms underlying the community-level accumulator-to-excluder shift documented in this study, and confirm or refine the preliminary phytostabilizer designation. Fourth, a dedicated Badam River sediment-sampling campaign is scheduled for August–September 2026. Fifth, a probabilistic Monte Carlo re-analysis of the human-health risk component is planned for the 2027 modeling campaign, incorporating site-specific occupational exposure parameters (localized inhalation, ingestion, and dermal adherence distributions for outdoor industrial workers in semi-arid urban settings) and a seasonal wind-blown dust factor; this analysis will replace the deterministic *CR* and *HI* point estimates reported here with full probability distributions, allowing direct evaluation of exceedance probability at the US EPA 10^{-4} and 10^{-6} thresholds. Together, these scheduled activities will deliver the species-, season-,

speciation-, and uncertainty-resolved evidence base required to support the operational deployment of the three-tier remediation framework proposed here.

Complete methodological details, supplementary data tables, and additional analytical results, including per-sample heavy-metal concentrations, computed pollution indices, and risk metrics for all sampled locations, are provided in the Supplementary Materials.

5. Conclusions

Integrated geochemical, vegetation, and risk assessment at an active Pb–Zn slag reprocessing site in Shymkent (Southern Kazakhstan) places it among the most severely contaminated Pb–Zn legacy sites documented in Central Asia and globally: cadmium and arsenic reached Geoaccumulation Class 6 across most of the impact zone, and enrichment factors for all six priority metals exceeded the anthropogenic-origin threshold by two to three orders of magnitude.

The principal contribution of this work is the identification of three distinct priority contaminants, depending on the assessment framework—lead by absolute mass loading, arsenic by human health risk (at worst-case points, >90% of the carcinogenic risk and hazard index), and cadmium by ecosystem risk. This disconnect between mass-based and toxicity-based prioritization argues for elevating arsenic and cadmium to co-priority status alongside lead at polymetallic Pb–Zn legacy sites, rather than targeting Pb in isolation. Composite vegetation analysis documented the bulk above-ground canopy burden but, by design, does not support species-level uptake inference; therefore, species-resolved tissue analysis is identified as a mandatory next step before any phytoremediation recommendation can be made (Sections 4.5 and 4.6).

The integrated framework deployed here is directly transferable to analogous Pb–Zn reprocessing legacy sites and supports a three-tier zonation for remediation prioritization: active engineered intervention within the 0–10 m perimeter, pilot interventions and further characterization in the 10–100 m zone, and monitored attenuation beyond 100 m. By coupling secondary resource recovery with contamination control, this evidence-based framework advances the sustainable rehabilitation of metallurgical legacy land and contributes to UN Sustainable Development Goals 3, 11, 12, and 15.

Supplementary Materials: The following supporting information can be downloaded at: https://www.mdpi.com/article/10.3390/su18136742/s1, Table S1: Manuscript: Arsenic and cadmium as co-priority contaminants alongside lead at a Pb–Zn slag reprocessing site in Southern Kazakhstan. Per-sample heavy-metal concentrations (As, Cd, Cr, Cu, Fe, Hg, Mn, Ni, Pb, Zn) and computed pollution indices (*CF*, *Igeo*, *EF*, *PLI*, m_{Cd}, RI), bioconcentration factors, and human-health and ecosystem risk metrics for all 24 transect soil samples, 2 background reference samples, and 4 composite plant tissue samples.

Author Contributions: Conceptualization, Z.P. and A.A. (Akbota Aitimbetova); methodology, Z.P.; validation, Z.P., A.A. (Akbota Aitimbetova), and A.A. (Azhar Abubakirova); formal analysis, Z.P.; investigation, Z.P., A.A. (Akbota Aitimbetova), and A.A. (Azhar Abubakirova); resources, Z.P.; data curation, Z.P.; writing—original draft preparation, Z.P.; writing—review and editing, A.A. (Akbota Aitimbetova) and A.A. (Azhar Abubakirova); visualization, A.A. (Akbota Aitimbetova); supervision, Z.P.; project administration, Z.P.; funding acquisition, Z.P. All authors have read and agreed to the published version of the manuscript.

Funding: This research has been funded by the Science Committee of the Ministry of Education and Science of the Republic of Kazakhstan (Grant No. AP25795537) titled "Ecological assessment of the locations of lead-zinc slags on environmental objects and the development of technology for the reclamation of slag heaps".

Institutional Review Board Statement: Not applicable.

Informed Consent Statement: Not applicable.

Data Availability Statement: The raw data supporting the conclusions of this article will be made available by the authors on request. These include soil geochemical data, plant tissue analyses, pollution indices, and risk assessment metrics for all sampled locations.

Acknowledgments: The authors thank the site operator for granting access to the study area during the sample-collection campaign and the staff of the accredited Analytical Laboratory of LLP «KazEcoAnaliz» (Almaty, Kazakhstan) for analytical support.

Conflicts of Interest: The authors declare no conflicts of interest. The funding from the Science Committee of the Ministry of Education and Science of the Republic of Kazakhstan (Grant No. AP25795537) did not involve any commercial interest or influence on the research design, data collection, analysis, or conclusions.

Abbreviations

The following abbreviations are used in this manuscript:

ANOVA	Analysis of Variance
BCF	Bioconcentration Factor
BCR	Community Bureau of Reference (sequential extraction protocol)
CDI	Chronic Daily Intake
CF	Contamination Factor
CR	Carcinogenic Risk
DW	Dry Weight
ECHA	European Chemicals Agency
EF	Enrichment Factor
Eri	Individual ecological risk factor
GOST	State Standard (Gosudarstvennyy Standart)
HI	Hazard Index
HSD	Honest Significant Difference (Tukey post hoc test)
ICP-OES	Inductively Coupled Plasma Optical Emission Spectrometry
Igeo	Geoaccumulation Index
IRIS	Integrated Risk Information System
ISO	International Organization for Standardization
m_{Cd}	modified Degree of Contamination
MPC	Maximum Permissible Concentration
OECD	Organization for Economic Co-operation and Development
PEC	Predicted Environmental Concentration
PLI	Pollution Load Index
PNEC	Predicted No-Effect Concentration
RAGS	Risk Assessment Guidance for Superfund
RCR	Risk Characterization Ratio
RfD	Reference Dose
RI	Potential Ecological Risk Index
SD	Standard Deviation
SEM-EDS	Scanning Electron Microscopy—Energy-Dispersive Spectroscopy
SF	Slope Factor
TF	Transfer Factor
Tri	Toxic Response Factor
UCC	Upper Continental Crust
US EPA	United States Environmental Protection Agency

References

1. Zhou, H.; Yang, W.-T.; Zhou, X.; Liu, L.; Gu, J.-F.; Wang, W.-L.; Zou, J.-L.; Tian, T.; Peng, P.-Q.; Liao, B.-H. Accumulation of Heavy Metals in Vegetable Species Planted in Contaminated Soils and the Health Risk Assessment. *Int. J. Environ. Res. Public Health* **2016**, *13*, 289. [CrossRef] [PubMed]
2. Pająk, M.; Błońska, E.; Szostak, M.; Gąsiorek, M.; Pietrzykowski, M.; Urban, O.; Derbis, P. Restoration of Vegetation in Relation to Soil Properties of Spoil Heap Heavily Contaminated with Heavy Metals. *Water Air Soil Pollut.* **2018**, *229*, 392. [CrossRef] [PubMed]
3. Zhao, Y.; Wang, J.; Zhang, G.; Liu, L.; Yang, J.; Wu, X.; Biradar, C.; Dong, J.; Xiao, X. Divergent Trends in Grassland Degradation and Desertification under Land Use and Climate Change in Central Asia from 2000 to 2020. *Ecol. Indic.* **2023**, *154*, 110737. [CrossRef]
4. Terzić, A.; Stojanović, J.; Jovanović, V.; Todorović, D.; Sokić, M.; Bojović, D.; Radulović, D. Exploring the Efficiency of Magnetic Separation and Gravity Concentration for Valorizing Pb-Zn Smelter Slag in a Circular Economy Framework. *Materials* **2024**, *17*, 3945. [CrossRef] [PubMed]
5. Nowińska, K.; Kokowska-Pawłowska, M. Mineralogy of Zinc and Lead Metallurgical Slags in Terms of Their Impact on the Environment: A Review. *Minerals* **2024**, *14*, 852. [CrossRef]
6. Gil-Loaiza, J.; Field, J.P.; White, S.A.; Csavina, J.; Felix, O.; Betterton, E.A.; Sáez, A.E.; Maier, R.M. Phytoremediation Reduces Dust Emissions from Metal(Loid)-Contaminated Mine Tailings. *Environ. Sci. Technol.* **2018**, *52*, 5851–5858. [CrossRef] [PubMed]
7. Kicińska, A. Physical and Chemical Characteristics of Slag Produced during Pb Refining and the Environmental Risk Associated with the Storage of Slag. *Environ. Geochem. Health* **2021**, *43*, 2723–2741. [CrossRef] [PubMed]
8. Salim, Y.; Issayeva, A.; Kidirbayeva, K.; Zhumadulayeva, A.I.; Dossybayeva, G.; Bozhbanbayeva, N.; Ashirbayeva, S. Influence of Lead-Zinc Slags of the Shymkent City on the Environment. *J. Ecol. Eng.* **2022**, *23*, 83–89. [CrossRef]
9. Junusbekov, M.M.; Akbasova, A.D.; Seidakbarova, A.D.; Koishiyeva, G.Z.; Sainova, G.A. Ecological Assessment of Soil Contamination by Heavy Metals Affected in the Past by the Lead–Zinc Mining and Processing Complex in Kentau, Kazakhstan. *Environ. Monit. Assess.* **2023**, *195*, 586. [CrossRef] [PubMed]
10. Faurat, A.; Yessimova, D.; Satybaldiyeva, G.; Kuatbayev, A.; Utarbayeva, A.; Kaliyeva, A.; Akhmetov, K.; Mulk Khan, S.; Ahmad, Z.; Rakhmanov, S. Assessing the Spatial Distribution and Sources of Heavy Metal Pollution in the Snow Cover: A Case Study from Pavlodar, Northeastern Kazakhstan. *PLoS ONE* **2025**, *20*, e0322300. [CrossRef] [PubMed]
11. Zhyrgalova, A.; Yelemessov, S.; Ablaikhan, B.; Aitkhozhayeva, G.; Zhildikbayeva, A. Assessment of Potential Ecological Risk of Heavy Metal Contamination of Agricultural Soils in Kazakhstan. *Braz. J. Biol.* **2024**, *84*, e280583. [CrossRef] [PubMed]
12. Wang, L.; Lv, Y.; Huang, S.; Liu, Y.; Li, X. The Evolution of Research on C&D Waste and Sustainable Development of Resources: A Bibliometric Study. *Sustainability* **2023**, *15*, 9141. [CrossRef]
13. Kowalska, J.B.; Mazurek, R.; Gąsiorek, M.; Zaleski, T. Pollution Indices as Useful Tools for the Comprehensive Evaluation of the Degree of Soil Contamination—A Review. *Environ. Geochem. Health* **2018**, *40*, 2395–2420. [CrossRef] [PubMed]
14. Nadgórska-Socha, A.; Ptasiński, B.; Kita, A. Heavy Metal Bioaccumulation and Antioxidative Responses in Cardaminopsis Arenosa and Plantago Lanceolata Leaves from Metalliferous and Non-Metalliferous Sites: A Field Study. *Ecotoxicology* **2013**, *22*, 1422–1434. [CrossRef] [PubMed]
15. Yang, L.; Ge, S.; Liu, J.; Iqbal, Y.; Jiang, Y.; Sun, R.; Ruan, X.; Wang, Y. Spatial Distribution and Risk Assessment of Heavy Metal(Oid)s Contamination in Topsoil around a Lead and Zinc Smelter in Henan Province, Central China. *Toxics* **2023**, *11*, 427. [CrossRef] [PubMed]
16. Ettler, V. Soil Contamination near Non-Ferrous Metal Smelters: A Review. *Appl. Geochem.* **2016**, *64*, 56–74. [CrossRef]
17. Angelovičová, L.; Lodenius, M.; Tulisalo, E.; Fazekašová, D. Effect of Heavy Metals on Soil Enzyme Activity at Different Field Conditions in Middle Spis Mining Area (Slovakia). *Bull. Environ. Contam. Toxicol.* **2014**, *93*, 670–675. [CrossRef] [PubMed]
18. Tembo, B.D.; Sichilongo, K.; Cernak, J. Distribution of Copper, Lead, Cadmium and Zinc Concentrations in Soils around Kabwe Town in Zambia. *Chemosphere* **2006**, *63*, 497–501. [CrossRef] [PubMed]
19. Wang, S.; Han, Z.; Wang, J.; He, X.; Zhou, Z.; Hu, X. Environmental Risk Assessment and Factors Influencing Heavy Metal Concentrations in the Soil of Municipal Solid Waste Landfills. *Waste Manag.* **2022**, *139*, 330–340. [CrossRef] [PubMed]
20. Tleuova, Z.; Snow, D.D.; Mukhamedzhanov, M.; Ermenbay, A. Relation of Hydrogeology and Contaminant Sources to Drinking Water Quality in Southern Kazakhstan. *Water* **2023**, *15*, 4240. [CrossRef]
21. Piatak, N.M.; Parsons, M.B.; Seal, R.R. Characteristics and Environmental Aspects of Slag: A Review. *Appl. Geochem.* **2015**, *57*, 236–266. [CrossRef]
22. *GOST R 58595-2019*; Soils. Sampling. GOST: Moscow, Russia, 2019.
23. *GOST 17.4.3.01-2017*; Nature Protection (SSOP). Soils. General Requirements for Sampling. Interstate Council for Standardization, Metrology and Certification: Moscow, Russia, 2017.
24. *GOST 17.4.4.02-2017*; Nature Protection. Soils. Methods for Sampling and Preparation of Soil for Chemical, Bacteriological, Helminthological Analysis. Interstate Council for Standardization, Metrology and Certification: Moscow, Russia, 2017.

25. *ISO 18512:2007*; Soil Quality. Guidance on Long and Short Term Storage of Soil Samples. International Organization for Standardization: Geneva, Switzerland, 2007.
26. *EPA Method 6010D*; Inductively Coupled Plasma-Atomic Emission Spectrometry. United States Environmental Protection Agency: Washington, DC, USA, 2023.
27. *ISO 17294-2:2016*; Inductively Coupled Plasma Mass Spectrometry (ICP-MS)—Part 2: Sample Introduction System. International Organization for Standardization: Geneva, Switzerland, 2016.
28. Rudnick, R.L.; Gao, S. Composition of the Continental Crust. In *Treatise on Geochemistry*; Elsevier: Amsterdam, The Netherlands, 2014; pp. 1–51. ISBN 978-0-08-098300-4.
29. European Chemicals Agency (ECHA). Information on Chemicals—Registered Substances Database. Available online: https://echa.europa.eu/information-on-chemicals/registered-substances (accessed on 9 June 2026).
30. Hakanson, L. An Ecological Risk Index for Aquatic Pollution Control. A Sedimentological Approach. *Water Res.* **1980**, *14*, 975–1001. [CrossRef]
31. Müller, G. Index of Geoaccumulation in Sediments of the Rhine River. *GeoJournal* **1969**, *2*, 108–118.
32. Sutherland, R.A. Bed Sediment-Associated Trace Metals in an Urban Stream, Oahu, Hawaii. *Environ. Geol.* **2000**, *39*, 611–627. [CrossRef]
33. Tomlinson, D.L.; Wilson, J.G.; Harris, C.R.; Jeffrey, D.W. Problems in the Assessment of Heavy-Metal Levels in Estuaries and the Formation of a Pollution Index. *Helgoländer Meeresunters.* **1980**, *33*, 566–575. [CrossRef]
34. Abrahim, G.M.S.; Parker, R.J. Assessment of Heavy Metal Enrichment Factors and the Degree of Contamination in Marine Sediments from Tamaki Estuary, Auckland, New Zealand. *Environ. Monit. Assess.* **2007**, *136*, 227–238. [CrossRef]
35. *SanRaN RK 4.01.071.04*; Sanitary-Epidemiological Requirements for the Safety of Soil; Sanitary Regulations and Norms of the Republic of Kazakhstan. Ministry of Health of the Republic of Kazakhstan: Astana, Kazakhstan, 2004.
36. Baker, A.J.M. Accumulators and Excluders -strategies in the Response of Plants to Heavy Metals. *J. Plant Nutr.* **1981**, *3*, 643–654. [CrossRef]
37. U.S. Environmental Protection Agency. Integrated Risk Information System (IRIS) Database. Available online: https://www.epa.gov/iris (accessed on 9 June 2026).
38. US EPA. *Exposure Factors Handbook: 2011 Edition (Final)*; U.S. Environmental Protection Agency, National Center for Environmental Assessment, Office of Research and Development: Washington, DC, USA, 2011.
39. U.S. Environmental Protection Agency. *Risk Assessment Guidance for Superfund (RAGS), Volume I: Human Health Evaluation Manual*; U.S. Environmental Protection Agency: Washington, DC, USA, 2023. Available online: https://www.epa.gov/risk/risk-assessment-guidance-superfund-rags-part (accessed on 9 June 2026).
40. Ahatović, A.; Čakar, J.; Subašić, M.; Hasanović, M.; Murtić, S.; Durmić-Pašić, A. *Plantago lanceolata* L. from Serpentine Soils in Central Bosnia Tolerates High Levels of Heavy Metals in Soil. *Water Air Soil Pollut.* **2020**, *231*, 169. [CrossRef]
41. Skrynetska, I.; Karcz, J.; Barczyk, G.; Kandziora-Ciupa, M.; Ciepał, R.; Nadgórska-Socha, A. Using Plantago Major and Plantago Lanceolata in Environmental Pollution Research in an Urban Area of Southern Poland. *Environ. Sci. Pollut. Res.* **2019**, *26*, 23359–23371. [CrossRef] [PubMed]
42. Ali, H.; Khan, E.; Sajad, M.A. Phytoremediation of Heavy Metals—Concepts and Applications. *Chemosphere* **2013**, *91*, 869–881. [CrossRef] [PubMed]
43. Rauret, G.; López-Sánchez, J.F.; Sahuquillo, A.; Rubio, R.; Davidson, C.; Ure, A.; Quevauviller, P. Improvement of the BCR Three Step Sequential Extraction Procedure Prior to the Certification of New Sediment and Soil Reference Materials. *J. Environ. Monit.* **1999**, *1*, 57–61. [CrossRef] [PubMed]

Disclaimer/Publisher's Note: The statements, opinions and data contained in all publications are solely those of the individual author(s) and contributor(s) and not of MDPI and/or the editor(s). MDPI and/or the editor(s) disclaim responsibility for any injury to people or property resulting from any ideas, methods, instructions or products referred to in the content.

toxics

MDPI

Article

Exceedance Probability and Toxicity-Value Sensitivity in Health-Risk Assessment of a Pb–Zn Slag Reprocessing Site Under the 2025 IRIS Arsenic Values

Zhaksylyk Pernebayev [1], Akmaral Issayeva [1,*], Togzhan Baiduisenova [2,*], Mahmood-ur-Rahman Ansari [3], Akbota Aitimbetova [1] and Kural Nurseiit [1]

[1] LLP Centre for Scientific Research and Ecological Expertise KazEcoHolding, Shymkent 160012, Kazakhstan; pernebayev.zh@kazecoholding.kz (Z.P.); a.aitimbetova@kazecoholding.kz (A.A.); k.nurseit1507@mail.ru (K.N.)
[2] Department of Biology, Zhanibekov University, Shymkent 160012, Kazakhstan
[3] Department of Bioinformatics and Biotechnology, Government College University Faisalabad, Faisalabad 38000, Pakistan; mahmoodansari@gcuf.edu.pk
* Correspondence: aitimbet.btq@gmail.com (A.I.); baiduisenova.togzhan@okmpu.kz or baiduisenovattt@mail.ru (T.B.)

Abstract

Screening-level risk assessments report single-point estimates of carcinogenic risk (CR) and hazard index (HI), conveying neither the probability of exceedance nor its sensitivity to revised toxicity values. We examined both at an active lead–zinc slag reprocessing site in Shymkent, Kazakhstan, by reanalysing a published dataset (24 soil samples) with Monte Carlo simulation for an adult outdoor worker, under the toxicity values of the source assessment and under the January 2025 IRIS values for inorganic arsenic. Under the original values, the probability of exceeding CR = 10^{-4} was 70% (95% bootstrap interval 59–80%) and of exceeding HI = 1 was 82%. Applied to the same concentrations, the 2025 values gave a 21-fold higher mean risk and exceedance probabilities of 99% and 97%. The screening conclusion therefore holds under both sets of values, whereas the quantitative estimate does not. Arsenic concentration dominated output variance. Because ingestion and dermal contact carry over 99% of the worker's risk, risk reduction requires measures that interrupt these pathways: engineered capping of the heap perimeter, restricted access, and occupational hygiene. Phytostabilization gave no modelled benefit to on-site workers; its value lies in limiting off-site dust, which was not modelled. Arsenic bioaccessibility testing and denser sampling are priorities.

Keywords: probabilistic risk assessment; Monte Carlo simulation; exceedance probability; toxicity value revision; arsenic; sensitivity analysis; Central Asia

Check for updates

Academic Editor: Luis Alberto Henríquez-Hernández

Received: 7 September 2026
Revised: 30 September 2026
Accepted: 5 October 2026
Published: 7 October 2026

Copyright: © 2026 by the authors. Licensee MDPI, Basel, Switzerland. This article is an open access article distributed under the terms and conditions of the Creative Commons Attribution (CC BY) license.

1. Introduction

Reprocessing of historical lead–zinc (Pb–Zn) slag occupies an uneasy position in the circular-economy agenda. Secondary recovery of residual metals diverts material from permanent disposal and reduces demand for primary extraction, yet the same operations disturb consolidated waste bodies and can remobilise legacy contaminants where containment, dust suppression and runoff control are inadequate [1–4], a pattern documented across nonferrous smelting sites worldwide [5]. Few regions in Central Asia carry a Pb–Zn metallurgical legacy on the scale of southern Kazakhstan, and the slag heap of the former Shymkent lead plant—accumulated over roughly seven decades of pyrometallurgical operation and currently

under active reprocessing—is among the most severely contaminated sites documented in the region [6–8]. Decisions about such sites are increasingly framed as sustainability trade-offs: how much intervention is warranted, where, and on what evidence.

The evidence base for site-management decisions is predominantly deterministic. Assessments typically report single-point estimates of carcinogenic risk (CR) and hazard index (HI), computed from mean or maximum measured concentrations combined with default exposure factors, and compare these against regulatory thresholds. Such an estimate answers whether a threshold is exceeded by the calculated value. It does not answer how probable exceedance is across the range of plausible exposures at the site, which is the quantity a manager weighing intervention against cost requires. Probabilistic methods, for which formal guidance exists within the same regulatory framework [9], supply that quantity by propagating distributions rather than point values through the exposure model, and by permitting the contribution of each input to output variance to be ranked so that data-collection effort can be directed where it reduces uncertainty most [10,11]. Applications in mining and smelter settings are now well established: probabilistic assessments have been reported for soils around Pb/Zn smelters [12], for mining-area soils with Monte Carlo simulation coupled to an improved exposure model [13], and for age-stratified receptor groups (a receptor being the person or population group whose exposure is modelled) where exceedance probabilities were reported separately by population subgroup [11,14], and for source-resolved assessment across a linked water–soil–crop system [15]. A smaller number of studies have applied deterministic and probabilistic models to the same dataset; one such comparison, across 444 paired soil–crop samples, reported that conventional deterministic methods underestimate risk for the most exposed 15–25% of the population [10]. Adoption in the post-Soviet Central Asian context, however, appears limited relative to the scale of the metallurgical legacy there.

A second and less-examined source of uncertainty is the toxicity values themselves. Slope factors and reference doses are periodically revised as epidemiological evidence accumulates, and a revision can move a risk estimate by more than the spatial variability the assessment was designed to characterize. In January 2025 the US EPA revised its assessment of inorganic arsenic, raising the oral slope factor from 1.5 to 32 per $mg \cdot kg^{-1} \cdot d^{-1}$ on the basis of a Bayesian hierarchical dose–response meta-analysis of bladder and lung cancer endpoints, and lowering the oral reference dose; the inhalation unit risk was not revised [16]. The revision has now been in force for over a year and a half, during which the stock of assessments of arsenic-dominated sites completed under the superseded values has remained in use without recomputation; such assessments are not directly comparable with those completed after the revision, and the site-management decisions resting on them have not been revisited. The practical consequences of the transition have been addressed in regulatory guidance and in the consultancy literature, chiefly through recomputation of generic screening levels, and agency guidance on applying the revised cancer slope factor was issued in 2026 [17]. Whether the site-specific management conclusions of completed assessments survive the revision is a different question, answerable only site by site, and has not, to the authors' knowledge, been examined in the peer-reviewed literature for Pb–Zn metallurgical legacy sites.

Arsenic is a particularly consequential case. It combines a high slope factor with a tendency toward spatially discrete enrichment at smelter and slag sites, so that the risk estimate for an arsenic-dominated location is effectively a function of a single toxicity value applied to a strongly skewed concentration distribution. Both components of that product were affected by the 2025 revision: the revised oral slope factor of 32 per $mg \cdot kg^{-1} \cdot d^{-1}$ was obtained by combining endpoint-specific values for bladder (17.6) and lung (21.3) cancer [16], and the oral reference dose was lowered to 6.0×10^{-5} $mg \cdot kg^{-1} \cdot d^{-1}$ on the

basis of ischemic heart disease and type 2 diabetes endpoints [16]. Where arsenic dominates a site's risk profile, the sensitivity of that profile to the revision is correspondingly large and cannot be inferred without recomputation.

Both questions are addressed here at an active Pb–Zn slag reprocessing site in Shymkent, Southern Kazakhstan, using the geochemical dataset published in [8]. The source assessment reported deterministic CR and HI estimates for an adult occupational receptor together with a three-tier remediation zonation. The same receptor is used here: an adult outdoor worker on the site. Children, residents of the adjacent districts (Figure 1b) and other potentially sensitive groups are not modelled, and the results should not be read as applying to them. This scope bears most directly on the conclusions about phytostabilization and off-site dust transport, which concern exposure pathways and populations beyond the site worker (Section 4.5). The present paper draws on that published dataset rather than on new field sampling; its contribution is the probabilistic and toxicity-value-sensitivity framework applied to it, and the general result that framework yields—that at arsenic-dominated sites the qualitative management conclusion and the quantitative risk estimate have different robustness properties, the former surviving both input variability and a toxicity-value revision while the latter survives neither. The same 24 transect samples are reanalysed probabilistically under two parameterizations. The first retains the toxicity values applied in the source assessment, so that the two analyses remain directly comparable; the second uses the values currently in effect. Exceedance probabilities, sensitivity rankings and scenario projections are reported under each.

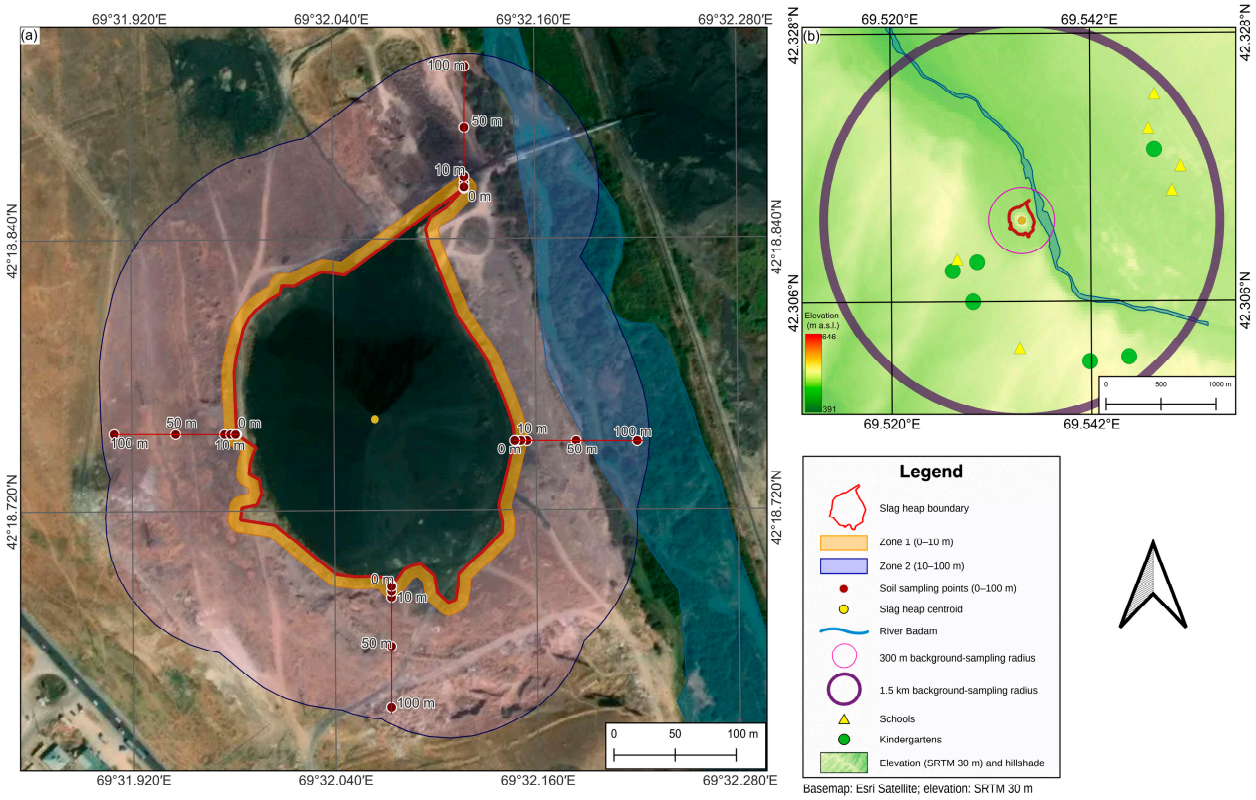


Figure 1. Study site. (**a**) Slag heap boundary and centroid (42.3125° N, 69.5342° E), the four sampling transects with points at 0, 1, 5, 10, 50 and 100 m from the heap edge (points at 1 and 5 m are not labelled), exposure Zone 1 (0–10 m) and Zone 2 (10–100 m), and the Badam River. (**b**) Surroundings of the heap: elevation (m a.s.l.) from the SRTM 30 m digital elevation model with hillshade, the Badam River, schools and kindergartens, and circles of 300 m and 1.5 km radius marking the distances at which the two reference samples were collected. Basemap: Esri Satellite.

Because the present analysis reuses a recently published dataset, its relation to the source assessment is set out explicitly in Table 1. Pernebayev et al. [8] reported the geochemistry, pollution indices, plant biomonitoring, ecosystem risk and deterministic human-health estimates for the site, and identified a probabilistic reanalysis of the human-health component as a planned follow-up. None of those results is repeated here. The present study carries out the probabilistic reanalysis with the data available, extends it to the toxicity values currently in force, quantifies the uncertainty attached to the result, and tests the zonation and intervention priorities proposed in [8] against the risk distributions.

Table 1. Relation of the present study to the source assessment [8].

Aspect	Reported in [8]	New in the Present Study
Data	24 transect and 2 reference soil samples, ten elements (ICP-OES)	Same dataset reused; no new sampling
Contamination indices, plant biomonitoring, ecosystem risk	CF, Igeo, EF, PLI, mCd, RI; bulk canopy ratios; PEC/PNEC	Not repeated
Human-health risk	Deterministic point estimates (site mean CR 7.0×10^{-4}, worst case 4.3×10^{-3}; HI 4.3 and 26.6)	Full distributions of CR and HI; exceedance probabilities; position of the point estimates within the distributions
Toxicity values	Values in force before 2025	Reassessment under the January 2025 IRIS arsenic values; effect of the revision separated from the effect of probabilistic treatment
Uncertainty	Not quantified	Sensitivity of CR and HI to all inputs; bootstrap sampling uncertainty; alternative distributions, inter-metal dependence and analytical error
Zonation	Three-tier zonation by distance from the heap	Tested against modelled risk; ordering of zones not resolved by the data
Interventions	Qualitative three-tier framework	Time-resolved scenario projections with sensitivity to efficiency assumptions
Principal conclusion	Arsenic dominates human-health risk; risk exceeds the screening level	Qualitative conclusion holds under both sets of toxicity values; quantitative estimate changes 21-fold because of the toxicity values alone

The specific objectives were to: (i) Fit and validate concentration distributions for eight priority metals; (ii) quantify CR and HI as full probability distributions and report exceedance probabilities against the 10^{-6}, 10^{-4} and HI = 1 screening levels; (iii) locate the previously published point estimates within those distributions; (iv) repeat the analysis under the 2025 IRIS arsenic values and determine which conclusions are altered; (v) rank the contribution of each stochastic input to output variance; and (vi) evaluate the published zonation and project risk under alternative intervention scenarios. Although developed at one site, the framework and its findings apply to any assessment in which a single strongly skewed contaminant governs the risk profile, and the procedure for testing whether a management conclusion survives a toxicity-value revision is transferable to the wider stock of arsenic-dominated assessments completed before January 2025.

2. Materials and Methods

2.1. Study Area

The study site is an active Pb–Zn slag reprocessing facility in Shymkent, Southern Kazakhstan (centre of the slag heap: 42.3125° N, 69.5342° E). The surrounding Turkestan Region is semi-arid (Köppen BSk [18]), receiving roughly 400 mm of precipitation annually; easterly and westerly winds prevail and govern which directions dust from the heap travels. The Badam River flows along the eastern side of the heap, between the heap

and the former lead-smelter site; the A-2 highway and residential areas lie to the west. A detailed description of site geology, hydrogeology, slag mineralogy (SEM-EDS: PbS, ZnS, ZnO, PbO, Fe_2O_3; slag pH 7.5–8.5) is given in Pernebayev et al. [8].

The heap lies on a terrace of the Badam River valley at the foot of dissected piedmont slopes (Figure 1b), so that surface runoff from these slopes during spring snowmelt and rainfall events is directed across the site toward the river. The zonal soils of the piedmont belt of the Turkestan Region are loamy sierozems [19]; around the heap, however, soils are disturbed by slag reprocessing and vehicle traffic. Soil agrochemical and water-physical properties, slope gradients and erosion rates were not measured in the source campaign and are not available for the present reanalysis. The nearest residential buildings lie about 250 m west of the heap boundary. Gridded population estimates (WorldPop, 2020, constrained and adjusted to United Nations estimates, 100 m resolution [20]) indicate approximately 1300 residents within 500 m of the heap centre and 10 500 within 1 km; one school (about 570 m) and three kindergartens (about 480–750 m) lie within 1 km of the heap boundary (Figure 1b).

2.2. Data Source

No new field sampling was conducted for this study. The geochemical dataset comprises 24 transect soil samples and two distal reference samples collected on 24 April 2026 and published as Supplementary Table S1 of [8]. Sampling followed GOST R 58595-2019 [21], GOST 17.4.3.01-2017 [22] and GOST 17.4.4.02-2017 [23]; samples were collected at a 0–50 cm depth along four transects oriented to the cardinal points, sampled at 0, 1, 5, 10, 50 and 100 m from the heap perimeter. Reference samples were collected at 300 m and 1.5 km. Two of the six authors of the present paper (Z.P. and A.A.) are authors of [8]; the present work is therefore in part a reassessment by the original investigators of their own published dataset, undertaken to test whether the management conclusions drawn there survive treatment of input variability and the subsequent revision of arsenic toxicity values. The dataset is published under a CC BY licence and the analysis reported here can be reproduced independently from it using the supplied code.

At each sampling point a composite sample of approximately 1 kg was formed from five increments collected by the envelope method (GOST 17.4.4.02-2017 [23]) over the 0–50 cm layer with a steel shovel, and placed in a polyethylene bag. Each point is therefore represented by a single depth-integrated composite; no depth-resolved data were obtained. Samples were transported in insulated cool boxes and were received by the laboratory on the day of collection (24 April 2026), as recorded in the test protocols. According to METAR records from the Shymkent airport station (ICAO: UAII) [24], light showers fell during the night and morning of 23 April 2026 and ended by about 10:00 local time; 24 April was dry and clear, with light winds of 1–4 $m \cdot s^{-1}$ and relative humidity falling from about 90% before dawn to about 30% in the afternoon. The samples were delivered unprocessed, and preparation before acid digestion was carried out by the laboratory. The heap, the four transects, Zones 1 and 2 and the Badam River are shown in Figure 1a.

The 0–50 cm interval is deeper than the surface layer normally considered for incidental ingestion and dermal contact. It was retained because the receptor is a worker at an active reprocessing site, where excavation, loading and vehicle traffic bring soil from below the immediate surface into contact with workers, so that exposure is not confined to the uppermost centimetres. Because the samples are depth-integrated, concentrations in the surface layer may be higher or lower than the values modelled here. This uncertainty was bounded by scaling all concentrations by 0.5 and 2.0 (Table S3): under the 2025 IRIS values $P(CR > 10^{-4})$ remained between 97.8% and 99.8% across this range, and under the source-assessment values it ranged from 53.1% to 83.4%.

Ten elements—As, Cd, Cr, Cu, Fe, Hg, Mn, Ni, Pb and Zn—were determined by ICP-OES (Shimadzu ICPE-9000) after acid digestion, in accordance with method M 02-902-157-10, at the accredited Analytical Laboratory of LLP KazEcoAnaliz (Almaty, Kazakhstan; accreditation certificate KZ.T.02.1017, issued 25 February 2026). Analyses were performed 27 April–5 May 2026 under Order No. 23-26 (Test Protocols No. 23-01 and No. 23-02, dated 5 May 2026). Quality control was carried out under the laboratory's internal procedures within the scope of its accreditation. The test protocols issued to the authors report the results, method, instrument and analytical conditions (25.2–25.4 °C; relative humidity 54–55%), but do not include batch-level quality-control records; element-specific recoveries of certified reference materials, blank values and replicate statistics were therefore not available for the present reanalysis. None of the 24 transect samples returned a value below the reporting limit for any of the eight modelled metals: the only soil reporting limit stated in the protocols, 0.1 mg·kg^{-1} for Hg, lies below the lowest transect Hg value (0.12 mg·kg^{-1}), so no substitution of censored values was required. To bound the effect of analytical error on the modelled distributions, measured concentrations were (i) scaled uniformly by 0.8 and 1.2 and (ii) perturbed by random multiplicative errors of 10% and 20% relative standard deviation before refitting (200 replicates each); results are given in Table S3.

Eight metals were carried forward into the risk model: Pb, Zn, Cd, Cu, As, Hg, Ni and Cr. The model is centred on arsenic, but the other seven metals were retained because carcinogenic risk and the hazard index are, by definition, sums across all contaminants of potential concern, and because the dominance of arsenic is a result to be demonstrated rather than assumed. Retaining them allows the contribution of each metal to total CR and HI to be quantified (Section 3.5). Fe and Mn were not treated as contaminants of potential concern: Fe concentrations (104–9570 mg·kg^{-1}) were below its upper-crustal abundance (39 200 mg·kg^{-1} [8]) at every transect point, and Mn (61–358 mg·kg^{-1}) did not exceed the Kazakhstan MPC at any point.

For the zonal analysis (Section 2.6), samples were assigned to two zones following the three-tier framework proposed in [8]: Zone 1, 0–10 m (n = 16) and Zone 2, 10–100 m (n = 8). The third tier (>100 m) contains no transect samples and was not modelled.

2.3. Concentration Distributions

Lognormal distributions were fitted to each metal by maximum likelihood on log-transformed concentrations across the 24 transect samples. The lognormal assumption was tested by the Shapiro–Wilk statistic applied to the log-transformed values (α = 0.05). With 24 observations per element the test has limited power, so non-rejection is treated as consistency with the lognormal model rather than as confirmation of it; normal quantile–quantile plots for all eight metals are provided as Figure S1 in the Supplementary Material. As a further check, lognormal, gamma and Weibull distributions were fitted by maximum likelihood to each metal and compared by the Akaike information criterion (AIC) and the Kolmogorov–Smirnov test, and the full risk analysis was repeated with each alternative model (Section 3.1; Table S4).

Six of the eight metals were consistent with a lognormal model (Table 2). Zn (W-test $p < 0.001$) and Hg ($p < 0.001$) were not. Hg exhibits a bimodal distribution—37.9–47.4 mg·kg^{-1} at four of the six western-transect points against 0.12–0.98 mg·kg^{-1} at seventeen of the remaining eighteen—consistent with the two distinct depositional processes identified in [8], and its geometric standard deviation (6.31) is more than 1.5× that of any other element. For these two metals, concentrations were resampled empirically from the measured values with a multiplicative lognormal kernel (σ = 0.15) to avoid imposing a parametric form the data do not support. A parametric model was therefore used where the Shapiro–Wilk test on log values did not reject lognormality ($p \geq 0.05$) and empirical resampling where it did.

The kernel smooths the 24 discrete measured values so that simulated concentrations are not restricted to exactly those values; σ = 0.15 is about one tenth of the standard deviation of the log-transformed concentrations (1.26 for Zn and 1.84 for Hg), so it does not alter the shape of the distributions. Because Zn and Hg together contribute about 0.3% of the mean hazard index, results are insensitive to this choice: for σ between 0 and 0.30 no reported probability changed by more than 0.1 percentage point (Table S4).

Table 2. Fitted distribution parameters for the 24 transect samples.

Metal	GM	GSD	AM	Min	Max	Shapiro–Wilk p (log)	Model
Pb	776.9	3.86	1754	72.6	9350	0.339	lognormal
Zn	822.3	3.51	1254	7.79	2870	<0.001	empirical
Cd	22.4	3.65	53.7	3.51	290	0.108	lognormal
Cu	405.5	2.68	684	80.1	4230	0.638	lognormal
As	658.2	3.94	1753	95.2	10,900	0.176	lognormal
Hg	1.19	6.31	8.0	0.12	47.4	<0.001	empirical
Ni	10.2	1.94	12.4	2.31	27.1	0.373	lognormal
Cr	6.88	2.22	9.4	1.79	36.9	0.955	lognormal

GM—geometric mean; GSD—geometric standard deviation; AM—arithmetic mean. All concentrations in $mg \cdot kg^{-1}$.

Sample 260 (eastern transect, 100 m), which returned anomalously low Fe and Zn in the source study, was retained: it was excluded from enrichment-factor calculations in [8] on normalization grounds that do not apply to the present analysis.

2.4. Probabilistic Risk Model

Human-health risk was modelled for an adult outdoor-worker receptor only following the US EPA RAGS framework [25], with three exposure pathways: incidental soil ingestion, inhalation of resuspended particulates and dermal contact. Chronic daily intake (CDI, $mg \cdot kg^{-1} \cdot d^{-1}$) was calculated for each pathway as in [8], preserving the model structure so that the two analyses differ only in the treatment of input variability.

Three sources of uncertainty are distinguished and treated separately. Variability—the spatial variation in concentrations across the site and inter-individual variation in exposure factors—is represented by the input distributions and propagated by the Monte Carlo simulation; this is what the exceedance probabilities describe. Parameter uncertainty—the uncertainty in the fitted distributions themselves, arising from the small number of samples and from the choice of distributional model—is quantified by bootstrap resampling and by the alternative concentration models described in Section 2.3 and below. Toxicity-value uncertainty is treated not probabilistically but as a comparison between two parameterizations (Section Toxicity Values), because the question it addresses is whether the conclusions survive a specific revision rather than how uncertain a given value is. The three are reported separately and are not combined into a single interval. The workflow of the analysis is summarized in Figure 2.

Exposure parameters were represented as distributions rather than point values (Table 3). Central values follow the US EPA Exposure Factors Handbook [26] and match the deterministic defaults used in [8], so that any divergence in output reflects distributional treatment alone and not a change in central assumptions.

Dermal absorption factors were metal-specific: As 0.030, Pb 0.006, and 0.001 for Zn, Cd, Cu, Hg, Ni and Cr. Following RAGS Part E, the dermal dose was expressed as an absorbed dose before multiplication by the slope factor, and the oral slope factor was adjusted to an absorbed-dose basis using a gastrointestinal absorption fraction of 1.0; absorption is therefore applied once and not twice.

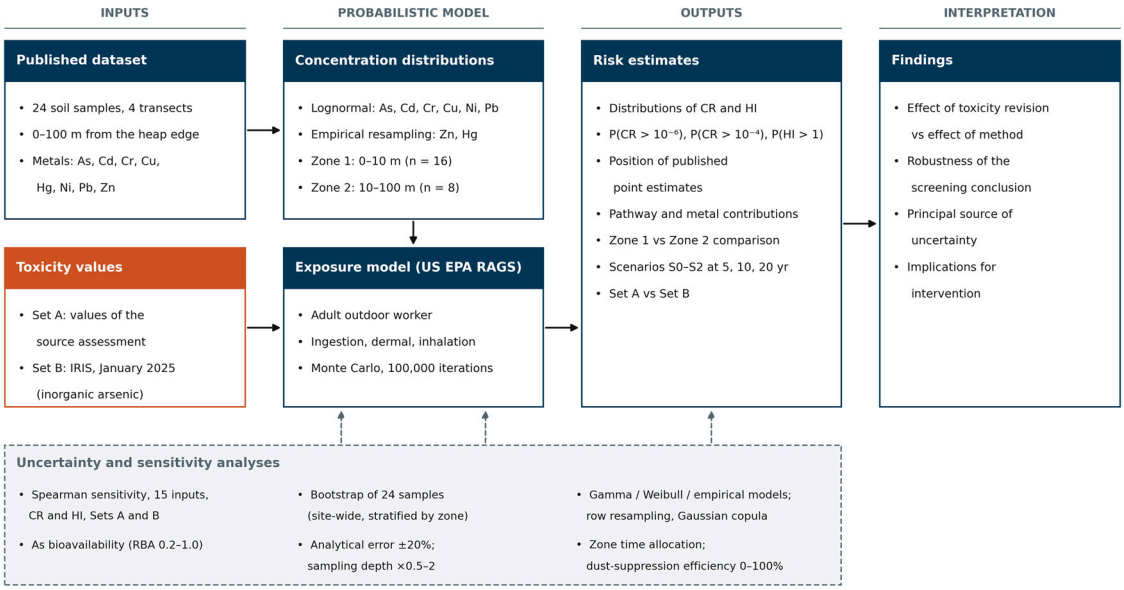


Figure 2. Workflow of the analysis. The published dataset of [8] is used to fit concentration distributions, which are propagated through the US EPA RAGS exposure model for an adult outdoor worker under two sets of toxicity values. Uncertainty and sensitivity analyses (bottom, dashed arrows) act on the concentration distributions, the exposure model and the outputs.

Table 3. Stochastic exposure parameters, adult outdoor-worker scenario.

Parameter	Distribution	Parameters	Central Value
Body weight (BW)	Normal, truncated to 40–130	$\mu = 70$, $\sigma = 12$ kg	70 kg
Soil ingestion rate (IngR)	Lognormal	GM = 50, GSD = 2.0 mg·d^{-1}	50 mg·d^{-1}
Inhalation rate (InhR)	Normal, truncated to 8–35	$\mu = 20$, $\sigma = 3$ m^3·d^{-1}	20 m^3·d^{-1}
Exposed skin area (SA)	Normal, truncated to 1500–5500	$\mu = 3300$, $\sigma = 660$ cm^2	3300 cm^2
Adherence factor (AF)	Lognormal	GM = 0.2, GSD = 2.0 mg·cm^{-2}	0.2 mg·cm^{-2}
Exposure frequency (EF)	Triangular	180/250/350 d·yr^{-1}	250 d·yr^{-1}
Exposure duration (ED)	Triangular	1/25/40 yr	25 yr
Particulate emission factor (PEF)	Fixed	1.36×10^9 m^3·kg^{-1}	—
Averaging time, carcinogenic	Fixed	70×365 d	—
Averaging time, non-carcinogenic	Fixed	ED $\times$ 365 d	—

Carcinogenic risk was computed as $CR = \Sigma(CDI_i \times SF_i)$ across metals and pathways for As, Cd, Cr and Ni; non-carcinogenic hazard as $HI = \Sigma(CDI_i / RfD_i)$ across all eight metals and three pathways. Slope factors and reference doses are listed in Table 4.

Results are interpreted against screening levels rather than binary thresholds. Following US EPA practice, carcinogenic risk is compared with the risk-management range of 10^{-6} to 10^{-4}: 10^{-6} is the point of departure below which risk is generally not of concern, and 10^{-4} the upper end of the range, above which remedial action is generally warranted [27]; values within the range call for site-specific judgement. An HI above 1 indicates that the estimated intake exceeds the reference dose and signals that further evaluation is needed; it is not a prediction that adverse effects will occur. Because total arsenic, default exposure parameters and a single occupational receptor are used, all results are screening-level estimates, and 'exceedance' refers to these screening levels throughout.

In the primary analysis, concentrations of the eight metals were sampled independently from their marginal distributions. Because the measured samples are paired multi-element observations, the effect of this assumption was tested with two alternatives that preserve the observed dependence: joint resampling of complete sample rows, with and without the

kernel described in Section 2.3, and a Gaussian copula combining the observed Spearman correlation matrix with the marginal distributions of Section 2.3 (Section 3.1; Table S4).

Table 4. Toxicity values applied under the two parameterizations.

Parameter (Inorganic Arsenic)	Set A	Set B	Basis of Set B
Oral slope factor, per $mg \cdot kg^{-1} \cdot d^{-1}$	1.5	32	Combined bladder (17.6) and lung (21.3) cancer slope factors; Bayesian hierarchical dose–response meta-analysis, logistic-power model; 11 bladder and 6 lung cancer studies. Updated 13 January 2025
Dermal slope factor, per $mg \cdot kg^{-1} \cdot d^{-1}$	1.5	32	Oral slope factor with GI absorption = 1.0
Inhalation slope factor, per $mg \cdot kg^{-1} \cdot d^{-1}$	15.1	15.1	Derived from IUR = 4.3×10^{-3} per $\mu g \cdot m^{-3}$ (1995), not revised in 2025
Oral RfD, $mg \cdot kg^{-1} \cdot d^{-1}$	3.0×10^{-4}	6.0×10^{-5}	Endocrine and cardiovascular systems; ischemic heart disease and type 2 diabetes; UF_C = 3; confidence medium/high. Rounded from osRfDs of 5.8×10^{-5} (type 2 diabetes) and 5.7×10^{-5} (ischemic heart disease). Updated 13 January 2025
Slope factors and RfDs, other seven metals	unchanged between sets	unchanged	IRIS

Arsenic risk was computed from total concentrations, which is equivalent to a relative oral bioavailability (RBA) of 1. Sensitivity to this assumption was examined by applying RBA values of 0.2, 0.4, 0.6 (the US EPA default for arsenic in soil [28]) and 0.8 to the ingestion pathway; dermal absorption is governed separately by the absorption factor, and the inhalation pathway was left unchanged (Section 3.3; Table S8).

Simulations were run with 100,000 iterations using the PCG64 generator (seed 20260827) in Python 3.11 with NumPy 2.4 [29] and SciPy 1.17 [30]. Convergence was verified by repeating the full analysis at 10 000 iterations under the same seed: exceedance probabilities agreed to within 0.9% and tail percentiles to within 5.1%, while the means of CR and HI agreed to within 1.6%. At 100,000 iterations the Monte Carlo standard error of an exceedance probability is at most 0.16 percentage points. This figure describes numerical precision conditional on the fitted distributions; it does not capture uncertainty arising from the limited number of measured samples, which is addressed below. The comparison is reproduced by the Supplementary Scripts.

Because the concentration distributions are fitted to 24 samples, their parameters are themselves uncertain. This uncertainty was quantified by nonparametric bootstrap. The 24 transect samples were resampled with replacement 1000 times; for each resample the lognormal parameters (As, Cd, Cr, Cu, Ni, Pb) were re-estimated and the empirical distributions (Zn, Hg) rebuilt, and the risk model was run with 10,000 iterations using the same exposure-parameter draws. The 2.5th and 97.5th percentiles across replicates are reported as 95% bootstrap intervals for the mean CR, mean HI and the exceedance probabilities. For the zonal comparison, a stratified bootstrap was applied, resampling Zone 1 (n = 16) and Zone 2 (n = 8) separately, and the ratio of mean CR between zones was recorded in each of 1000 replicates. With n = 24 these percentile intervals are approximate and indicate the order of magnitude of sampling uncertainty rather than exact coverage.

Toxicity Values

Set A comprises the toxicity values applied in the source assessment [8]. As a check on the present model implementation, the full deterministic model was evaluated at the RAGS point values on the measured concentrations, without recourse to any quantity reported in [8]. Under IRIS toxicity values throughout, site-mean carcinogenic risk is

6.44×10^{-4}, 8.0% below the published figure of 7.0×10^{-4}, and the worst-case sample yields 4.00×10^{-3} against a published 4.3×10^{-3}. Adding an oral slope factor for cadmium of 6.1 per $mg \cdot kg^{-1} \cdot d^{-1}$—a value issued in several national frameworks but not by IRIS—raises the site-mean result to 7.02×10^{-4}, within 0.3% of the published figure, the entire residual of 5.80×10^{-5} being attributable to that single term. The model structure is therefore reproduced; the element-wise apportionment differs solely through the treatment of cadmium described below, and all results reported here use IRIS values only. Any divergence between the deterministic and probabilistic results reported below reflects the treatment of input variability rather than a difference in model structure.

The oral and dermal slope factors applied to chromium are not issued by IRIS, which derives a carcinogenicity value for hexavalent chromium by the inhalation route only; the values used here were taken from national compilations and applied to total chromium, and chromium contributes 0.2% of total carcinogenic risk at this site. An inhalation RfC for inorganic arsenic has not been assessed under the IRIS programme. Route-specific inhalation and dermal reference doses used in the hazard index calculation were therefore derived by route extrapolation from published compilations rather than taken directly from IRIS, by applying a factor of 0.41 to the oral reference dose under either parameterization; this is noted in Section 4.6. Cadmium is classified by IRIS as carcinogenic by the inhalation route only, and no oral slope factor is issued for it; cadmium carcinogenicity is therefore restricted to the inhalation pathway throughout the present analysis, a pathway contributing less than 0.1% of intake under the RAGS default particulate emission factor. Assessments that apply an oral slope factor to cadmium, as some national frameworks do, will apportion a correspondingly larger share of total carcinogenic risk to that element.

2.5. Sensitivity Analysis

The contribution of each stochastic input to output variance was quantified by Spearman rank correlation between the sampled input values and each output—total CR and HI—across the 100,000 iterations, under both parameterizations. All fifteen stochastic inputs were included: the eight metal concentrations and the seven exposure parameters. An approximate contribution to output variance was obtained by normalizing the squared rank correlations to 100%. Rank correlation was preferred over Pearson correlation because the input–output relationships are monotonic but not linear, and because several inputs are strongly right-skewed.

2.6. Scenario Analysis

Risk trajectories were projected over 5-, 10- and 20-year horizons under three management scenarios, constructed by mechanism rather than by a uniform percentage reduction: no intervention in either zone (S0); engineered containment of Zone 1 (0–10 m), with no intervention in Zone 2 (S1); and engineered containment of Zone 1 combined with phytostabilization of Zone 2 (10–100 m) (S2).

Engineered containment was modelled as interruption of all three exposure pathways within the treated zone, consistent with regulatory guidance, which describes caps and covers as eliminating direct exposure to solid mining waste by creating a physical barrier and as reducing or eliminating fugitive dust emissions, rather than as producing a partial reduction in concentration [31]. An establishment lag of 1.0 yr was assumed for construction.

Phytostabilization was modelled as suppression of the inhalation pathway only, with ingestion and dermal contact retained, since a vegetative cover reduces dust emission without removing surface soil from contact. An establishment lag of 3.5 yr was applied, based on field data reporting 21–61% canopy cover after 41 months on compost-amended tailings [32].

The underlying flux basis is a documented reversal from net emission (2323 $g \cdot m^{-2} \cdot yr^{-1}$, unirrigated control) to net deposition (371 and 606 $g \cdot m^{-2} \cdot yr^{-1}$ at 16% and 32% canopy cover) [3]. These measurements were not converted into a fractional reduction in inhalation exposure; instead, the inhalation pathway was fully suppressed after the establishment lag, which represents the most favourable case for phytostabilization. Because the cited evidence indicates partial rather than complete cover, the dust-reduction efficiency was additionally varied from 0 to 100% in steps of 25%, so that the inhalation pathway was reduced by that fraction after the lag (Section 3.7; Table S6).

Both studies were conducted at the Iron King Mine and Humboldt Smelter Superfund site (Dewey-Humboldt, AZ, USA), on sulfidic mine tailings enriched in arsenic and lead under a semi-arid climate, where compost-amended plots were seeded with native plant species [3,32]. Canopy cover is the proportion of the ground surface covered by the vertical projection of plant foliage. The net emission or deposition flux is the difference between the mass of wind-blown particles leaving and arriving at a unit area of surface per year; a change from net emission to net deposition therefore indicates that the surface has ceased to act as a dust source. The cited setting is comparable to the Shymkent heap in climate and in the contaminants involved, which is why these data were used. It differs in substrate: the Shymkent slag is coarser (0.5–15 mm) and slightly alkaline (pH 7.5–8.5) [8], and no amendment or planting programme is in place at the site. Vegetation establishment on the slag may therefore be slower and less complete than in the cited trials, and the transferred values are treated as indicative rather than site-specific.

The projection horizon T governs the fraction of the exposure period over which an intervention is credited; it does not replace the exposure duration, which is sampled from its distribution as in Table 3. For each horizon T, the residual fraction of a suppressed pathway was computed as $1 - \max(0, (T - \text{lag})/T)$, i.e., the intervention is credited only for the portion of the exposure period during which it is operational.

Common random numbers were used across scenarios: concentrations were drawn once per zone and reused for all three scenarios, so that between-scenario differences reflect the modelled intervention alone and not simulation noise. Zonal results were combined assuming equal receptor time allocation between Zone 1 and Zone 2. In the absence of information on how workers divide their time, equal weighting was used as a neutral default; its influence was examined by repeating the scenario analysis for Zone 1:Zone 2 allocations of 100:0, 75:25, 25:75 and 0:100 (Section 3.7; Table S7).

2.7. Data and Code Availability

The source geochemical data are published as Supplementary Table S1 of [8]. Simulation code is provided as Supplementary Material and reproduces all reported values from the published dataset.

3. Results

3.1. Concentration Distributions

Fitted distribution parameters are given in Table 2 (Section 2.3). Geometric standard deviations ranged from 1.94 (Ni) to 6.31 (Hg), confirming substantial right-skew across all priority metals; for the four metals entering the carcinogenic-risk calculation they were 3.94 (As), 3.65 (Cd), 2.22 (Cr) and 1.94 (Ni). The ratio of arithmetic to geometric mean reaches 2.66 for As (1753 versus 658.2 $mg \cdot kg^{-1}$) and 2.40 for Cd (53.7 versus 22.4 $mg \cdot kg^{-1}$).

Six of the eight metals were consistent with a lognormal model (Shapiro–Wilk on log values, $p = 0.108$–0.955). Zn and Hg were not ($p < 0.001$ in both cases). The measured concentrations along the four transects, expressed as multiples of the Kazakhstan maximum permissible concentration, are mapped in Figure S2. Interpolated concentration surfaces

were not produced: with four radial transects, the sectors between them are unsampled, and interpolation would assign values to large areas without measurements.

The lognormal model had the lowest AIC for five of the six parametrically modelled metals (for As, ΔAIC = 8.5 relative to the gamma and 6.2 relative to the Weibull model); for Ni the three models were indistinguishable (ΔAIC < 0.5), and no model was rejected by the Kolmogorov–Smirnov test ($p \geq 0.16$; these p values are conservative because the parameters were estimated from the same data). Replacing the lognormal model with gamma or Weibull distributions, or using empirical resampling for all eight metals, changed $P(CR > 10^{-4})$ from 69.9% to 67.7–71.9% under Set A and from 99.3% to 95.5–99.8% under Set B (Table S4). The lighter upper tails of the gamma and Weibull models reduce the Set B probabilities by about four percentage points; no conclusion is altered. Normal quantile–quantile plots of the log-transformed concentrations (Figure S1) provide a check that does not depend on test power, and the bootstrap gives 95% intervals for the fitted As parameters of 397–1115 mg·kg^{-1} for the geometric mean and 2.59–5.23 for the geometric standard deviation (Table S2).

Pb, Zn, Cd, Cu and Ni were strongly inter-correlated (Spearman ρ = 0.80–0.90), whereas As was weakly and non-significantly correlated with all metals except Hg (ρ = 0.17–0.32; As–Hg ρ = 0.47, $p = 0.021$). Because As dominates both CR and HI and is nearly independent of the other metals, preserving the dependence structure had little effect. Under Set A, $P(CR > 10^{-4})$ was 68.1% with joint row resampling and 70.0% with the Gaussian copula, against 69.9% with independent sampling; under Set B it was 99.3–99.8% (99.3%). P(HI > 1) was 78.1–79.7% under Set A (82.1%) and 96.5–98.3% under Set B (97.3%) (Table S4). The independence assumption therefore does not materially affect the conclusions.

These departures have different causes. Mercury shows the largest dispersion of any element (GSD = 6.31, more than 1.5 times that of any other metal) and a clearly bimodal distribution: values of 37.9–47.4 mg·kg^{-1} at four of the six western-transect points against 0.12–0.98 mg·kg^{-1} at seventeen of the remaining eighteen, a separation of more than an order of magnitude with only three intermediate values (2.36 and 6.98 mg·kg^{-1} on the western transect and 2.44 mg·kg^{-1} elsewhere). This is consistent with the two distinct depositional processes identified in the source assessment [8] and is not adequately represented by any single unimodal parametric form. Zinc departs less dramatically but spans 7.79 to 2870 mg·kg^{-1}, and its lowest value comes from sample 260, retained here for the reasons given in Section 2.3. For both metals, empirical resampling preserves the observed structure without imposing a form the data do not support; neither metal contributes materially to carcinogenic risk, so the choice affects the hazard index only. The two modes of Hg correspond to two depositional settings—the western transect and the other three—rather than to a mixture within a single population. Empirical resampling reproduces both modes in the observed proportions, whereas a two-component mixture or a transect-stratified model fitted to six and eighteen observations would be poorly constrained; and because Hg contributes about 0.3% of the mean hazard index, the choice of Hg model does not affect any reported result.

For the four metals entering the carcinogenic-risk calculation the lognormal fits were satisfactory, and arsenic—which dominates the output (Section 3.5)—returned a p value of 0.176, below those of Cr (0.955) and Ni (0.373) but above that of Cd (0.108). The As distribution spans 95.2 to 10,900 mg·kg^{-1} across the 24 transect samples, a range of more than two orders of magnitude within a 100 m radius, which is the feature that makes a point-estimate summary problematic at this site.

3.2. Distributions of Carcinogenic Risk and Hazard Index

The distributions of CR and HI under both parameterizations are summarized in Table 5. Both are strongly right skewed under either parameterization. Under Set A the CR interquartile range spans 7.91×10^{-5} to 6.38×10^{-4} while the 99th percentile reaches 8.20×10^{-3}—two orders of magnitude above the first quartile—and the mean (7.38×10^{-4}) exceeds the median (2.26×10^{-4}) by a factor of 3.3. A mean that sits above the 75th percentile is characteristic of a distribution whose expectation is governed by its upper tail rather than by its central mass. The same structure appears in the hazard index (mean 8.03, median 3.12) and is preserved under Set B, since a slope factor scales the distribution without altering its shape. Figure 3 shows both distributions as exceedance curves, which give the probability of exceeding any level of CR or HI. In the extreme upper tail the simulated values exceed unity under Set B (maximum 7.34), where the linear low-dose extrapolation underlying the slope-factor model no longer holds; such iterations should be read as an indication of the weight of the tail rather than as risk estimates in the probabilistic sense.

Table 5. Distributions of CR and HI under both parameterizations.

Statistic	CR, Set A	CR, Set B	HI, Set A	HI, Set B
Mean	7.38×10^{-4}	1.57×10^{-2}	8.03	37.4
5th percentile	1.78×10^{-5}	3.63×10^{-4}	0.439	1.41
25th percentile	7.91×10^{-5}	1.66×10^{-3}	1.35	5.04
Median	2.26×10^{-4}	4.77×10^{-3}	3.12	13.0
75th percentile	6.38×10^{-4}	1.35×10^{-2}	7.58	34.2
95th percentile	2.86×10^{-3}	6.08×10^{-2}	29.2	141
99th percentile	8.20×10^{-3}	1.75×10^{-1}	78.3	386
Maximum	3.44×10^{-1}	7.34	3040	15,200

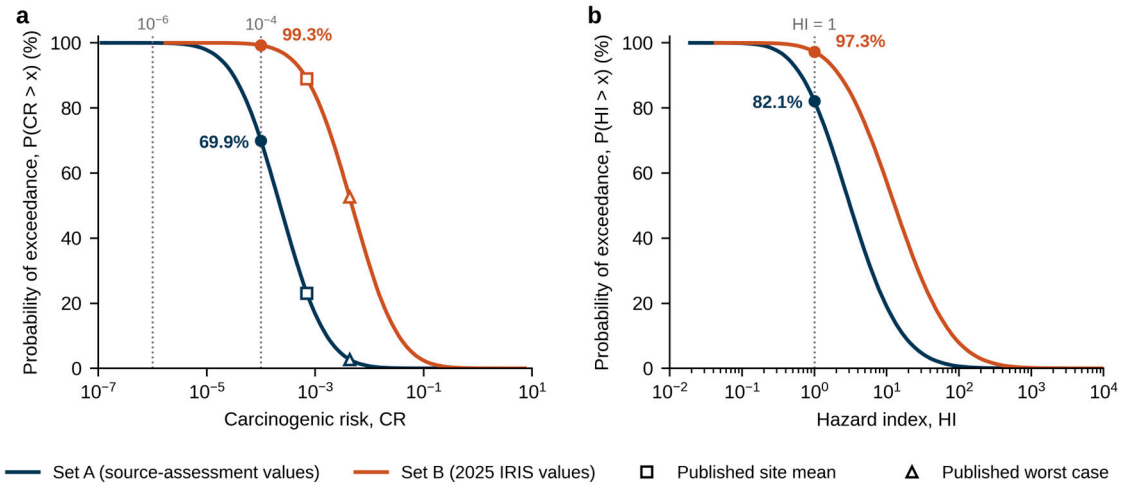


Figure 3. Exceedance curves for (**a**) total carcinogenic risk (CR) and (**b**) the hazard index (HI) across 100,000 Monte Carlo iterations, adult outdoor-worker scenario, under the toxicity values applied in the source assessment (Set A) and the values established by the January 2025 IRIS revision (Set B). Each curve gives the probability that the simulated value exceeds the level on the horizontal axis. Dotted lines mark 10^{-6} and 10^{-4}, the lower and upper ends of the US EPA risk-management range, and HI = 1; filled circles give the probability of exceeding 10^{-4} and HI = 1. Open symbols mark the site-mean (7.0×10^{-4}, squares) and worst-case (4.3×10^{-3}, triangles) point estimates reported for the same dataset in [8]: under Set A these are exceeded by 23.1% and 2.8% of simulated exposures, and under Set B by 89.0% and 52.7%.

3.3. Exceedance Probabilities

Exceedance probabilities against the screening levels are given in Table 6. Under Set A, exceedance of the 10^{-4} carcinogenic screening level is more likely than not (69.9%) but far from certain, and exceedance of 10^{-3} occurs in roughly one simulated exposure in six. Under Set B both statements change character: exceedance of 10^{-4} becomes effectively certain (99.3%) and exceedance of 10^{-3} becomes the majority outcome (84.0%). The non-carcinogenic endpoint behaves similarly, with P(HI > 1) rising from 82.1% to 97.3% and P(HI > 10) from 19.1% to 57.4%.

Table 6. Exceedance probabilities against screening levels.

Threshold	Set A	Set B
CR > 10^{-6}	99.98%	100.0%
CR > 10^{-5}	97.8%	100.0%
CR > 10^{-4}	69.9%	99.3%
CR > 10^{-3}	16.8%	84.0%
HI > 1	82.1%	97.3%
HI > 4	42.4%	80.1%
HI > 10	19.1%	57.4%

The distinction matters for how a conclusion is stated. Under Set A the defensible statement is that risk is more likely than not to exceed the upper end of the risk-management range; under Set B, that it almost certainly does. Neither statement is available from a point estimate, and the two differ in the degree of confidence a manager could attach to a decision to intervene.

Sampling uncertainty is considerably larger than numerical uncertainty (Table S2). Across 1000 bootstrap replicates, P(CR > 10^{-4}) ranged from 59% to 80% under Set A and from 98.4% to 99.9% under Set B (95% intervals), and P(HI > 1) from 72.5% to 90.1% and from 94.5% to 99.2%. In every replicate both exceedance probabilities remained above 50% under either parameterization.

Relative bioavailability of arsenic affects the Set A results more than the Set B results (Table S8). At the US EPA default RBA of 0.6, mean CR was 29% lower than with total arsenic, and P(CR > 10^{-4}) was 62.5% under Set A and 98.7% under Set B; at an RBA of 0.2 the corresponding probabilities were 49.5% and 97.2%. The reduction in mean CR is less than proportional to RBA because dermal contact, which carries 28% of CR, is not affected. P(HI > 1) remained above 72% under Set A and above 93% under Set B across the range.

3.4. Position of the Published Point Estimates

The position of each published point estimate within the simulated distributions is given in Table 7. With the source-assessment values, 23.1% of simulated exposures exceed the published site-mean CR and 2.8% exceed the published worst case. Substituting the current toxicity values shifts both figures to 89.0% and 52.7%: what was reported as the site worst case now falls near the median of the distribution.

Table 7. Position of the published point estimates within the simulated distributions.

Published Estimate	Value	Percentile, Set A	Percentile, Set B
Site-mean CR	7.0×10^{-4}	76.9	11.0
Worst-case CR	4.3×10^{-3}	97.2	47.3
Site-mean HI	4.3	59.7	21.5
Worst-case HI	26.6	94.3	69.2

Mean CR under Set B is 21.3× that under Set A; mean HI is 4.7×. The ratio for CR follows directly from the 21.3-fold increase in the arsenic oral slope factor, since ingestion and dermal contact together account for 99.8% of arsenic CR (inhalation 0.17%). Because the concentrations and the exposure model are identical under both parameterizations, this difference reflects the toxicity values alone; it implies no change in the contamination of the site or in the exposure of the worker.

The effect of moving from deterministic to probabilistic treatment is small compared with the effect of the toxicity-value revision. Evaluated at the RAGS central-tendency exposure values and site-mean concentrations, the present model gives CR = 6.4×10^{-4} under Set A and 1.37×10^{-2} under Set B; the corresponding probabilistic means are 7.4×10^{-4} and 1.57×10^{-2}, higher by a factor of 1.15 under either set. Replacing Set A with Set B multiplies CR by 21.2 in the deterministic and 21.3 in the probabilistic calculation. For HI the corresponding factors are 1.3 (probabilistic versus deterministic) and 4.7 (Set B versus Set A). The toxicity-value revision therefore moves the estimate by more than an order of magnitude, whereas the change in method moves it by 15–30%. What the probabilistic treatment adds is not a different central value but the distribution around it: the probability of exceeding 10^{-4} (69.9% under Set A, 99.3% under Set B) and HI = 1 (82.1% and 97.3%), and the position of the published point estimates within that distribution (Table 7). The published deterministic site-mean estimate of 7.0×10^{-4} [8] differs from the value reproduced here (6.4×10^{-4}) because it included a legacy oral slope factor for cadmium (Section Toxicity Values).

3.5. Contaminant Contributions and Sensitivity

Arsenic accounted for 99.8% of mean CR under both parameterizations, with Cr contributing 0.2% and Cd and Ni together less than 0.05%. Arsenic also dominated the non-carcinogenic endpoint, contributing 91.7% of mean HI under Set A, followed by Pb (6.9%) and Cd (1.0%).

Sensitivity ranking (Spearman ρ with total CR; Table 8) is unchanged between the two parameterizations, since a slope factor scales the output without altering rank order.

Table 8. Sensitivity of total carcinogenic risk to model inputs (Spearman rank correlation, 100,000 iterations). The seven metal concentrations other than As ($|\rho| \leq 0.005$) are not listed here; they are given, together with the full ranking for CR and HI under both parameterizations, in Table S5.

Input	ρ
As concentration	+0.867
Soil ingestion rate (IngR)	+0.292
Exposure duration (ED)	+0.268
Adherence factor (AF)	+0.133
Body weight (BW)	−0.109
Exposure frequency (EF)	+0.084
Exposed skin area (SA)	+0.040
Inhalation rate (InhR)	−0.004

Arsenic concentration dominates, exceeding the next-ranked input by a factor of three (Figure 4).

With all fifteen stochastic inputs included, the concentrations of the seven metals other than As show negligible rank correlation with CR ($|\rho| \leq 0.005$). For HI, As concentration again dominates (ρ = +0.852 under Set A and +0.904 under Set B, corresponding to about 79% and 85% of explained variance). The HI ranking differs from the CR ranking in two respects. Exposure duration has no influence on HI (ρ = −0.001), because for non-carcinogenic endpoints it cancels between intake and averaging time, whereas the adherence factor rises in rank (ρ = +0.242 under Set A) because dermal contact contributes 48% of mean HI against 28% of mean CR. Pb concentration is the only non-As metal with a detectable influence on

HI (ρ = +0.153 under Set A, about 2.5% of explained variance; +0.044 under Set B). The full ranking for both outputs and parameterizations is given in Table S5.

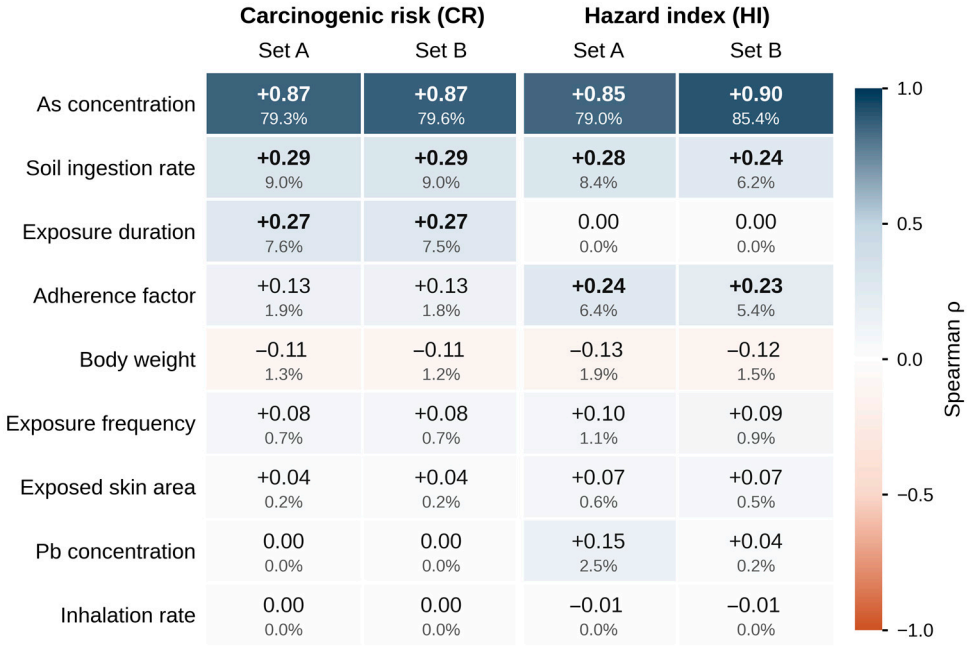


Figure 4. Sensitivity of total carcinogenic risk (CR) and the hazard index (HI) to the stochastic model inputs across 100,000 Monte Carlo iterations, under the source-assessment (Set A) and 2025 IRIS (Set B) toxicity values. Each cell gives the Spearman rank correlation between the input and the output (upper value; colour scale) and the approximate contribution of the input to output variance, obtained by normalizing the squared correlations of all fifteen inputs to 100% (lower value). Arsenic concentration dominates both outputs (ρ = +0.867 for CR under Set A), exceeding the next-ranked input by a factor of three. Exposure duration has no influence on HI, and Pb concentration is the only other metal with a detectable influence (HI, Set A). Concentrations of the remaining six metals ($|\rho| \leq 0.03$) are not included in the figure; they are reported, together with the full ranking, in Table S5.

Body weight carries the only negative correlation, as expected from its position in the denominator of the intake equation. The four exposure parameters that a site-specific occupational survey could realistically refine—exposure duration, ingestion rate, adherence factor and frequency—together rank well below arsenic concentration.

Inhalation rate shows negligible rank correlation ($\rho < 0.01$). This follows from the RAGS default particulate emission factor of 1.36×10^9 $m^3 \cdot kg^{-1}$, under which the inhalation chronic daily intake is more than three orders of magnitude smaller than the ingestion intake; the inhalation pathway contributes 0.17% of arsenic carcinogenic risk under Set A (0.01% under Set B), against 71.4% for ingestion and 28.4% for dermal contact. This pathway structure governs the scenario results reported in Section 3.7.

3.6. Zonal Risk Distribution

Risk was computed separately for the two zones of the published three-tier framework (Table 9, Figure 5).

Mean risk in Zone 2 is 1.81× that in Zone 1, and mean HI is 1.72× higher. Zone 1 nevertheless carries the higher exceedance probability (77.5% versus 60.3%).

These two statements are not contradictory and describe different features of the distributions. Zone 1 is uniformly contaminated: nearly all sampling points exceed 10^{-4}, but few reach extreme values. Zone 2 is spatially patchy: a majority of points exceed 10^{-4}, but the distribution carries substantially heavier upper values, driven by the western-

transect secondary maxima at 50 and 100 m (As 7610 and 7900 mg·kg^{-1}; Pb 7850 mg·kg^{-1} at 100 m). Mean risk is governed by the tail; exceedance probability by the bulk.

Table 9. Zonal risk, no-intervention scenario, 20-yr horizon.

Zone	*n*	Mean As (mg·kg^{-1})	Max As	Mean CR	P(CR > 10^{-4})	Mean HI
Zone 1 (0–10 m)	16	1557	10,900	5.72×10^{-4}	77.5%	7.0
Zone 2 (10–100 m)	8	2144	7900	1.04×10^{-3}	60.3%	12.0

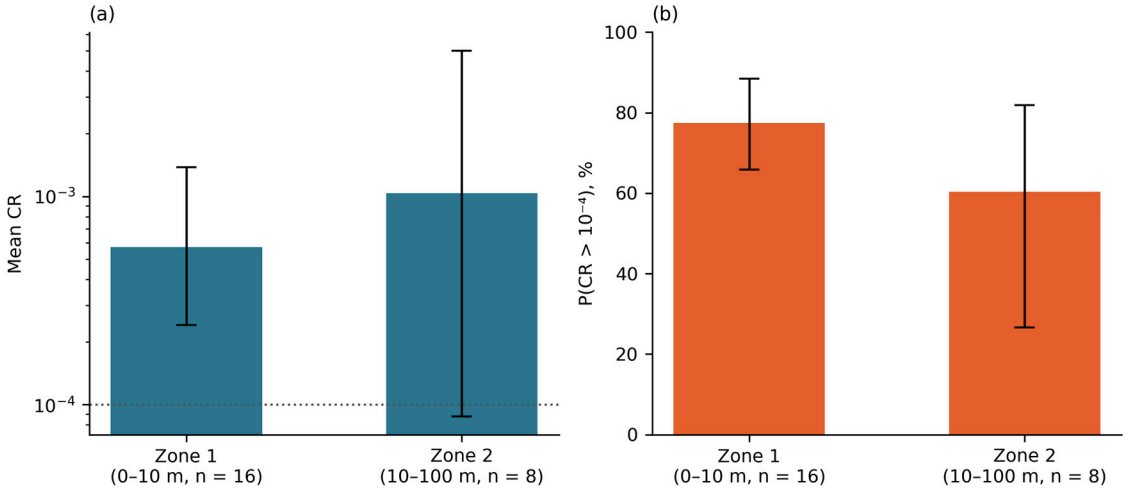


Figure 5. Zonal comparison at the 20-year horizon under the no-intervention scenario, Set A toxicity values: (**a**) Mean carcinogenic risk (logarithmic axis; the dotted line marks 10^{-4}) and (**b**) probability of exceeding 10^{-4}. Error bars show 95% stratified-bootstrap intervals (1000 replicates, zones resampled separately). Zone 2 has the higher point estimate of mean risk and Zone 1 the higher exceedance probability, but the intervals overlap widely and the zonal ordering is not resolved by the data (Section 3.6). The Zone 2 mean is carried by two of eight samples (Table 10).

Table 10. Leave-one-out stability of the Zone 2:Zone 1 mean-As ratio (Zone 1 mean As = 1557 mg·kg^{-1}, *n* = 16; full Zone 2 ratio = 1.38).

Sample Excluded	Transect	Distance (m)	As in Sample	Zone 2 Mean As	Ratio
247	South	50	193	2423	1.56
248	South	100	97.6	2436	1.56
253	North	50	183	2424	1.56
254	North	100	95.2	2437	1.56
259	East	50	194	2423	1.56
260	East	100	879	2325	1.49
265	West	50	7610	1363	0.88
266	West	100	7900	1322	0.85

The non-monotonic decay producing these secondary maxima was documented in [8], which reported that a simple radial dispersion model does not describe the contamination plume and declined to fit one. The consequence for remediation prioritization was not drawn there and is developed in Section 4.4.

Because the zonal comparison rests on eight outer-zone samples, its stability was tested by leave-one-out analysis on mean As concentration (Table 10).

Exclusion of either western-transect sample reverses the ordering; exclusion of any of the remaining six leaves the ratio at 1.49–1.56. The zonal comparison is therefore carried by two of eight samples, both on the transect identified in [8] as carrying the highest mean concentrations of Pb, Cd, Hg and As. The interpretation of this dependence is developed in Section 4.4.

Note that the Zone 2:Zone 1 ratio computed on mean As concentration (1.38) is lower than the ratio of mean modelled CR (1.81). The two are not directly comparable: risk is computed from fitted lognormal distributions, whose expectation is more sensitive to the upper tail than the arithmetic mean of the underlying samples. The larger ratio for risk than for mean concentration is the same tail effect described in Section 3.2, operating within rather than between frameworks.

The stratified bootstrap confirms that the zonal comparison is not resolved by the data: the 95% interval for the Zone 2:Zone 1 ratio of mean CR is 0.16–9.9, and Zone 2 exceeded Zone 1 in 68% of replicates.

3.7. Scenario Projections

Projected risk under the three management scenarios is given in Table 11 and Figure 6.

Relative mean CR under S1 (S0 = 1.000): 0.716/0.680/0.662 at 5/10/20 yr under Set A; 0.715/0.680/0.661 under Set B. Containment removes roughly a third of mean risk under either parameterization—the proportional benefit of intervention is invariant to the toxicity values, because a slope factor scales all scenarios equally. The revision therefore changes the absolute risk level but not the relative merit of the interventions.

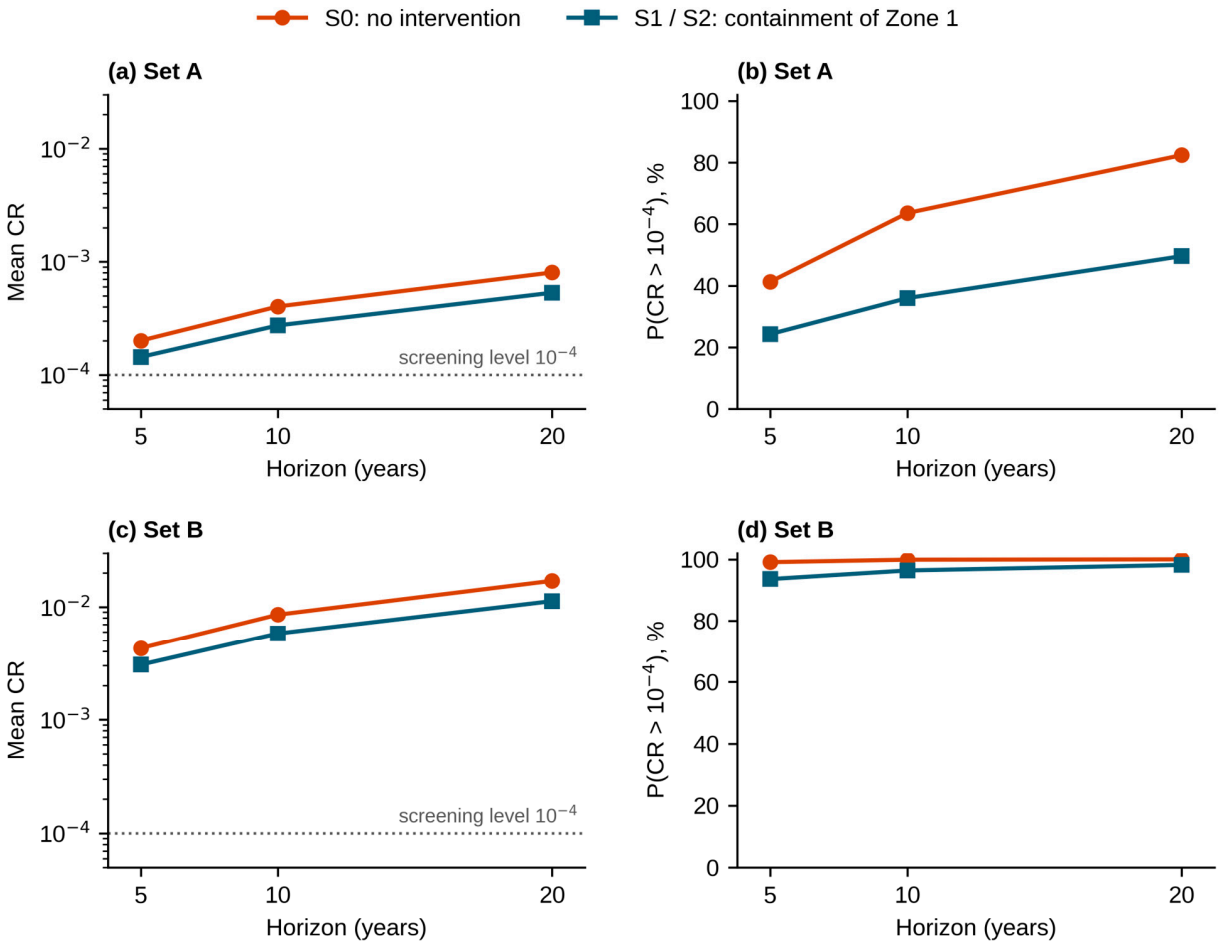


Figure 6. Projected risk under management scenarios at 5-, 10- and 20-year horizons under Set A (**a**,**b**) and Set B (**c**,**d**). (**a**,**c**) Mean carcinogenic risk on a common logarithmic axis; the dotted line marks the 10^{-4} screening level. (**b**,**d**) Probability of exceeding 10^{-4}. S0 = no intervention; S1 = engineered containment of Zone 1 (0–10 m); S2 = containment of Zone 1 plus phytostabilization of Zone 2 (10–100 m). S1 and S2 are plotted as a single series because they differ by less than 0.3% at every horizon.

Table 11. Scenario projections under both parameterizations.

Set A—Toxicity Values of the Source Assessment			
T (yr)	**Scenario**	**Mean CR**	**P(CR > 10^{-4})**
5	S0	2.01×10^{-4}	41.3%
5	S1/S2	1.44×10^{-4}	24.3%
10	S0	4.03×10^{-4}	63.6%
10	S1/S2	2.74×10^{-4}	36.0%
20	S0	8.05×10^{-4}	82.4%
20	S1/S2	5.33×10^{-4}	49.6%
Set B—2025 IRIS values			
T (yr)	**Scenario**	**Mean CR**	**P(CR > 10^{-4})**
5	S0	4.28×10^{-3}	99.1%
5	S1/S2	3.06×10^{-3}	93.6%
10	S0	8.56×10^{-3}	99.9%
10	S1/S2	5.82×10^{-3}	96.4%
20	S0	1.71×10^{-2}	100.0%
20	S1/S2	1.13×10^{-2}	98.2%

The result for S2 does not depend on the assumption of complete dust suppression. With the dust-reduction efficiency varied from 0 to 100%, mean CR under S2 differed from that under S1 by at most 0.14% under Set A and 0.006% under Set B (20-yr horizon), and the probability of exceeding 10^{-4} was unchanged at the reported precision (Table S6). This follows from the pathway structure: inhalation contributes 0.17% of mean CR under Set A and 0.01% under Set B (Section 3.5), so that complete suppression is an upper bound on the benefit of phytostabilization for the occupational receptor rather than an assumption on which the result depends.

The benefit of containing Zone 1 depends strongly on how the receptor divides time between the zones. At the 20-year horizon under Set A, mean CR under S1 relative to S0 was 0.05, 0.41, 0.66, 0.85 and 1.00 for Zone 1:Zone 2 allocations of 100:0, 75:25, 50:50, 25:75 and 0:100, and P(CR > 10^{-4}) under S1 was 5%, 38%, 50%, 56% and 60%, respectively (Table S7). Without intervention, P(CR > 10^{-4}) ranged from 60% to 84% under Set A and from 97% to 100% under Set B across these allocations. The screening conclusion therefore does not depend on the allocation, but the effectiveness of containment limited to Zone 1 does: it is substantial only if the worker spends most of the time within 10 m of the heap.

S1 and S2 remain indistinguishable under both sets (<0.3%).

4. Discussion

The Discussion distinguishes three kinds of statement. Observed results are properties of the measured concentrations and hold without further assumptions. Model-derived results—exceedance probabilities, sensitivity rankings and scenario outcomes—hold conditionally on the exposure model, the toxicity values and the distributional assumptions. Management implications depend in addition on assumptions that have not been validated at this site, notably occupancy, arsenic bioavailability, the respirable fraction implied by the particulate emission factor, and the choice of receptor; they are stated as conditional on those assumptions.

4.1. What a Point Estimate Does Not Convey

Under Set A the probabilistic mean (7.38×10^{-4}) and the published deterministic estimate (7.0×10^{-4}), computed at central-tendency exposure values, agree to within about 5% for this dataset, an agreement that depends on the shape of the distributions and should not be generalized to other sites. Deterministic evaluation at central parameter values

therefore approximates the distributional mean at this site, and the two frameworks do not disagree about central tendency.

They differ in what they report. The deterministic figure states that a calculated value exceeds 10^{-4}; the probabilistic analysis states that 69.9% of plausible exposures do. These are different quantities, and only the second is directly usable in a decision [9] that weighs the cost of intervention against the likelihood of harm. Similarly, the value reported as the site worst case is exceeded by 2.8% of simulated exposures—a figure that cannot be inferred from the point estimate, and that a manager might reasonably regard as either negligible or as requiring action depending on the receptor population size.

Two independent studies that applied both frameworks to a single dataset support the general position. A dual-model comparison across 444 paired soil–crop samples reported that deterministic methods underestimate risk for the most exposed 15–25% of an agricultural population [10]. A study of 740 topsoil samples in Guizhou, China, likewise found mean hazard index and carcinogenic risk values to be higher under the probabilistic approach, and noted that traditional deterministic values may underestimate arsenic risk specifically [33]—the element that dominates risk at the present site. At Shymkent the divergence in the mean is small (5%), which is itself informative: agreement in central tendency does not imply that the point estimate carries the same information as the distribution.

The practical recommendation is narrow and defensible: screening-level assessments at sites with strongly right-skewed concentration distributions should report exceedance probabilities alongside point estimates. This requires no additional sampling—only that the existing data be treated as a distribution [9].

The number of Monte Carlo iterations and the amount of empirical information are separate quantities. The 100,000 iterations fix the numerical precision of each estimate to within 0.16 percentage points, but they cannot add information beyond the 24 samples that define the concentration distributions. Bootstrap intervals, which reflect that limit, span roughly 20 percentage points for the site-wide exceedance probability under Set A and more than an order of magnitude for the ratio between zones (Sections 3.3 and 3.6). Probabilistic output from a small dataset is therefore most informative where it is robust to resampling—here, the site-wide conclusion under either set of toxicity values—and least informative where it is not, as for the zonal comparison.

4.2. Sensitivity to the Toxicity-Value Revision

The 2025 IRIS revision of inorganic arsenic raises mean CR at this site by a factor of 21.2 and mean HI by 4.7. The magnitude follows from the site's contamination profile: arsenic contributes 99.8% of carcinogenic risk, so the site's risk estimate is effectively a function of a single toxicity value.

The qualitative conclusion is unaffected. Under both parameterizations the 10^{-4} screening level is exceeded by a majority of simulated exposures (69.9% and 99.3%) and HI = 1 by a large majority (82.1% and 97.3%). The finding of [8] that risk at this site exceeds the screening levels, and that arsenic is its dominant driver, holds under either set of values and is in that sense robust.

The quantitative estimate is not. Under current values the point estimate previously reported as the site worst case falls at the 48.5th percentile—close to the median. This is a property of the revision, not of the earlier calculation [34]: the same concentrations and the same exposure model yield a risk estimate 21 times higher because one toxicity value changed. It does not indicate that contamination or exposure at the site has increased. A decision calibrated to the absolute magnitude of an estimate produced under either set—a remediation trigger, or a comparison against a site assessed at a different date—is therefore calibrated to the toxicity values in force at the time of assessment as much as to site conditions.

The generalizable point concerns comparability rather than correctness. Assessments of arsenic-dominated sites completed before and after January 2025 are not on the same scale. The discrepancy between them is larger than the spatial variability such assessments are designed to resolve. Where risk estimates are compared across sites or over time—as they routinely are in prioritization exercises—the toxicity-value vintage should be reported alongside the estimate [34,35]. Recomputation under current values is inexpensive where the underlying concentration data are published, as they were here. Exceedance probabilities are not, however, equally robust to every source of uncertainty: they were stable under the toxicity revision, sampling uncertainty and the alternative concentration models tested, but remained sensitive to occupancy and arsenic bioavailability, and for any receptor exposed mainly by inhalation they would depend on the particulate emission factor.

4.3. Arsenic Governs Precision Under Either Parameterization

Arsenic accounts for 99.8% of mean CR and 91.7% of mean HI, and its concentration shows a rank correlation with total CR ($\rho = +0.867$) exceeding that of the next-ranked input by a factor of three (Section 3.5). The four exposure parameters that a site-specific survey could realistically refine—exposure duration, ingestion rate, adherence factor and frequency—together account for a small fraction of output variance.

This shapes how additional resources should be allocated. A site-specific occupational exposure survey, which is the conventional response to uncertainty in a screening-level assessment, would reduce output variance marginally. A finer-resolution sampling of arsenic, particularly along the eastern transect where the 10,900 $mg \cdot kg^{-1}$ hotspot was recorded as a single point flanked by markedly lower values, would reduce it substantially. Sensitivity analysis converts an intuition about data gaps into a defensible allocation of survey effort, and this is among the more useful and least-used products of probabilistic assessment.

The dominance of arsenic also reinforces the co-priority argument made in [8] and reported at comparable Pb–Zn smelting sites elsewhere [36–38]: at polymetallic Pb–Zn legacy sites, the contaminant with the largest mass burden is not the contaminant that drives risk. Probabilistic treatment widens this divergence rather than narrowing it, because arsenic combines a high slope factor with the heaviest distributional tail among the priority metals, a behaviour with a mineralogical basis: at non-ferrous smelting sites arsenic partitions largely into reducible and residual phases and is hosted in discrete mineral grains rather than dispersed through the soil matrix, producing pronounced heterogeneity at metre scale [39,40].

Comparison with other assessments places these results in a regional and international context. Within Kazakhstan, the only nationwide stochastic assessment of urban soils identified Shymkent as one of the four most contaminated of 22 cities, together with Balkhash, Ust-Kamenogorsk and Ridder, and found carcinogenic risks well above the screening level, driven mainly by ingestion of lead by children [41]. That assessment was based on state monitoring data for Pb, Cd, Cu, Zn and Cr and did not include arsenic. The present results indicate that at a slag reprocessing site within the same city arsenic, rather than lead, governs risk, so that assessments omitting arsenic may understate risk where Pb–Zn metallurgical residues are present. In Kentau, a single-industry town of the same region with a long history of Pb–Zn ore processing, surface soils remain contaminated with Zn, Cd, Pb and Cu [7], which indicates that such residues persist as long-term sources. Internationally, the closest analogue is a probabilistic assessment of arsenic-contaminated allotment-garden soils in the former gold- and arsenic-mining town of Złoty Stok, Poland, where total As ranged from 433 to 1148 $mg \cdot kg^{-1}$ [42]. There, 54% of simulated adult exposures reached a carcinogenic risk of 10^{-4}, ingestion and dermal contact accounted for nearly all risk while inhalation was negligible, total As and the soil ingestion rate

were the principal drivers, and adjusting ingestion for measured bioaccessibility reduced ingestion-related risk by 89%. The pathway structure and sensitivity ranking found here are consistent with those results despite differences in receptor and exposure assumptions, and the size of the bioaccessibility effect reported there indicates that the lower end of the RBA range examined in Section 3.3 is realistic for mining-affected soils.

4.4. Distance from Source Is a Poor Proxy for Risk

The three-tier zonation proposed in [8] prioritizes the 0–10 m perimeter for engineered intervention, the 10–100 m band for phytostabilization, and beyond 100 m for monitored attenuation. The third tier contains no transect samples and was not modelled here, so the present analysis bears on the ordering of the first two tiers only. The ordering follows the intuition of radial decay from a point source.

The present analysis does not confirm that ordering on risk grounds. Mean CR in Zone 2 (10–100 m) is 1.81× that in Zone 1 (0–10 m), and mean HI is 1.72× higher (Section 3.6). The mechanism is visible in the source data: the western transect carries As concentrations of 7610 mg·kg^{-1} at 50 m and 7900 mg·kg^{-1} at 100 m, and Pb of 7850 mg·kg^{-1} at 100 m—a secondary maximum at the outer edge of Zone 2.

This result depends on those two samples. Leave-one-out analysis (Section 3.6, Table 10) shows that excluding either the 50 m or the 100 m western sample reverses the comparison, reducing the Zone 2:Zone 1 mean-As ratio from 1.38 to 0.88 and 0.85 respectively; excluding any of the remaining six samples leaves the ratio at 1.49–1.56. Two of eight samples therefore carry the finding.

This dependence is taken to be informative rather than disqualifying, for two reasons. The two samples are not analytical outliers. They lie on the western transect, which [8] identified as carrying the highest mean concentrations of four priority metals, oriented along the prevailing wind regime, away from the Badam River and toward the A-2 highway and adjacent residential areas. Their values also sit within a broadly elevated arsenic profile along that transect—3890 mg·kg^{-1} at 0 m, 7610 at 50 m and 7900 at 100 m—rather than standing isolated within it. More importantly, the sensitivity is itself the finding: where two samples in eight can reverse the risk ordering between zones, a distance-stratified design with $n = 8$ beyond the perimeter does not resolve the risk surface, and any zonation derived from it—including the ordering proposed in [8] and the reversal suggested here—rests on insufficient support.

What the data do establish is limited. The stratified bootstrap interval for the Zone 2:Zone 1 ratio of mean CR (0.16–9.9) includes values well below and well above unity, so the present design cannot determine whether risk beyond the 10 m perimeter is lower or higher than within it. Pernebayev et al. [8] documented the non-monotonic concentration pattern and declined to fit a radial dispersion model on that basis, while retaining a distance-ordered zonation in its management recommendations. The present results indicate that this zonation is not supported by the risk data, but they equally do not support a reversed ordering.

Zone 1 nevertheless carries the higher exceedance probability (77.5% versus 60.3%). The zones therefore differ in the character of their contamination, not merely in its degree: Zone 1 is uniformly and reliably contaminated; Zone 2 is patchily and severely so. Mean risk responds to the tail; exceedance probability responds to the bulk. A management framework built on either statistic alone will misallocate effort, and the two should be reported together.

The generalizable point is that at sites where deposition is wind-controlled and runoff redistributes coarse fragments along topographic gradients, distance from the source perimeter is a poor proxy for risk. Zonation should follow the measured risk surface, and a

sampling design stratified by distance rather than by expected risk will not resolve that surface at reasonable cost. Directional stratification weighted toward the prevailing wind vector, with denser sampling where secondary maxima have already been observed, would support zonation decisions that the present design cannot.

4.5. The Receptor Determines Which Intervention Appears Effective

Containment of Zone 1 reduces mean CR to 0.660 of the no-intervention value at the 20-year horizon when time is divided equally between the zones; the reduction ranges from 95% to none as the share of time spent in Zone 1 falls from 100% to zero (Section 3.7). Adding phytostabilization of Zone 2 produces no additional reduction: S1 and S2 differ by less than 0.3% at every horizon (Section 3.7).

This follows directly from the sensitivity analysis. Phytostabilization was modelled as suppression of dust emission, which acts on the inhalation pathway; inhalation contributes 0.17% of worker CR under Set A and 0.01% under Set B under the RAGS default particulate emission factor of 1.36×10^9 $m^3 \cdot kg^{-1}$, and shows negligible rank correlation with output ($\rho < 0.01$). Within this model, an intervention acting on a pathway that carries almost none of the modelled risk cannot reduce that risk. This is a model outcome for the on-site occupational receptor under the default particulate emission factor, not a general statement about the performance of phytostabilization, whose benefit lies in reducing off-site dust transport and exposure of receptors not modelled here.

This result must not be read as evidence against phytostabilization. It is a statement about the receptor, not the measure. The occupational receptor modelled here stands on the contaminated surface; dust generated at mining and metallurgical sites is nonetheless a documented source of measurable exposure in adjacent settlements [43,44]; ingestion and dermal contact dominate, and a vegetative cover does not remove soil from contact. The receptor that phytostabilization protects is the off-site resident, for whom the transport pathway—wind-driven dispersion of fine particulates—is the exposure pathway. Pernebayev et al. [8] reported Pb at 205 $mg \cdot kg^{-1}$ (12× upper continental crust) at a reference point 1.5 km from the heap, indicating that this transport is operative at the kilometre scale in the prevailing wind regime.

The general implication is methodological. Where a risk assessment is used to compare interventions, the choice of receptor silently determines the ranking. An occupational-only assessment will systematically favour barrier measures over emission-control measures, because barriers act on the pathways that dominate on-site exposure. Site-management frameworks derived from single-receptor assessments therefore encode a preference that is an artefact of scope rather than a property of the interventions. Extension of the present analysis to a residential receptor is the most direct route to resolving this, and is identified as the priority next step (Section 4.6).

4.6. Limitations

Single sampling campaign. All concentration data derive from one campaign (24 April 2026). How metal mobility shifts between seasons in this semi-arid setting, where moisture arrives episodically, is therefore not captured; the fitted distributions describe spatial rather than temporal variability.

Total concentrations. No sequential extraction was performed, so the bioavailable fraction is unknown. Total concentrations were used throughout, which is conservative for risk estimation but limits inference about mobility. Fractionation is identified as a priority for the next campaign.

Temporal representativeness. The analysis rests on a single sampling campaign (24 April 2026) at an active reprocessing site. Concentrations may since have changed

through continued reprocessing, earthworks or redistribution by wind and runoff, and seasonal variation was not captured; the results describe the site as sampled rather than its current state.

Mercury. Mercury was modelled from total concentrations in soil through the particulate pathways of the RAGS model. Volatilization of elemental mercury and mercury speciation were not considered, although inhalation can be an important route of mercury exposure near metallurgical residues [45] and mercury in settled dust can vary seasonally in semi-arid settings [46]. Because Hg contributes a small share of the modelled hazard index, this omission does not affect the conclusions for the occupational receptor, but it would matter for residential receptors and children.

Analytical quality control. Element-specific analytical quality-control data (certified reference material recoveries, blanks, replicate precision) were not reported in the laboratory test protocols and could not be included. A systematic analytical bias of ±20% altered the probability of exceeding 10^{-4} by about 5 percentage points or less under either parameterization (Table S3), indicating that the conclusions are not sensitive to analytical error of this magnitude.

Sampling depth. Soil was sampled as 0–50 cm depth-integrated composites, and surface-layer (0–5 or 0–10 cm) concentrations, which are most relevant to incidental ingestion and dermal contact, were not measured separately. A twofold difference between surface and depth-integrated concentrations would not change the conclusions under the 2025 toxicity values (Table S3).

Toxicity values. The arsenic slope factors and reference doses under both parameterizations were taken directly from the primary IRIS records. Route-specific inhalation and dermal reference doses required for the hazard index are not issued under the IRIS programme and were obtained by route extrapolation from published compilations, in which such values vary between sources. Carcinogenic risk is unaffected, since it draws only on IRIS slope factors; hazard index values carry this additional uncertainty.

Zone areas and receptor time allocation. Zone boundaries follow the buffer rings of [8], described there as estimated. Combined risk assumes equal receptor time allocation between Zone 1 and Zone 2, an assumption rather than a survey result; repeating the analysis for allocations from 100:0 to 0:100 shows that this assumption governs the estimated benefit of containment but not the screening conclusion (Section 3.7). Results are therefore reported as relative risk ratios rather than absolute exposures, and zonal results are given separately so that alternative weightings can be applied.

Sample size. The fitted distributions rest on 24 samples, and bootstrap intervals for the site-wide exceedance probabilities span roughly 20 percentage points under Set A (Section 3.3); the probabilities should therefore be read to the nearest ten percentage points rather than to one decimal place. Eight samples support the zonal comparison, the direction of the difference is not robust to the exclusion of either western-transect sample, and the stratified bootstrap interval for the Zone 2:Zone 1 ratio spans values on both sides of unity (Section 3.6). The zonal comparison is therefore unresolved by the present design.

Arsenic bioavailability. Carcinogenic risk was computed from total soil arsenic, which is equivalent to assuming a relative bioavailability of unity. The US EPA recommends a default relative bioavailability of 60% for arsenic in soil [28], and in vivo measurements on soils from mining and smelting sites report values well below unity [47]. The estimates reported here are therefore upper bounds with respect to this parameter; applying RBA to the ingestion pathway reduces mean CR by 29% at the default of 0.6 and by 57% at 0.2 (Section 3.3). Under Set B the probability of exceeding 10^{-4} remains above 97% across this range. Under Set A it falls to 62.5% at the default and to 49.5% at 0.2, so that with the superseded toxicity values and low bioavailability, exceedance would be about as likely as

not. A site-specific bioaccessibility measurement would therefore matter for conclusions drawn under the superseded values, but not under those currently in force.

Particulate emission factor. The RAGS default particulate emission factor was retained rather than derived site-specifically. This parameter governs the magnitude of the inhalation pathway, and the negligible reduction attributed to phytostabilization in the scenario analysis follows from it. The respirable fraction of the slag, which is the property this factor represents, was not characterized. Aerodynamic or laser-diffraction sizing of the respirable fraction, and a particulate emission factor derived from it, would be required before the S1–S2 comparison could be treated as quantitative rather than indicative; emission from tailings and slag surfaces is governed by the respirable fraction and surface condition rather than by bulk composition, and site-specific factors derived from dispersion measurement differ substantially from generic defaults [48,49].

Intervention efficiencies. Scenario parameters are literature-derived. The scenarios constitute a parametric analysis of the sensitivity of risk to the documented range of intervention performance, not a site-specific engineering forecast. For phytostabilization, the dust-reduction efficiency was varied from 0 to 100% without effect on the conclusions (Section 3.7).

Single receptor. Only an adult occupational receptor was modelled. Extension to a residential receptor would require soil data from residential and sensitive land uses. The nearest housing lies about 250 m west of the heap and about 10,500 people live within 1 km of its centre (Section 2.1), but soil was not sampled at residential locations, so no such analysis is attempted here. As set out in Section 4.5, this scope determines the relative ranking of interventions, and the omission of a residential receptor is the principal limitation on the management conclusions.

5. Conclusions

Probabilistic reanalysis of a published dataset from an active Pb–Zn slag reprocessing site shows that the January 2025 IRIS revision of inorganic arsenic changes the quantitative risk estimate far more than any modelling choice: for the same measured concentrations, the mean carcinogenic risk estimated for the adult outdoor worker was 21-fold higher, and the estimated probability of exceeding the upper end of the US EPA risk-management range (10^{-4}) increased from about 70% (95% bootstrap interval 59–80%) to over 98%. The qualitative screening conclusion of [8] therefore holds under both sets of toxicity values, whereas estimates made before and after the revision are not comparable; this conclusion is robust to sampling uncertainty and to the alternative concentration models tested, but remains conditional on the occupancy, bioavailability and particulate-emission assumptions of the exposure model. Relative to the published deterministic assessment, the probabilistic analysis changes the central estimate for this dataset by only about 15%, but adds what a point estimate cannot convey: the probability of exceedance and the position of the published values within the distribution. The principal source of uncertainty is the arsenic concentration distribution, which dominates output variance and rests on 24 samples. This small spatial dataset leaves the ordering of risk between the zones unresolved, and the restriction to a single occupational receptor means that the results do not extend to residents or children.

Supplementary Materials: The following supporting information can be downloaded at: https://www.mdpi.com/article/10.3390/toxics14100894/s1, Figure S1: normal quantile–quantile plots of the log-transformed concentrations of all eight metals, with Shapiro–Wilk p values; Figure S2: measured concentrations along the four transects as multiples of the Kazakhstan maximum permissible concentration; Table S2: bootstrap uncertainty due to the limited number of samples, site-wide and by zone; Table S3: sensitivity to analytical error and sampling depth; Table S4: goodness of fit of alternative distributions, risk under alternative concentration models and dependence

structures, and kernel width; Table S5: rank-correlation sensitivity of CR and HI to all stochastic inputs; Table S6: sensitivity of scenario S2 to the dust-reduction efficiency of phytostabilization; Table S7: sensitivity to the allocation of time between zones; Table S8: sensitivity to the relative bioavailability of arsenic. Script S1: 'S1_reproduce_all.py', which reproduces every result of the primary analysis from the published source dataset (fixed random seed 20260827); File S2: 'S2_expected_output.txt', the console output of Script S1; File S3: 'requirements.txt', the library versions used; Script S4: 'S4_revision_block1.py', 'S4_revision_block2.py' and 'S4_revision_block3.py', which reproduce the analyses in Tables S2–S8 and Figure S2, and 'S4_revision_figures.py', which reproduces Figures 3–6; File S5: 'S5_revision_output.txt', the console output of Script S4. The scripts require Supplementary Table S1 of [8], publicly available under a CC BY licence at https://doi.org/10.3390/su18136742; that dataset is not duplicated here.

Author Contributions: Conceptualization, Z.P., A.I., A.A.; methodology, Z.P., A.I., A.A., T.B.; software, A.A., T.B.; validation, Z.P., A.I., M.-u.-R.A.; formal analysis, A.I., Z.P., T.B., M.-u.-R.A.; investigation, A.A., K.N.; data curation, Z.P., T.B.; writing—original draft preparation, Z.P., A.I., A.A.; writing—review and editing, T.B., M.-u.-R.A.; visualization, A.A.; supervision, A.I., M.-u.-R.A.; project administration, Z.P., A.I.; funding acquisition, Z.P. All authors have read and agreed to the published version of the manuscript.

Funding: This research was funded by the Science Committee of the Ministry of Science and Higher Education of the Republic of Kazakhstan, grant number AP25795537, "Ecological assessment of the locations of lead-zinc slags on environmental objects and the development of technology for the reclamation of slag heaps".

Institutional Review Board Statement: Not applicable.

Informed Consent Statement: Not applicable.

Data Availability Statement: The source geochemical data analysed in this study are openly available as Supplementary Table S1 of reference [8] at https://doi.org/10.3390/su18136742. The simulation code and its console output are provided in the Supplementary Materials. Further inquiries can be directed to the corresponding authors.

Acknowledgments: The authors thank the accredited Analytical Laboratory of LLP KazEcoAnaliz (Almaty, Kazakhstan) for the analytical work underlying the source dataset. During the preparation of this study, the authors used a large language model (Claude Opus 4.1, Anthropic; accessed via claude.ai, 2026) to assist with literature searching, drafting and editing of the text, writing the Python code of Script S1, and preparing the graphical abstract, and Grammarly Pro (Grammarly, 2026) for English language proofreading. All computational results were independently reproduced from the supplied script, all toxicity values were verified against the primary IRIS records, and all cited sources were checked against their published records. The authors have reviewed and edited the output and take full responsibility for the content of this publication.

Conflicts of Interest: Authors Zhaksylyk Pernebayev, Akmaral Issayeva, Akbota Aitimbetova and Kural Nurseiit were employed by LLP Centre for Scientific Research and Ecological Expertise KazEcoHolding. The remaining authors declare that the research was conducted in the absence of any commercial or financial relationships that could be construed as a potential conflict of interest.

Abbreviations

The following abbreviations are used in this manuscript:

ABS	Dermal absorption factor
AF	Adherence factor
AT	Averaging time
BW	Body weight
CDI	Chronic daily intake
CR	Carcinogenic risk
ED	Exposure duration

EF	Exposure frequency
GM	Geometric mean
GSD	Geometric standard deviation
HI	Hazard index
ICP-OES	Inductively coupled plasma optical emission spectrometry
IngR	Soil ingestion rate
InhR	Inhalation rate
IRIS	Integrated Risk Information System
IUR	Inhalation unit risk
MPC	Maximum permissible concentration
PEF	Particulate emission factor
RAGS	Risk Assessment Guidance for Superfund
RfD	Reference dose
SA	Exposed skin area
SF	Slope factor
US EPA	United States Environmental Protection Agency

References

1. Terzić, A.; Stojanović, J.; Jovanović, V.; Todorović, D.; Sokić, M.; Bojović, D.; Radulović, D. Exploring the Efficiency of Magnetic Separation and Gravity Concentration for Valorizing Pb–Zn Smelter Slag in a Circular Economy Framework. *Materials* **2024**, *17*, 3945. [CrossRef]
2. Nowińska, K.; Kokowska-Pawłowska, M. Mineralogy of Zinc and Lead Metallurgical Slags in Terms of Their Impact on the Environment: A Review. *Minerals* **2024**, *14*, 852. [CrossRef]
3. Gil-Loaiza, J.; Field, J.P.; White, S.A.; Csavina, J.; Felix, O.; Betterton, E.A.; Sáez, A.E.; Maier, R.M. Phytoremediation Reduces Dust Emissions from Metal(loid)-Contaminated Mine Tailings. *Environ. Sci. Technol.* **2018**, *52*, 5851–5858. [CrossRef] [PubMed]
4. Kicińska, A. Physical and Chemical Characteristics of Slag Produced during Pb Refining and the Environmental Risk Associated with the Storage of Slag. *Environ. Geochem. Health* **2021**, *43*, 2723–2741. [CrossRef] [PubMed]
5. Ettler, V. Soil Contamination near Non-Ferrous Metal Smelters: A Review. *Appl. Geochem.* **2016**, *64*, 56–74. [CrossRef]
6. Salim, Y.; Issayeva, A.; Kidirbayeva, K.; Zhumadulayeva, A.I.; Dossybayeva, G.; Bozhbanbayeva, N.; Ashirbayeva, S. Influence of Lead–Zinc Slags of the Shymkent City on the Environment. *J. Ecol. Eng.* **2022**, *23*, 83–89. [CrossRef]
7. Junusbekov, M.M.; Akbasova, A.D.; Seidakbarova, A.D.; Koishiyeva, G.Z.; Sainova, G.A. Ecological Assessment of Soil Contamination by Heavy Metals Affected in the Past by the Lead–Zinc Mining and Processing Complex in Kentau, Kazakhstan. *Environ. Monit. Assess.* **2023**, *195*, 586. [CrossRef] [PubMed]
8. Pernebayev, Z.; Aitimbetova, A.; Abubakirova, A. Integrated Geochemical, Vegetation, and Risk Assessment of a Pb–Zn Slag Reprocessing Site in Southern Kazakhstan: Implications for Sustainable Remediation Prioritization. *Sustainability* **2026**, *18*, 6742. [CrossRef]
9. US EPA. *Risk Assessment Guidance for Superfund: Volume III—Part A, Process for Conducting Probabilistic Risk Assessment*; EPA 540-R-02-002; Office of Emergency and Remedial Response, U.S. Environmental Protection Agency: Washington, DC, USA, 2001.
10. Wang, X.; Xu, F.; Gui, Y.; Liu, Y. Enhancing Health Risk Assessment for Soil Heavy Metal(loid)s Using a Copula-Based Monte Carlo Simulation Method. *Ecotoxicol. Environ. Saf.* **2025**, *300*, 118419. [CrossRef] [PubMed]
11. Panqing, Y.; Abliz, A.; Xiaoli, S.; Aisaiduli, H. Human Health-Risk Assessment of Heavy Metal–Contaminated Soil Based on Monte Carlo Simulation. *Sci. Rep.* **2023**, *13*, 7033. [CrossRef] [PubMed]
12. Guo, G.; Zhang, D.; Wang, Y. Probabilistic Human Health Risk Assessment of Heavy Metal Intake via Vegetable Consumption around Pb/Zn Smelters in Southwest China. *Int. J. Environ. Res. Public Health* **2019**, *16*, 3267. [CrossRef] [PubMed]
13. Sun, L.; Wang, X.; Liu, Y.; Huang, J.; Xi, S.; Shi, L.; Song, Y.; Qi, M.; Guo, C. Improved Model for Human Health Risk Assessment of Soil Heavy Metal(loid)s in a Mining Area of Southeastern China. *Ecotoxicol. Environ. Saf.* **2025**, *306*, 119312. [CrossRef] [PubMed]
14. Shetty, B.R.; Pai, B.J.; Salmataj, S.A.; Naik, N. Assessment of Carcinogenic and Non-Carcinogenic Risk Indices of Heavy Metal Exposure in Different Age Groups Using Monte Carlo Simulation Approach. *Sci. Rep.* **2024**, *14*, 29906. [CrossRef] [PubMed]
15. Jia, X.; Fu, H.; Ding, D.; Ren, X.; Zhao, P.; Chen, X.; Luo, X.; Guo, B.; Xu, H.; Sheng, Z.; et al. Source-Oriented Health Risk Assessment of Potentially Toxic Elements in the Water–Soil–Crop System Using Monte Carlo Simulation: A Case Study of the Laoguan River Basin, China. *Toxics* **2025**, *13*, 952. [CrossRef] [PubMed]
16. US EPA. Integrated Risk Information System (IRIS): Inorganic Arsenic, CASRN 7440-38-Oral Slope Factor And reference Dose. Updated 13 January. Available online: https://iris.epa.gov/ChemicalLanding/&substance_nmbr=278 (accessed on 30 August 2026).
17. Agency for Toxic Substances and Disease Registry (ATSDR). How to Use the Newly Revised Cancer Slope Factor (CSF) for Inorganic Arsenic. In *ATSDR Newsletter for Health Assessors*; U.S. Department of Health and Human Services: Atlanta, GA, USA, 2026.

18. Beck, H.E.; Zimmermann, N.E.; McVicar, T.R.; Vergopolan, N.; Berg, A.; Wood, E.F. Present and Future Köppen-Geiger Climate Classification Maps at 1-km Resolution. *Sci. Data* **2018**, *5*, 180214. [CrossRef] [PubMed]
19. Salim, Y.; Yerimbetova, A.; Baiduisenova, T.; Uspabayeva, A.; Abildayeva, R.; Balgabekova, A.; Ashirbayeva, S.; Tleukeyeva, A. Soil Pollution with Heavy Metals in Turkestan Region. *J. Ecol. Eng.* **2023**, *24*, 31–38. [CrossRef] [PubMed]
20. Bondarenko, M.; Kerr, D.; Sorichetta, A.; Tatem, A.J. *Census/Projection-Disaggregated Gridded Population Datasets for 189 Countries in 2020 Using Built-Settlement Growth Model (BSGM) Outputs*; WorldPop, University of Southampton: Southampton, UK, 2020. [CrossRef]
21. *GOST R 58595-2019*; Soils Sampling. Standartinform: Moscow, Russia, 2019.
22. *GOST 17.4.3.01-2017*; Nature Protection (SSOP); Soils—General Requirements for Sampling. Interstate Council for Standardization, Metrology and Certification: Moscow, Russia, 2017.
23. *GOST 17.4.4.02-2017*; Nature Protection; Soils—Methods for Sampling and Preparation of Soil for Chemical, Bacteriological, Helminthological Analysis. Interstate Council for Standardization, Metrology and Certification: Moscow, Russia, 2017.
24. Reliable Prognosis. Weather Archive at Shymkent Airport (UAII), METAR, 22–24 April 2026. Available online: https://rp5.kz (accessed on 27 September 2026).
25. US EPA. *Risk Assessment Guidance for Superfund (RAGS), Volume I: Human Health Evaluation Manual*; U.S. Environmental Protection Agency: Washington, DC, USA, 2023. Available online: https://www.epa.gov/risk/risk-assessment-guidance-superfund-rags-part (accessed on 30 August 2026).
26. US EPA. *Exposure Factors Handbook: 2011 Edition (Final)*; National Center for Environmental Assessment, Office of Research and Development: Washington, DC, USA, 2011.
27. US EPA. *Role of the Baseline Risk Assessment in Superfund Remedy Selection Decisions*; OSWER Directive 9355.0-30; U.S. Environmental Protection Agency: Washington, DC, USA, 1991.
28. US EPA. *Recommendations for Default Value for Relative Bioavailability of Arsenic in Soil*; OSWER 9200.1-113; U.S. Environmental Protection Agency: Washington, DC, USA, 2012.
29. Harris, C.R.; Millman, K.J.; van der Walt, S.J.; Gommers, R.; Virtanen, P.; Cournapeau, D.; Wieser, E.; Taylor, J.; Berg, S.; Smith, N.J.; et al. Array Programming with NumPy. *Nature* **2020**, *585*, 357–362. [CrossRef] [PubMed]
30. Virtanen, P.; Gommers, R.; Oliphant, T.E.; Haberland, M.; Reddy, T.; Cournapeau, D.; Burovski, E.; Peterson, P.; Weckesser, W.; Bright, J.; et al. SciPy 1.0: Fundamental Algorithms for Scientific Computing in Python. *Nat. Methods* **2020**, *17*, 261–272. [CrossRef] [PubMed]
31. ITRC (Interstate Technology & Regulatory Council). *Mining Waste Treatment Technology Selection: Technology Overview of Capping/Covers and Grading*; Interstate Technology & Regulatory Council, Mining Waste Team: Washington, DC, USA, 2010; Available online: https://projects.itrcweb.org/miningwaste-guidance/to_capping_covers.htm (accessed on 30 August 2026).
32. Gil-Loaiza, J.; White, S.A.; Root, R.A.; Solís-Dominguez, F.A.; Hammond, C.M.; Chorover, J.; Maier, R.M. Phytostabilization of Mine Tailings Using Compost-Assisted Direct Planting: Translating Greenhouse Results to the Field. *Sci. Total Environ.* **2016**, *565*, 451–461. [CrossRef] [PubMed]
33. Li, Q.; Li, D.; Wang, Z.; Sun, D.; Zhang, T.; Zhang, Q. Integrated Deterministic and Probabilistic Methods Reveal Heavy Metal-Induced Health Risks in Guizhou, China. *Toxics* **2025**, *13*, 515. [CrossRef] [PubMed]
34. National Research Council. *Review of EPA's Integrated Risk Information System (IRIS) Process*; The National Academies Press: Washington, DC, USA, 2014. [CrossRef] [PubMed]
35. Vieira Silva, A.; Öberg, M. Selection of the Critical Effect Size Alters Hazard Characterization—A Retrospective Analysis of Key Studies Used for Risk Assessments of PFAS. *Front. Toxicol.* **2025**, *7*, 1525089. [CrossRef] [PubMed]
36. Yang, L.; Ge, S.; Liu, J.; Iqbal, Y.; Jiang, Y.; Sun, R.; Ruan, X.; Wang, Y. Spatial Distribution and Risk Assessment of Heavy Metal(Oid)s Contamination in Topsoil around a Lead and Zinc Smelter in Henan Province, Central China. *Toxics* **2023**, *11*, 427. [CrossRef] [PubMed]
37. He, J.; Peng, Z.; Zeng, J.; Ke, W.; Zhu, F.; Jiang, J.; Xue, S. Source Apportionment and Quantitative Risk Assessment of Heavy Metals at an Abandoned Zinc Smelting Site Based on GIS and PMF Models. *J. Environ. Manag.* **2023**, *336*, 117565. [CrossRef] [PubMed]
38. Luo, X.; Wu, C.; Lin, Y.; Li, W.; Deng, M.; Tan, J.; Xue, S. Soil Heavy Metal Pollution from Pb/Zn Smelting Regions in China and the Remediation Potential of Biomineralization. *J. Environ. Sci.* **2023**, *125*, 662–677. [CrossRef] [PubMed]
39. Ke, W.; Zeng, J.; Zhu, F.; Luo, X.; Feng, J.; He, J.; Xue, S. Geochemical Partitioning and Spatial Distribution of Heavy Metals in Soils Contaminated by Lead Smelting. *Environ. Pollut.* **2022**, *307*, 119486. [CrossRef] [PubMed]
40. Zeng, J.; Luo, X.; Cheng, Y.; Ke, W.; Hartley, W.; Li, C.; Jiang, J.; Zhu, F.; Xue, S. Spatial Distribution of Toxic Metal(Loid)s at an Abandoned Zinc Smelting Site, Southern China. *J. Hazard. Mater.* **2022**, *425*, 127970. [CrossRef] [PubMed]
41. Ramazanova, E.; Lee, S.H.; Lee, W. Stochastic Risk Assessment of Urban Soils Contaminated by Heavy Metals in Kazakhstan. *Sci. Total Environ.* **2021**, *750*, 141535. [CrossRef] [PubMed]
42. Olabode, K.; Lewińska, K.; Komorowicz, I. Human Health Risk and Remedial Goal Assessment Using Monte Carlo Simulation: A Case Study of Arsenic Contaminated Allotment Gardens in Southern Poland. *Environ. Geochem. Health* **2026**, *48*, 571. [CrossRef] [PubMed]
43. Nkosi, V.; Wichmann, J.; Voyi, K. The Potential Health Costs of PM10 Impacts on a Gold Mine Village during Company Liquidation. *Minerals* **2022**, *12*, 169. [CrossRef]

44. Khan, M.M.H.; Kurniawan, T.A.; Chandra, I.; Lei, T.M.T. Modeling PM10 Emissions in Quarry and Mining Operations: Insights from AERMOD Applications in Malaysia. *Atmosphere* **2025**, *16*, 369. [CrossRef]
45. Morton Bermea, O.; Castro-Larragoitia, J.; Arellano Álvarez, Á.A.; Pérez-Rodríguez, R.J.; Leura-Vicencio, A.; Schiavo, B.; Salgado-Martínez, E.; Razo-Soto, I.; Hernández-Álvarez, E. Mercury in Blood of Children Exposed to Historical Residues from Metallurgical Activity. *Expo. Health* **2021**, *13*, 281–292. [CrossRef]
46. Schiavo, B.; Meza-Figueroa, D.; Morton-Bermea, O.; Vizuete-Jaramillo, E.; Robles-Morua, A. Seasonal Variation of Mercury in Settled Dust from Brick Kiln Pollution in Sonora, Mexico: Ecological Risk and Human Health Implication. *Atmos. Pollut. Res.* **2023**, *14*, 101787. [CrossRef]
47. Bradham, K.D.; Scheckel, K.G.; Nelson, C.M.; Seales, P.E.; Lee, G.E.; Hughes, M.F.; Miller, B.W.; Yeow, A.; Gilmore, T.; Serda, S.M.; et al. Relative Bioavailability and Bioaccessibility and Speciation of Arsenic in Contaminated Soils. *Environ. Health Perspect.* **2011**, *119*, 1629–1634. [CrossRef] [PubMed]
48. Ilie, A.M.C.; Vaccaro, C.; Rogers, J.; Sansalone, J. Modelling the Dispersion of Particulate Matter (PM10) via Wind Erosion from Opencast Mining—Moldova Nouă Tailings Ponds, Romania. *Environ. Monit. Assess.* **2023**, *195*, 1518. [CrossRef] [PubMed]
49. Lee, S.-h. Particle Size Effects in Gaussian-Based Air Quality Modeling of Mine Dust: A Review with Mechanistic Numerical Demonstration. *Mining* **2026**, *6*, 44. [CrossRef]

Disclaimer/Publisher's Note: The statements, opinions and data contained in all publications are solely those of the individual author(s) and contributor(s) and not of MDPI and/or the editor(s). MDPI and/or the editor(s) disclaim responsibility for any injury to people or property resulting from any ideas, methods, instructions or products referred to in the content.